Experimental Investigations of Surface Roughness Effect on Functional Applications of Tube Extrusion Punch Using Magnetorheological Finishing Process

A Thesis Submitted in Fulfillment of the Requirement for the Award of the Degree of

MASTER OF ENGINEERING

in

Production Engineering

Submitted by

ANIRUDH CHANA

Roll No. 801685002

Under Supervision of

Dr. Anant Kumar Singh
Associate Professor

THAPAR INSTITUTE
OF ENGINEERING & TECHNOLOGY
(Deemed to be University)

MECHANICAL ENGINEERING DEPARTMENT

THAPAR INSTITUTE OF ENGINEERING & TECHNOLOGY
(A DEEMED TO BE UNIVERSITY), PATIALA, PUNJAB – 147004, INDIA

JULY, 2018

DECLARATION

I, **Anirudh Chana** hereby declare that the work presented in this thesis entitled "**Experimental Investigations of Surface Roughness Effect on Functional Applications of Tube Extrusion Punch Using Magnetorheological Finishing Process**" in fulfilment of the requirement for the award of degree of **Master of Engineering (Production Engineering)** submitted at Mechanical Engineering Department, Thapar Institute of Engineering & Technology (Deemed to be University), Patiala is an authentic record of work carried out under supervision of **Dr. Anant Kumar Singh** (Associate Professor, Mechanical Engineering Department, Thapar Institute of Engineering & Technology from August, 2017 to July, 2018. The matter presented in this has not been submitted either in part or full to any other university or institute for the award of any other degree.

(Anirudh Chana)

Date: 9/8/2018

(801685002)

(Anant Kumar Singh)

(Associate Professor)

Mechanical Engineering Department,

Thapar Institute of Engineering & Technology

(A Deemed to be University), Patiala, Punjab.

Date: 09/08/2018

Dedicated

to

my family

for their endless love, support and encouragement

ACKNOWLEDGEMENT

I would first like to thank my thesis advisor **Dr. Anant Kumar Singh** (Associate Professor, Mechanical Engineering Department, Thapar Institute of Engineering & Technology). The door to his office was always open whenever I ran into a trouble spot or had a question about my research or writing. He steered me in the right direction whenever he thought I needed it. His guidance helped me in all the time of research and writing of this thesis.

I would like to thank **Mr. Jaswant Singh** (General Manager), **Mr. Rajeev kumar** (Engineer Head, Forging Department) and their colleagues for helping me in understanding the process and discussing the problems faced during extrusion operation at GNA Axles Ltd., Hoshiarpur (Punjab). I am really thankful to them for allowing me to use their extrusion punch in my thesis work and allowing me to test it in the industry

I also place on record, my sense of gratitude to one and all, who directly or indirectly, have impart their hand in this venture.

ABSTRACT

Surface finish has great influence on functional properties such as wear resistance and power loss. Finishing process not only has to reduce surface roughness but also improve the surface accuracy and minimize the surface defects. In metal forming process, surface roughness plays the vital role in deciding the efficiency of the process. Rough surface results in more power loss and abrasion of dies and punches during metal forming operations. Non homogenous strain of material due to high surface roughness in forming process results in heterogeneity of properties of end products. Demand for surface finishing of dies and moulds in metal forming processes is increased. The industrial application for surface finishing requirement has various benefits. Surface finish is required to improve the service life of the extrusion punch used in tube extrusion process. In industry, the finishing of the extrusion punch is performed mainly by grinding process. Surface roughness of 480nm is achieved at the industry by the grinding process. A fixture of magnetorheological (MR) finishing process is developed in this research to finish the ferromagnetic cylindrical extrusion punch made of H13 material up to nano-level. The present MR finishing tool performance has been analyzed for finishing of extrusion punch through magnetostatic simulation. The study on the mechanism of material removal during MR finishing of extrusion punch is also done. The surface roughness model is validated experimentally. The percentage error is found in the range of 5% to 15.65%. Response surface methodology (RSM) using central composite design has been used for designing the experiments and regression analysis. The effect of process parameters like tool rotation, tool reciprocating feed, workpiece rotation and current are studied and optimized. Experiments are performed using the optimum parameters. Surface roughness are reduced from 380nm to 50nm in 50 minutes. Finishing of the extrusion punch has been done using optimum parameters on the designed fixture. Surface roughness value of punch reduced to 70nm from 480nm in 25hrs. After finishing, extrusion punch is tested in industry for improvement in tube extrusion process and found their better functional life as compared to the grinded surface.

Keywords *: Extrusion punch , Magnetorheological polishing fluid, H13 die steel, Magnetic iron particles, Surface roughness.*

TABLE OF CONTENT

LIST OF TABLES

LIST OF FIGURES

ABBREVIATIONS

ANOVA	Analysis of Variance
BEMRF	Ball End Magnetorheological Finishing
BHN	Brinell Hardness Number
CAD	Computer Aided Design
CMP	Chemo-Mechanical Polishing
CIP	Carbonyl Iron Particle
CV	Coeffecient of Variation
DRMRF	Dual Rotation Magnetorheological Finishing
EIP	Electrolytic Iron Particle
FEA	Finite Element Analysis
FMAB	Flexible Magnetic Abrasive Brush
I-CNT	Iron Carbonyl Nano-Tubes
MR	Magnetorheological
MRF	Magnetorheological Finishing
MRP	Magnetorheological Polishing
MRAFF	Magnetorheological Abrasive Flow Finishing
SEM	Scan Electron Microscopy
S-FMAB	Static Flexible Magnetic Abrasive Brush
SiC	Silicon Carbide
VHN	Vicker Hardness Number

NOMENCLATURE

D_s	Diameter of wheel (mm)
a	Depth of cut (mm)
l_c	Length of contact (mm)
V_s	Velocity of wheel (m/min)
F_n	Normal force (N)
F_t	Tangential force (N)
F_a	Axial force (N)
R_n	Resisting normal force (N)
R_s	Resisting shear force (N)
d_μ	Diameter of particle (μm)
m	Mesh size of particle
V	Volume of MR polishing fluid (mm^3)
$Ø_{IP}$	Volume fraction of iron particles in MR polishing fluid
N_{IPC}	Number of iron particles in a chain
B	magnetic flux density (T)
μ_o	Magnetic permeability of free space (m kg s^{-2} A^{-2})
H	Magnetic strength at a point (A/m)
M	Magnetization of a particle (A m^2/kg)
H_{xij}	Magnetic strength along x-axis (A/m)
H_{yij}	Magnetic strength along y-axis (A/m)
H_{zij}	Magnetic strength along z-axis (A/m)
I	Current through electromagnetic coil (A)
a_j	Radius of coil varying in y direction (mm)
z_i	Varying distance from measuring point along z-axis (mm)
x	Distance form measuring point along x-axis (mm)
y	Distance from measuring point along y-axis (mm)
d_g	Gauge diameter of wire (mm)
F_m	Normal magnetic force (N)
m_{ip}	Mass of iron particle (kg)
χ_m	Mass of magnetic susceptibility (m^3/kg)

F_{ind}	Indenting force on abrasive particles (N)
H_{BHN}	Brinell hardness number (kgf/mm^2)
D_{abr}	Diameter of abrasive particle (μm)
D_i	Indenting diameter (m)
t	Depth of indentation (m)
A	Area of groove generated by abrasive (m^2)
V_a	Volume removed by abrasive particle (m^3)
L_a	Actual contact length of abrasive (m)
A'	Area of circular tool tip (mm^2)
N_s	Number of active abrasives
V^i	Material removal in ith stroke (mm^3)
R_w	Radius of cylindrical workpiece (mm)
h	Total height of material removed (μm)
Ra^i	Surface roughness in ith stroke (nm)
Ra^{i-1}	Surface roughness in (i-1)th stroke (nm)
β	Helix angle (degree)
p	Pitch of helix (mm)
D	Diameter of workpiece (mm)
F	Feed of tool (cm/min)
T'	Time taken to complete path in one rotation along helix (s)
R	Rotational speed of workpiece (rpm)
N_h	Number of active abrasive due to helix effect
T	Tool rotation (rpm)
A_1	Finished surface area of specimen (mm^2)
A_2	Surface area of extrusion punch (mm^2)

CHAPTER 1

INTRODUCTION

1.1 INTRODUCTION

Finishing operation is the final stage of any part manufactured by either casting, forging, forming or machining. Finishing operation increase the cost upto 10 to 15 percent of production cost [1]. Finishing operation is also a value added operation which results in increase of cost as well as lead time. Due to this reason, there is need of better finishing process to reduce time and cost. Finishing operation had become a very important process of many manufacturing system because of the functional requirement of part, safety and aesthetics made it important to enhance surface qualities before using it in sub-assembly [1]. The problems related to friction such as wear resistance and power loss are greatly influenced by surface roughness [2]. Finishing processes not only need to overcome these problems but also be able to achieve accuracy as well as minimum surface defects [1]. The surface qualities enhancing methods can be classified in to following sections [1].

- Surface roughness reduction
- Bulk properties improvement techniques (heat treatment)
- Resistant to corrosion (galvanizing)

Surface finish enhancing methods can be classified into two categories namely traditional and advanced finishing processes .

1.2 TRADITIONAL FINISHING PROCESSES

1.2.1 Honing

Honing is used to finish the internal as well as outer cylindrical surface. It can be used for both metallic as well as non metallic workpieces [1]. It is used to remove the errors associated with the preceding machining operations such as out of roundness and [1]. Honing is done by using the honing tool (or stick) which consists of Al_2O_3 or SiC abrasives bonded by resin as shown in Figure 1.1. The lay pattern obtained on the workpiece is generally cross-hatched due to synchronic rotational as well as translational motion of tool. The cross-hatched pattern provides good lubricating on retaining surface [3]. Surface finish that can be attained by this process is in range of 50 nm to 100 nm [1]. The tolerance that can be achieved by this process is $\pm$ 2 μm [1].

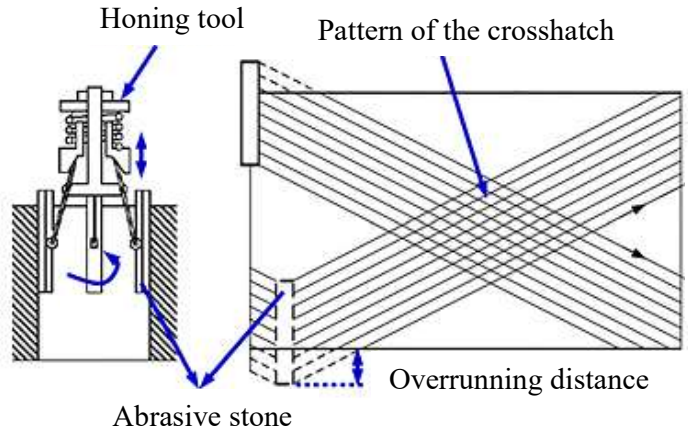

Figure 1.1 Mechanism of material removal in honing [4]

1.2.2 Grinding

The abrasive particles bonded on grinding wheel removes the material in form of micro-chips as shown in Figure 1.2. In Figure 1.2, depth of cut (a), diameter of wheel (D_s), Velocity of wheel (V_s) and length of contact (L_c) is shown. In this process a thin layer of workpiece is removed which is as low as 1 µm [5]. During grinding operation the abrasive particles get blunt, chips removed get trapped between the abrasive particles. Grinding wheel needed to be glazed, which remove the fractured abrasives. To maintain the circularity of the wheel, the truing is done. The main drawback of grinding is high heat generation. High heat generation results in thermal cracks, residual stresses etc. [1].

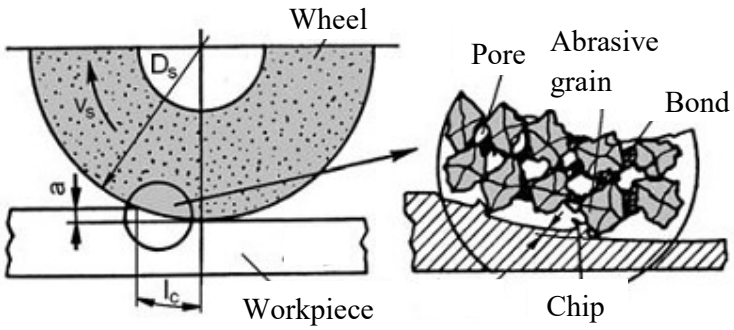

Figure 1.2 Mechanism of material removal in grinding [6]

1.2.3 Lapping

Lapping is done to improve the surface finish obtained after grinding as well as honing [5]. Lapping is done to achieve the close fit tolerance, better accuracy, remove minor imperfection in shape [5]. Lapping is done by placing the loose abrasives between the lap and workpiece as shown in Figure 1.3.

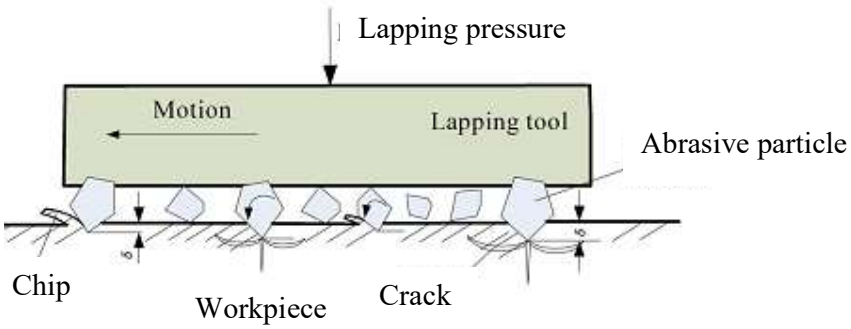

Figure 1.3 Mechanism of material removal in lapping[7]

All the traditional surface quality improvement processes discussed above have a major limitation of shape and size of the workpiece that can be finished. Honing is suitable for cylindrical parts. For cylindrical as well as flat surfaces lapping is used. Defects such as cracks, thermal stresses are produced in grinding operation due to generation of excessive heat. In all these processes controlling of in-process forces is not possible which leads to non-controllable surface finish.

1.3 ADVANCED FINISHING PROCESSES

The development in materials results in high strength, high temperature resistant materials which make it difficult to machined by traditional methods. To use these materials and machining to desire shape and size, the non traditional processes have to be used [1]. High precision machinability is needed in the manufacturing world, which can be achieved by the advanced finishing methods [3]. The limitations of traditional finishing methods has been overcome by advanced finishing methods. In traditional finishing processes, the limitation of shape and size has been overcome by use of loose abrasive which can enter in to any complex cavities. The use of smart fluids results in the in-process control of forces acting during finishing operation. Rheological properties of smart fluid changes under the influence of magnetic field.

1.3.1 Abrasive Flow Machining (AFM)

This process was identified as early as 1960. This process is suitable for deburring, polishing of cylindrical components [1]. In this process a visco-elastic medium is used to remove the material from the cylindrical cavity by moving to and fro by two vertically opposed extruded cylinder as shown in Figure 1.4. The finishing performance can be accelerated by improving the rheological properties of visco-elastic medium [9]. The viscosity of the visco-elastic medium play a vital role in finishing operation [10]. Figure 1.4 shows the forces F_n (normal force) and F_t (tangential force) acting during AFM. The indentation on the workpiece surface

is due to normal force (radially). Material is removed in form of micro chips by tangential force (axially)

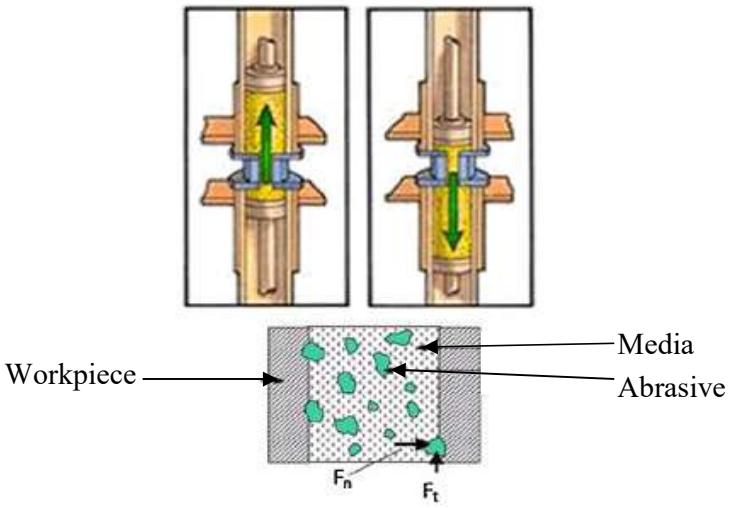

Figure 1.4 Mechanism of abrasive flow machining (AFM)[8]

1.3.2 Magnetorheological Finishing (MRF)

The finishing of precision lenses is very difficult because they are made of brittle material. Initially manufacture of a lens's involved two operations grinding and finishing. The profile required for lens was obtained by grinding [5]. The cracks and surface defects after grinding was removed by finishing operation [5]. Grinding and finishing are non-controllable processes and high local pressure generates during operation which results in sub surface damage.

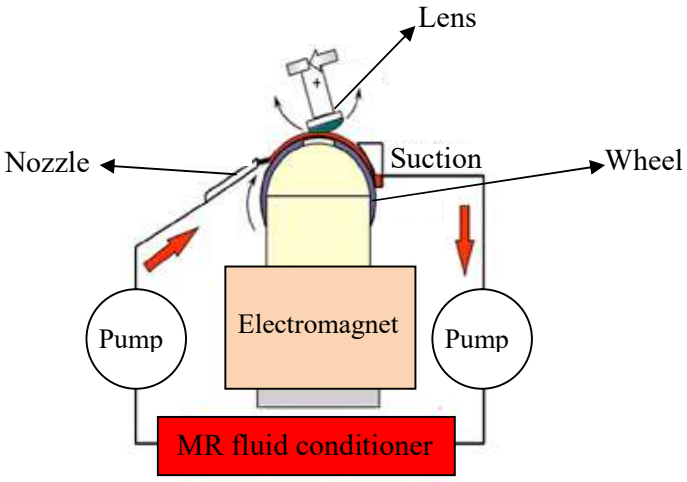

Figure 1.5 Schematic of MRF [8]

To overcome this problem magnetorheological finishing (MRF) process was developed in 1996 at centre of optics manufacturing at Rochester [11]. This process uses the magnetorheological fluid which is known as smart fluid. The Smart fluid is a colloidal

suspension of iron particles and abrasive particles. Smart fluid under the influence of magnetic field changes its properties. The MR polishing fluid ribbon is created between the workpiece and the wheel as shown in Figure 1.5. Under the influence of magnetic field, properties of ribbon changes which results in finishing of workpiece.

1.3.3 Magnetorheological Abrasive Flow Finishing (MRAFF)

The limitation of controlling of forces in AFM has been overcome in this process by use of magnetorheological (MR) polishing fluid. This process uses MR polishing fluid, which under the influence of magnetic field changes its rheological properties and is controlled by use of magnetic field. This process can finish complex external as well as internal geometries up to nano-level surface finish. Figure 1.6 shows the working mechanism of this process.

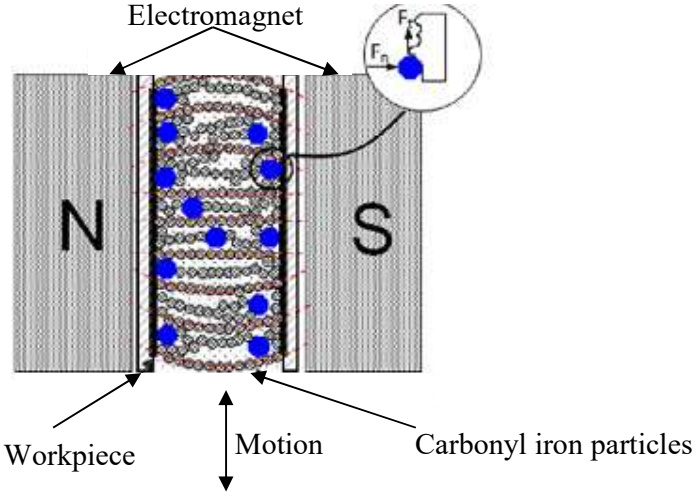

Figure 1.6 Mechanism of MRAFF[8]

1.3.4 Chemo-Mechanical Polishing (CMP)

This process was developed for semiconductor manufacturing industries. It is a planarization process in which the material is removed by chemical as well as mechanical action [12]. In this process finishing take place in two steps. Firstly, reaction take place between workpiece and fluid. Secondly reaction products is abraded by mechanical action [13]. In this process, layer of silica slurry resting on the rotating polishing pad is pressed by semiconductor wafer. The mechanism for this process is shown in Figure 1.7. This process overcame many problems such as pitting, scratching etc. and results in smooth surface [14].

1.3.5 Elastic Emission Machining (EEM)

EEM was developed as early as 1976 [15]. The material is removed at atomic level by mechanical method to give mirror like surface finish. Figure 1.8 shows the mechanism of EEM. The abrasive particles strike the atom or group of atoms on surface of workpiece and remove it .Material is removed at nano-level, so the finish is also obtained in the nano-meter

range of 0.2 nm to 0.4 nm [1]. Size and type of abrasive particles effect the efficiency of material removal in this process.

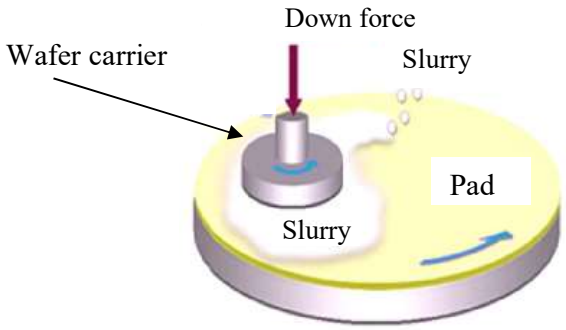

Figure 1.7 Mechanism of chemo-mechanical polishing[8]

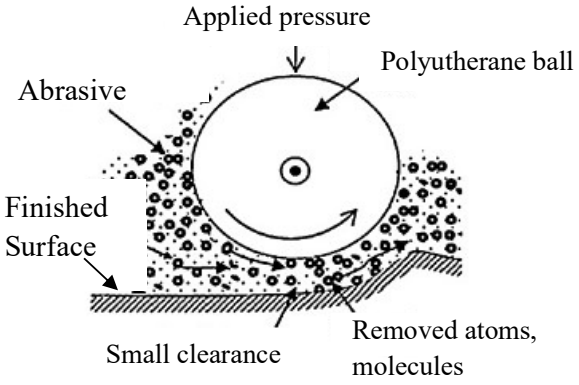

Figure 1.8 Mechanism of elastic emission machining[8]

In the present research work, an industrial application was searched for the nano-surface finishing requirement. Tube extrusion process was found in GNA Axles Ltd. in Hoshiarpur, Punjab, India. In that process, the surface finish improvement was needed on punch as well as container mold for their improvement in functional life. Because at present the industry uses surface finish by grinding up to 0.48 µm. In tube extrusion process losses due to friction occur during punch - billet - container interaction. After going through literature survey, It was found that friction plays the vital role in losses during extrusion process. So the main objective of this research was decided to improve the functional performance of the process by enhancing the surface quality. The mechanism of tube extrusion is shown in Figures 1.9 (a) and (b) respectively. Tube extrusion is performed in three stages on the vertical press. The hot billet is heated to temperature of 1250^0 C and placed in mold container. In stage 1, an impression is made at the top of billet surface. The punch is pierced through the hot billet to some length in stage 2. During piercing, the punch surface area is in contact with the billet

pierced surface. To reduce the frictional effect on the punch, glass lubricant is applied on the punch surface at each stage. In the stage 3, punch pierced completely through billet. Billet is in contact with punch as well as container in stage 3, friction losses also occur in that region . The spindle is produced from this process as shown in Figure 1.9 (c).

The two main factors was found which arises due to friction.

- Power loss to overcome friction
- wearing of die due to friction between die and billet

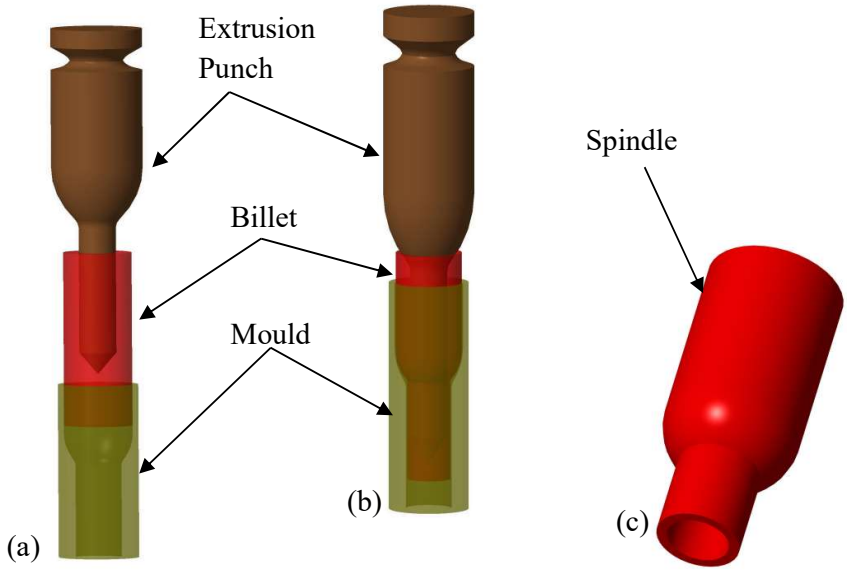

Figure 1.9 Tube extrusion process (a) stage 2 of tube extrusion, (b) stage 3 of tube extrusion and (c) end product from tube extrusion (spindle)

In the industry, die surface is finished by grinding. The surface roughness achieved at the working area of die was about 0.48 µm. In the present research, the surface roughness of the die was reduced to nano-level surface finish (µm) by the use of magnetic field assisted finishing process. After surface finishing the die, it was tested at the industry to find out the improvement of their functional life in the extrusion process.

1.4 MAGNETORHEOLOGICAL POLISHING FLUID

Magnetorheological (MR) polishing fluid is a smart fluid. MR polishing fluid is the suspension of magnetic iron particles and non-magnetic abrasive particles in carrier medium such as oil, mineral oil, etc. MR polishing fluid act as Newtonian fluid in the absence of magnetic field. Under the effect of magnetic field, MR polishing fluid act as non-Newtonian fluid [8] shown in Figure 1.10. For non-Newtonian behaviour Herschel-bulkley model was considered [16]

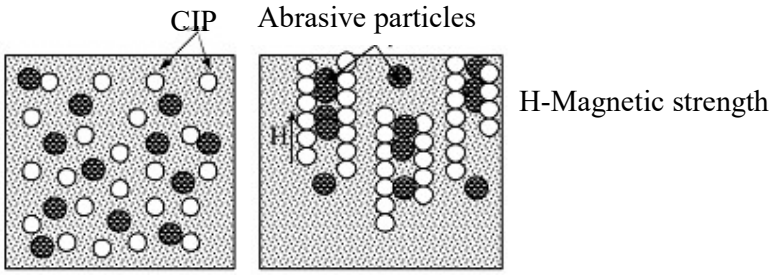

Figure 1.10 Effect of magnetic field on magnetorheological polishing fluid [1]

Dipoles are created under the influence of external magnetic field. Figure 1.11 shows that the dipoles attracting each other to form chains of magnetic iron particles. Response time of MR fluid is very small in milliseconds [16]. Magnetic lines of forces moves from region of higher flux gradient to region of lower flux gradient. The magnetic iron particles move toward region of higher magnetic flux and non-magnetic abrasive move toward region of lower magnetic flux [8].

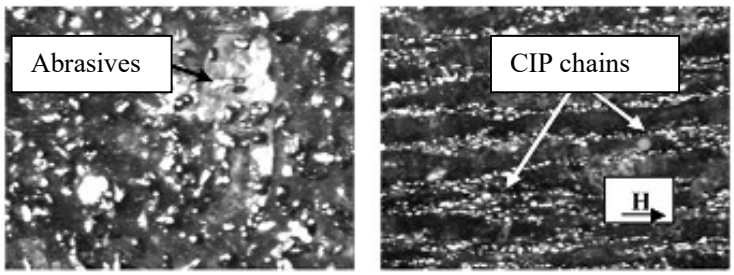

Figure 1.11 Chain formation in MR polishing fluid [1]

1.5 ESSENTIAL FEATURES OF MAGNETORHEOLOGICAL (MR) POLISHING FLUID

- The concentration of magnetic and abrasive particles must be at optimum level
- In the absence of magnetic field, MR fluid should have low viscosity
- Under the effect of magnetic field MR polishing fluid must have high yield strength
- Resistance to corrosion
- MR fluid should have good re-dispersibility
- The lumps of particles in MR fluid should be less

1.6 COMPONENTS OF MAGNETORHEOLOGICAL (MR) POLISHING FLUID

MR polishing fluid plays the major role in finishing process based on magnetic field. MR polishing fluid is the suspension of micron sized abrasive and iron particles in carrier medium with additives [1]. Rheological behaviour of MR polishing fluid is influenced by magnetic field [16]. The rheological properties of MR polishing fluid includes viscosity and shear

strength. Rheological behaviour of MR polishing fluid changes with change in temperature and chemical composition of MR polishing fluid.

The main components of MR polishing fluid are :

- Abrasive particles
- Magnetic particles
- Carrier medium
- Stabilizer / Additive

1.6.1 Abrasive Particles

The roughness peaks on workpiece surface is removed by the abrasive particles trapped in the iron particle chains. Removal of material depends on the properties of abrasive particles used for finishing. The most important characteristics of abrasive particle affecting wear rate are size, hardness and geometry [17].

Commonly used abrasive particles are :

- Silicon Carbide (SiC)
- Carbon boron nitride (CBN)
- Alumina (Al_2O_3)
- Hematite
- Quartz

The hardness and fracture toughness of these abrasives is shown in Figure 1.12.

1.6.2 Magnetic Particles

The magnetic particles are the main component of the MR polishing fluid. These particles forms the chain in the working gap under the effect of magnetic field. In these chains, the abrasive particles get trapped and perform the finishing operation. The rheological properties of the MR polishing fluid plays a very vital role in finishing. Magnetic particles must have high magnetic saturation and low coercivity for good rheological properties of MR polishing fluid. Dipoles are formed in the working gap on applying magnetic field. Dipole attracts each other and form the chain structure. Commonly used magnetic particles are :

- Carbonyl iron particles (CIP)
- Electrolytic iron powder (EIP)

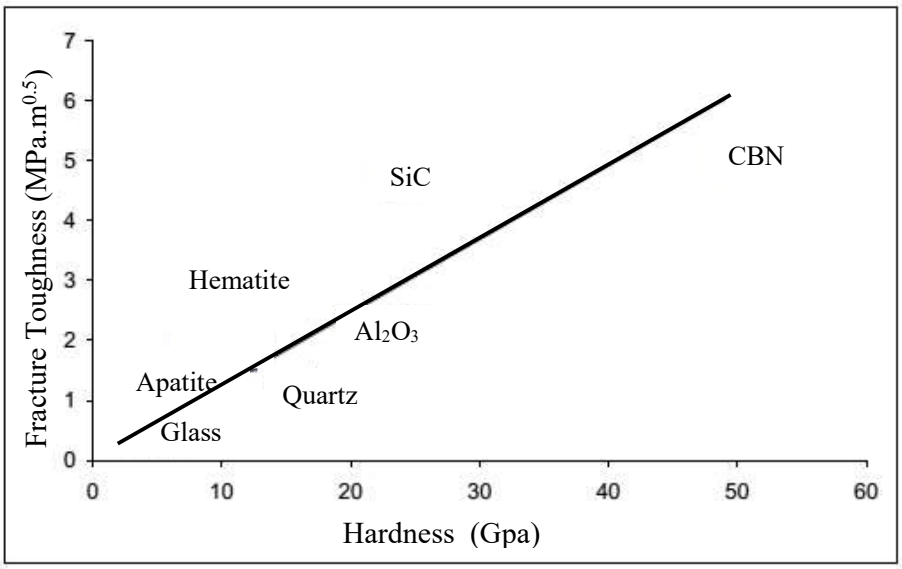

Figure 1.12 Fracture toughness at varying hardness for different abrasives [17]

1.6.3 Carrier Medium

The suspension of abrasives and magnetic particles take place in carrier medium. The desirable properties of carrier medium are low freezing point, high boiling point and resist corrosion. Carrier medium are generally oil based or water based [16]. Oil based carrier medium has high viscosity which results in good performance in against the sedimentation[16] .

1.6.4 Stabilizer / Additives

For the proper dispersion of abrasive particles and magnetic particles in MR polishing fluid, the stabilizers are added. Grease or other thixotropic additives are added to MR polishing fluid to improve stability in aqueous based MR polishing fluid. Some additives are necessary to be added to prevent oxidation of suspended magnetic particles. Stabilizer such as glycerol are added to improve suspension of particles in MR polishing fluid [16].

1.7 MAGNETORHEOLOGICAL (MR) FLUID BASED FINISHING PROCESSES

MR fluid based finishing processes are demanding nowadays. MR fluid based finishing processes can finish different shapes and size of components. In these processes controlling of forces acting during finishing can also be controlled by controlling magnetic field [1]. The processes related to finishing of cylindrical workpieces are ball end magnetorheological finishing (BEMRF), MR finishing process for external cylindrical workpiece and cylindrical workpiece magnetic abrasive finishing assisted by vibration.

1.7.1 Ball End Magnetorheological Finishing (BEMRF)

The MRF can finish only specific shapes of surface such as concave, convex etc. This limitation was overcome in the BEMRF. In BEMRF [18], the ball end tool tip was used, which can finish flat as well as curvature surface. In the working gap magnetic field is applied across tool tip.

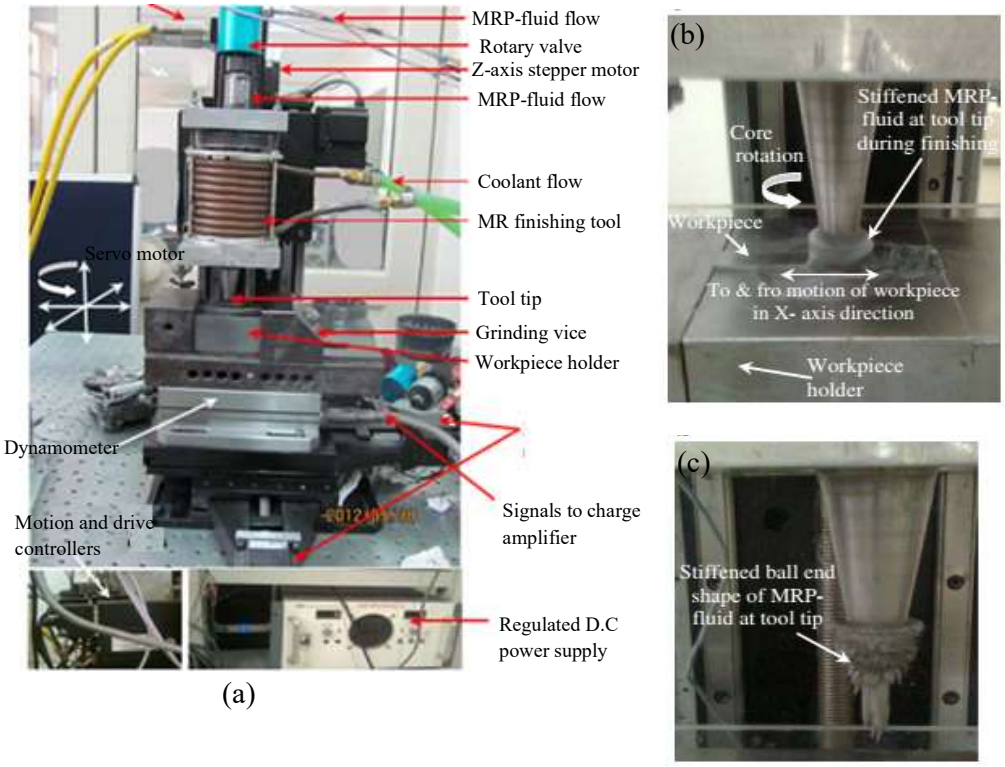

Figure 1.13 Ball end magnetorheological (MR) finishing (a) experimental setup, (b) stiffened MR polishing fluid during machining, (c) stiffened ball end at tool tip [18]

Magnetorheological polishing (MRP) fluid is induced through electromagnetic coil on the tool tip which take the form of ball brush. The relative motion between the ball end brush and workpiece is responsible for finishing. This process can finish the surface of ferromagnetic as and non ferromagnetic material. Figure 1.13 (a) shows the experimental set-up developed for this process. Figures 1.13 (a) and (b) represent the brush formed during activation of magnetic field across tool tip.

1.7.2 Magnetorheological (MR) External Cylindrical Finishing Process

This process can finish external cylindrical surface made of ferromagnetic as well as non ferromagnetic materials [19]. In this process the cylindrical workpiece is rotated against the MRF tool. Generally for finishing of cylindrical components, traditional finishing processes

are used in industries. Defects are associated by use of traditional finishing processes such as cracks, scratches and residual stresses [1]. MRF process can make its way in automobile, aerospace and machine tool industries. This process overcome the problems of in process controlling of forces which give rise to surface defects associated with traditional finishing processes [1]. The MRF experimental setup designed for finishing of cylindrical workpiece can be seen in the Figure 1.14 (a). In the working gap, MR polishing fluid is applied as shown in Figure 1.14 (b). The performance of this process was also checked for flat tool tip and curved tool tip [20]. The Surface roughness value was reduced by 54.41 % for flat tool tip and 80.88% for curved tool tip [20].

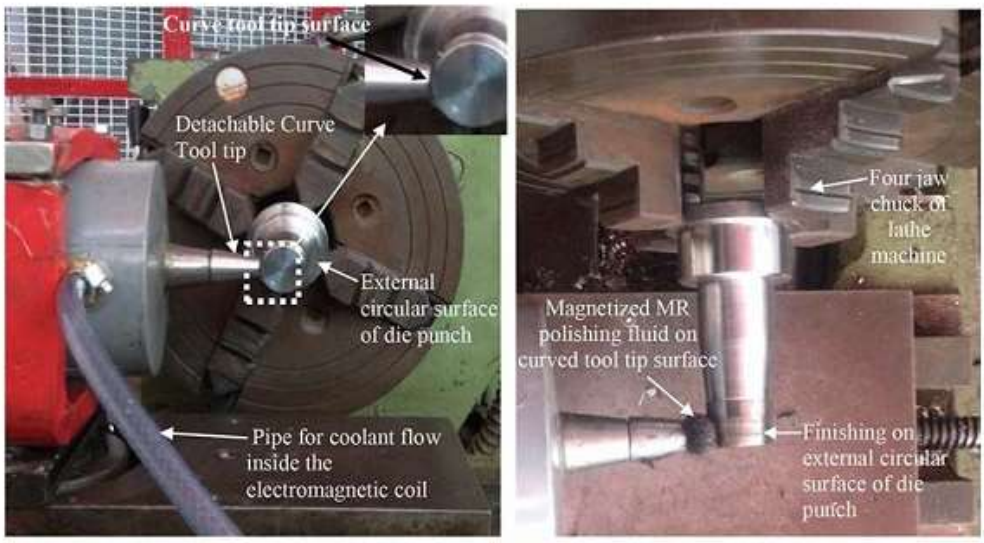

(a) (b)

Figure 1.14 Magnetorheological finishing (a) Experimental setup for external cylindrical surface finishing and (b) Magnetized MR polishing fluid [19]

1.7.3 Vibration Assisted Cylindrical Magnetorheological (MR) Finishing

Development in the field of material science results in new material. Traditional finishing methods faces difficulty while finishing these materials. This process is developed to finish the cylindrical workpiece of high hardness. The cylindrical workpiece is placed between the two electromagnetic poles in this process [21]. The electromagnetic poles are excited by supplying the current through the coil of electromagnet. In the working gap between the tool and workpiece, magnetic flux gradient is created. MR polishing fluid is supplied in the working gap which take the form of the brush to perform the finishing operation. The setup developed for this process is shown in Figure 1.15.

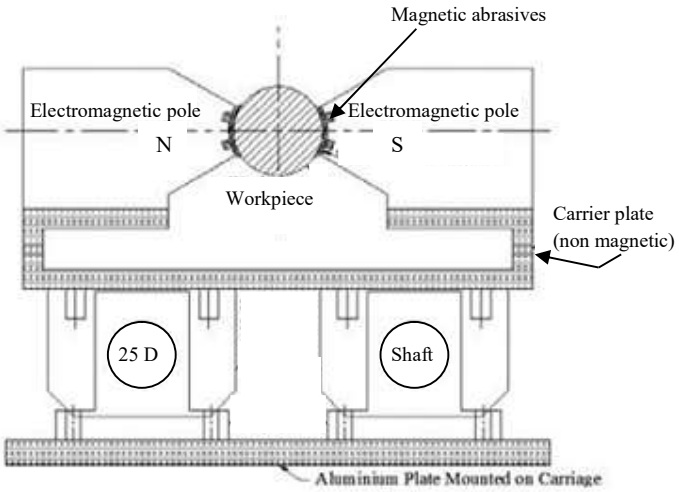

Figure 1.15 Experimental setup for vibration assisted cylindrical finishing process [21]

1.8 ADVANVANTAGES OF MAGNETORHEOLOGICAL (MR) POLISHING FLUID BASED PROCESSES

- Capable to finish the workpiece up to nano-level
- Can finish complex shapes and geometry
- Forces acting during finishing is controlled by controlling the magnetic field
- Reduces sub-surface defects (scratch, micro cracks)

1.9 NEED OF NANO-FINISHING

Finishing of engineering components is necessary to improve

- Reduction in wear due to friction
- Resistance from oxidation and corrosion
- Loss of power due to friction
- Aesthetic appearance
- optical properties

CHAPTER 2
LITERATURE REVIEW

In this chapter, the literature review related to the proposed research work is reported. After going through the literature review , gaps were analyzed which are also discussed. Objectives of the project were decided based on literature review and industrial application.

2.1 LITERATURE REVIEW

Jung *et* al. [22] used sintered iron-carbonyl nano-tubes (I-CNT) compound abrasives for magnetorheological (MR) finishing of hard and brittle materials. An experiment was performed on wheel type MR finishing setup using Al_2O_3 - TiC hard disk slider as a workpiece material. While performing the experiment with diamond abrasive it was found that with increase in RPM, material removal rate increases upto some extent and start decreasing afterwards. The main reason behind this was the domination of centrifugal force on carbonyl iron particles (CIP) chains which results in deformation of chain. In case of increase in gap, MRR reduces with increase of working gap and MRR increases with reduction in working gap. The main reason behind this variation is that magnetic flux density has inverse relation with working gap. The problem was solved by using I-CNT abrasives, these abrasives have high cohesive strength and are ferromagnetic in nature. These abrasives chains does not get deform easily under the effect of magnetic field. This results in increase in MRR even at high RPM as well as reduction in tool aging effect i.e. constant MRR attained for longer period.

Song *et* al. [23] investigated on finishing performance with magnetorheological (MR) polishing fluid under magnetic field. In this study an experiment was performed on a pin-on-disk apparatus for material removal and surface roughness. The material used as a workpiece was steel(SM45C), brass, Aluminium(AL606I). It was found that steel samples achieves a better surface finish as compared to brass and aluminium i.e. surface roughness of material is inversely proportional to its hardness. The magnetic field has great impact on reduction of surface roughness and increase in MRR for steel samples. The material removal rate increases with load and rotational speed for steel samples. Surface finish decreases with increase of load and rotational speed for steel samples. Better surface finish can be achieved with high concentration of magnetic particles in MR polishing fluids.

Wang *et* al. [24] investigated on the magnetorheological (MR) finishing method for wire electric discharge machined (WEDM) pierced die cavity. In this study, the finishing of WEDM is performed as after wire electric discharge machining melted layer on machined

surface is produced containing micro cracks and residual stresses which results in reduction in mould life. Initially for finishing of WEDM pierced die cavity a permanent magnet was cut in the shape of cavity and used as tool for finishing of die cavity in MRF process. The main drawback of this method is that for different cavity different shapes of magnet to be needed. To overcome this problem, the core that is obtained after WEDM is used as tool for polishing of die cavity. In this study, the core was used as a tool for MR finishing of die cavity. A tool was designed using a core and permanent magnet was attached axially along a rod. The workpiece was submerged in the tub of MR polishing fluid in which the tool was made to reciprocate through cavity. After the experiment, it was found that flat surface roughness was reduced to 0.303 μm to 0.132 μm and surface roughness of corner with radius was reduced from 0.303 μm to 0.278 μm.

Wang *et* al. [25] improved surface texture by dual rotation magnetorheological finishing (DRMRF). In this study the problem of directional texture and groove angles in MRF is eliminated to improve the surface quality. An experiment was performed in which rotating wheel is used as a tool on which MR polishing fluid is supplied and it is attached to the wheel under the influence of magnetic field. A fresh MR polishing fluid is supplied at one end and collected at other end. It was found that in earlier developed MR finishing, the directional texture as well as concentrated groove angles are formed which reduces the surface quality. In order to overcome this problem a dual rotation MRF was developed in which along the wheel rotation, a rotation is provided along radial direction. After performing the experiment with DRMRF directional texture as well as concentrated groove angles was eliminated. Even the surface finish was improved using the dual rotation magnetorheological finishing.

Singh *et* al. [26] investigated on the flexible magnetic abrasive brush (FMAB). Static flexible magnetic abrasive brush (S-FMAB) has limitation of non uniform strength. The reason for non-uniform strength is non homogenous mixing of abrasive and iron particles. In S-FMAB the current supplied is DC to electromagnet, the chain is of carbonyl iron particles (CIP) and abrasives is formed to perform the operation. At some places, the workpiece has high peaks and at some places have low peaks, the only reason behind this is inhomogeneous mixing of abrasives as well as CIPs and the abrasives have been worn out and needed to be refreshed. Limitation of S-FMAB was overcome by supplying the pulsating current to electromagnet. This pulsating current allow the mixing of CIPs and abrasives in regular interval which improves the roughness obtained as compared to S-FMAB.

Jayswal *et* al. [27] studied the effect of slot in magnet on induced normal magnetic force. It was found that machining pressure is maximum on abrasive particles for slotted pole surface

rather than magnet with no slots. It was also found that region under the slot have negative force acting on abrasive particles which signifies zero penetration depth in workpiece.

Sidpara *et* al. [16] investigated the rheological behaviour of magnetorheological polishing (MRP) fluid. The experiment was performed on a machine setup MCR 301 rheometer in which the abrasives are placed on a sandblasted measuring plate on which a sand blasted tool master is pressed and rotated. Magnetic field is also applied by electric coils fixed in fixtures in such a way that the magnetic lines of forces is perpendicular to base of machine on which abrasive is placed. In the experiment, the effect of temperature, composition of MR fluid and magnetic field on the yield strength and viscosity of MR fluid was observed. As the temperature increases shear thinning take place which results in decrease in yield stress. In this experiment, the composition of MR polishing fluid consists of abrasives, carbonyl iron particles (CIPs) and water . It has been found that as the concentration of CIPs increases, it results in increase in yield strength and viscosity of MR polishing fluid. With increase in concentration of abrasives, viscosity decreases whereas yield stress decreases, if CIPs concentration is below 35% or else increases. If the concentration of water increases it result in decrease in yield stress as well as viscosity. Lastly increase in magnetic field results in increase in viscosity and yield stress.

Singh *et* al. [28] investigated on the material removal mechanism in ball end magnetorheological finishing process(BEMRF). In this study, an experiment was performed on a ferromagnetic workpiece. There are two types of wear mechanism investigated in this research based on strength of magnetic field namely three - body wear mechanism and two - body wear mechanism. In two-body wear mechanism, the strength of magnetic field is sufficient to hold the MR fluid column. The abrasive particles in MR polishing fluid are held tightly and remove material. Whereas in three body mechanism, the strength of magnetic field is not sufficient to hold the MR polishing fluid firmly. Due to which abrasives particles act as different body from MR polishing fluid column and starts rolling during finishing. If the strength of the magnetic field is more two - body wear mechanism will take place else three - body wear mechanism. The main reason behind the change in mechanism is the strength of magnetic field holding the CIPs as chain structure in which abrasives are trapped. After investigating about mechanism, its effect on surface roughness and surface quality was studied. It was found that when magnet field induced, normal force increases surface roughness decreases and when normal force decreases surface roughness increases.

Sidpara and Jain [29] investigated on forces on the freeform surface in magnetorheological fluid based finishing process. In this study, an experiment was performed to measure the

effect of various parameters such as angle of curvature of workpiece, rotational speed of tool and feed rate on forces acting during this process. The effect of these parameters were studied on three components of forces namely normal, tangential and axial force. The experiment was performed on a CNC milling machine and a permanent magnet was used to create the magnetic field. The replica of knee joint made of stainless steel is the workpiece used in this experimentation. On increasing the angle of curvature of the workpiece, the forces acting on workpiece decreased. On increasing the rotational speed of the tool, forces increased up to some extent and start decreases afterward. On increasing the feed rate same pattern is observed as in case of rotational speed of tool. The magnitude of forces first increases and start decreasing after optimum value.

Maan *et* al. [30] performed the nano finishing using magnetorheological fluid based finishing process on permanent mould punch. In this study, an experiment was performed on two setups. One setup was used for finishing of cylindrical surface and second one was used for finishing of bottom surface of cylindrical workpiece. The workpiece material was P20 tool steel which is ferromagnetic in nature and having hardness of 45HRC. After the experiment, it was found that average surface roughness value of flat surface of permanent mould die punch was reduced to 30 nm from 1080 nm in 120 minutes. The average roughness value of external cylindrical surface was reduced to 80 nm from 630 nm in 120 minutes. Metallurgical microscopic study and mirror images demonstrated significant enhancement in surface quality of finished surface of permanent die punch as compared to its initial surfaces.

Bedi and Singh [31] finished the ferromagnetic blind hole type surface using magnetorheological finishing processs. In this study the experiment was performed in which the workpiece was held in the vice where as tool was mounted on a bracket which move on a slide. The translation motion along slide as well as rotational motion of tool was provided by servo motors. The workpiece used was blind hole type cavity of EN31. Two different tools were designed for finishing of this type of cavity. One tool was designed for finishing of cylindrical surface whereas second one was designed for finishing of bottom flat surface. After performing the experiment it was found that surface roughness of inner lateral as well as bottom surface was reduced by 67.7% and 69.5% respectively, in 90 minutes . SEM analysis was also performed and it was found that surface defects such as grooves, cavity, scratch, axial groove and ploughed material were reduced.

Bedi and Singh [32] finished ferromagnetic cylindrical honed surface using magnetorheological process. In this study, an experiment was performed on a honed ferromagnetic cylindrical surface. Initially the problem faced was that the magnets are placed

outside the cylinder and magnetic field was produced from outside as a result the magnetic flux density was higher at the circumference of the ferromagnetic cylinder than the MR polishing fluid. As a result, the MR polishing fluid start sticking to the workpiece surface and machining cannot be performed. Then a tool was designed to overcome this problem. Tool consists of mild steel core on which electromagnets are placed. That tool was made to move axially as well as rotate while machining of the workpiece and it was found that the magnetic flux density is now high at the tool surface rather than the workpiece surface. So now there is no sticking of the MR pollishing fluid on the workpiece surface and machining can be done easily. After the experiment has been performed it was further investigated for change in roughness, parallelity, roundness and straightness of cylindrical surface and it was found to be reduced to minimum level. The surface roughness was reduced by 77.4% after 90 minutes of finishing.

Ohmori *et* al. [33] developed centerless grinding process using electrolytic in-process dressing (EID) and truing. In this method, the dressing and truing of metal bonded grinding wheel is done during the centerless grinding operation as shown in Figure 2.1. The experimentation was performed for small cylindrical workpieces. The material used for experimentation was Si_3N_4, die steel and ZrO_2. The results obtained after experimentation shows a significant improvement in surface quality as compared to traditional grinding operation.

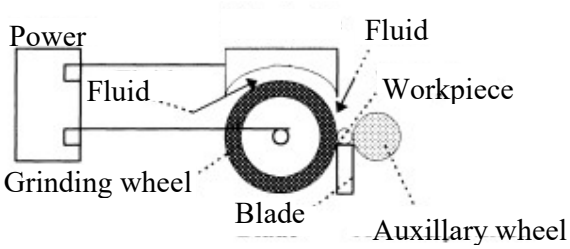

Figure 2.1 Schematic for the centerless grinding using EID[34]

Hochang and Pa [34] developed a new method of electro-polishing for round bars and tubes. Formed electrodes were used in this process. This process eliminates the use of expensive equipments or higher material removal rate as conventional electro-chemical machining. The round bars or tubes which are produced by manufacturing processes can be polished using disc form electrodes. Five different designs of electrodes were designed. Experimentation was performed using these electrodes on different die materials. Experimental setup was designed as shown in Figure 2.2. The experimental parameters were rotational speed of workpiece, electric current, electrode geometry pulse rate and electrode feed rate. It was

found that smoothest surface is obtained using pin - on - edge disc electrode because of the largest discharge space available as compared to other form electrodes.

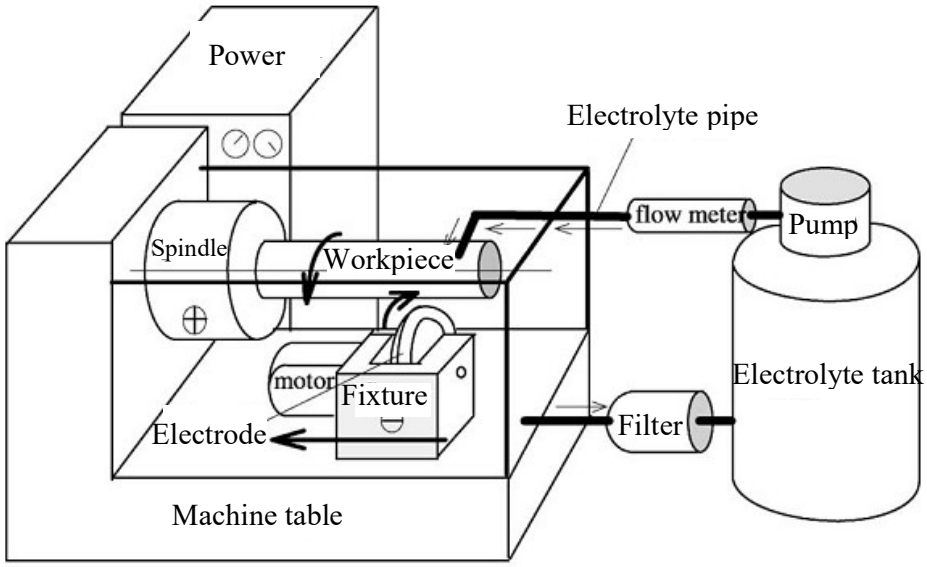

Figure 2.2 Schematic for electro-polishing process using disc-form electrodes[35]

Hassan *et* al. [35] investigated on the performance of brass cylindrical component using response surface methodology. In this process a ball burnishing tool was designed as shown in Figure 2.3. The balls used in the tool was chromium steel balls of 65 HRC. A cylindrical brass workpiece was used in this experiment. Experiment was performed on the colchester master 2500 lathe. The cylindrical workpiece was held in the chuck at one end and on the other end by revolving center on the lathe. The designed tool was held in the tool post on lathe while machining. Experimental parameters were number of passes of tools and force on ball of ball burnishing tool. It was found that surface roughness was reduced to 0.172 μm from 5.2 μm at force of 203 N in two passes.

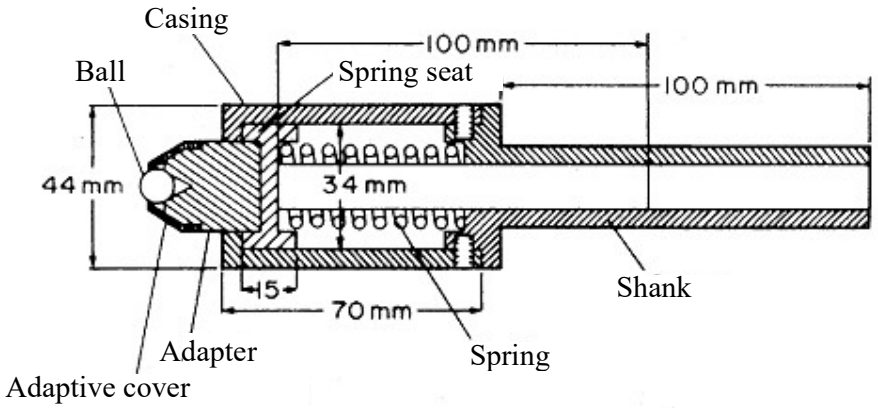

Figure 2.3 Design of ball burnishing tool[36]

Arif *et* al. [36] investigated on the defects in the hollow extrusion products. It was found that billet thermal gradient and billet - die - container friction effects the material flow during the process. Friction results in power loss during process as well as breaks the lubricant film between the billet and die. Broken lubricant get trapped at the dead metal zone and passes on to the extruded product. These lubricant traces in extruded product emerges as sub - surface defects. During the heat treatment of the product, blistering take place at these locations. Friction between the billet and die surface offers great resistance to the material flow during the process

Ebrahimi *et* al. [37] analyzed the tube extrusion process using upper bound approach. The power lost on frictional surface and discontinuous velocity surfaces was evaluated using velocity field. Optimization of total power was done with respect to die angle. Friction factor as well as reduction in area effects the optimum angle. The experimental and theoretical data was validated by load-displacement curve.

Gattmah *et* al. [38] investigated on the hot extrusion process of hollow tube by use of finite element method. FEM was done to see the effect of displacement of ram, reduction in area, semi die angle and friction coefficient on extrusion force and surface temperature. It was found that reduction in area and coefficient of friction have strong effect. Extrusion pressure increases for 0.35 coefficient of friction for 13 % and 25 % reduction area. Extrusion pressure shows no significant change for for 37 % and 48 % reduction in area for 0.2 coefficient of friction.

Alam and Jha [39] proposed the mathematical model for ball end magnetorheological finishing. In working gap magnetic flux density has been calculated by considering the magnetization of ferromagnetic workpiece. BCC unit cell structure for 19µm CIP's and 18 µm SiC particles was proposed. Normal indenting force as well as shear force model has been developed in this research. Indenting force has been calculated by using the brinell model of hardness. Roughness model was developed to measure the accuracy of the proposed model. Roughness was calculated theoretically and compared to the experimental data. The experiment was performed on flat surface mild steel workpiece. Experiment was performed for different current intensity for 10 minutes. The error in theoretical and experimental data ranges from 7 % to 32 %. This error occurred due to the assumptions made during modelling of process.

Jain *et* al. [40] done the mathematical model for material removal and surface roughness in abrasive flow machining. Material removal was calculated for AFM. Material removal was calculated geometrically as well as in the form of surface roughness. Number of active

abrasives were calculated to calculate the net material removal by active abrasives in single stroke. Surface roughness model was developed for single stroke of operation. Theoretical model was used to analyse the effect of various parameters on abrasive flow machining.

Jha and Jain [41] proposed the mathematical modelling for the magnetorheological abrasive flow machining. The principle for unit cell of MR polishing fluid particles was discussed in detail in this research. Unit cell structure for different size of abrasive particles and carbonyl iron particles (CIPs) was derived for MR finishing fluid. The number of active abrasive were calculated by studying a unit cell containing particles. The rate of finishing decreases with decrease of size of abrasive particles. As the size of abrasive particles decreases, indenting force as well as shear force decreases which results in decrease of finishing rate. The magnetization of the magnetic particles depend on the size of particles. Magnetic force model was developed for MRAFF. Magnetic flux was calculated to measure the normal indenting force. Normal indenting force was calculated using brinell hardness model. Roughness model was also developed to measure the accuracy of model. Surface roughness calculated theoretically for different abrasive and magnetic particles. . The error in the theoretical and experimental data ranges from -4 % to 133 % for 200 finishing cycles. This error is due to the assumptions made before modelling of surface roughness.

2.2 GAPS IN LITERATURE REVIEW

- Permanent magnet was used for producing the magnetic field in the polishing gap. The finishing performance can be improved by replacing permanent magnet by electromagnet. Use of electromagnet will results in increase of magnetic flux in gap by increasing current of electromagnet [24]. Even if the electromagnet is used pulsating current can be supplied so that MR polishing fluid mixing can take place which results in improvement in surface finish [26].
- Effect of composition of MR polishing fluid, temperature and magnetic field was observed on yield stress and viscosity of MR polishing fluid during operation. It was found that with increase in temperature water get evaporated which results in destruction of iron particles chains as a result yield stress as well as viscosity decreases .If the concentration of water increases, it also results in decrease of yield stress as well as viscosity[16]. Some other fluids which are having high cohesive strength can be used instead of water to improve the performance of process or some compound can be used to increase the cohesive strength of our carrier medium.
- Increase in concentration of iron particles results in increase in yielding strength [16].

- Surface defects obtained in hollow extrusion due to breaking down of lubricant layer at high ram speed and high friction. Breaking of lubrication film as well as resistance to material flow is due to friction between die and billet respectively [36].
- The extrusion pressure is greatly affected by coefficient of friction as well as percentage reduction in area of billet [38].

2.3 IMPORTANCE OF PROPOSED PROJECT IN CONTEXT TO CURRENT STATUS

From the literature review it was found that the traditional finishing processes are mostly used for finishing the punch surface. Even after using these traditional finishing processes, the finished surface gets many defects such as scratches, micro grooves and directional textures. Therefore, to improve the further surface quality the MR polishing fluid based finishing process is required. MR polishing fluid based finishing processes are capable to improve surface finishing at nano-level, therefore the MR finishing process can be more useful to improve surface characteristics of punch after the traditional finishing processes. In proposed research, the functional applications of punch would be investigated before and after using the improved MR-finishing process.

2.4 PROBLEM FORMULATION

- Heterogeneity in final product due to surface roughness [36]. Strain homogeneity is effected by friction between surfaces of billet. The strain in material do not take place uniformly results in change in mechanical properties of end product[36].
- Glass lubricant is used to reduce the friction between the die and billet to reduce the frictional effect [36]. The glass film breaks during the operation due to friction on surfaces and mix in to the extruded product. During the heat treatment of product, the trapped lubricant in the final product results in blistering.
- Power loss due to friction between the billet and die surface [37]. It was found that extrusion forces increases up to 0.35 coefficient of friction for 13% and 25% reduction of area [38].
- Reduction in tool life due to abrasion as well as thermal cracking [36]. The abrasion from the surface of the die and mould is due to mechanical wear. The factors which are responsible for mechanical wear are sliding velocity, surface finish, contact area etc.[36].

2.5 OBJECTIVES

- To finish the extrusion punch cylindrical surface using MR finishing process for improving its functional life.
- Design and fabricate the experimental fixture for finishing the tube extrusion punch surface.
- Study the mechanism of material removal for MR finishing of external cylindrical surface of extrusion punch.
- Parametric study for nano-finishing the extrusion punch material using response surface methodology for better process performance.
- Finish the industrial extrusion punch on the fabricated fixture and test the finished extrusion punch surface for its functional life during operation in industry.

CHAPTER 3

ANALYSIS OF MECHANISM OF MATERIAL REMOVAL DURING MAGNETORHEOLOGICAL SURFACE FINISHING OF EXTRUSION PUNCH

Magnetic fluid based finishing processes demand is increasing due to its ability in improvement on surface characteristics as compared to traditional finishing processes. Magnetic fluid based finishing processes are precision finishing processes. These processes are time consuming but producing better surface quality as compared to traditional finishing processes. In this chapter, the mechanism of material removal is analyzed through development of surface roughness model. This includes study the various parameters effecting the performance of the process. Variation on the performance of the process is discussed for different machining parameters. The efficiency of the process in term of surface roughness reduction and time can be improved by studying the effect of various parameters. The magnetorheological (MR) polishing fluid is the main component of any magnetic fluid based finishing process. The unit cell structure is derived for the composition of MR polishing fluid used. The unit cell structure was used to calculate the active abrasive particles and the magnetic iron particles in the working gap. For validation of the roughness model, the experiments were performed. Percentage error was calculated for the difference in theoretical and experimental data.

3.1 COMPOSITION OF MAGNETORHEOLOGICAL (MR) POLISHING FLUID

The finishing process of any magnetic fluid based finishing processes depends on MR polishing fluid. The finishing capability of this process is determined by rheological properties of MR polishing fluid. The MR polishing fluid was selected on the basis of literature review and is reported in Table 3.1.

Table 3.1 Composition of MR polishing fluid

Components	% Volume concentartion
Iron particles of 400 mesh size	30
Abrasive particles of 800 mesh size	15
Carrier medium (Parrafin oil and AP3 greese)	55

MR polishing fluid composition plays the vital role in deciding the rheological behaviour of the fluid. When the MR polishing fluid is applied in the region of magnetic flux density, dipoles are created. Chain structures of iron particles are formed by dipole interaction in the region of magnetic flux. The yield strength of the chain structure depends on the strength of magnetic field.

3.2 MAGNETIC FIELD BASED FINISHING PROCESS

The cylindrical workpiece surface is finished by the use of MR polishing fluid in this process. MR polishing fluid rheological behaviour is controlled by the magnetic field. The working gap of 0.6mm is created between the tool face and cylindrical workpiece surface. In the working gap, MR polishing fluid is supplied. MR polishing fluid under the effect of magnetic field take the form of brush. The workpiece is given the rotational motion. The tool is given the rotational as well as reciprocation motion. Material is removed due to relative motion between the tool and workpiece surfaces in the form of micro chips.

3.3 MECHANISM OF MATERIAL REMOVAL DURING EXTERNAL CYLINDRICAL FINISHING WITH MAGNETIC FIELD BASED FINISHING PROCESS

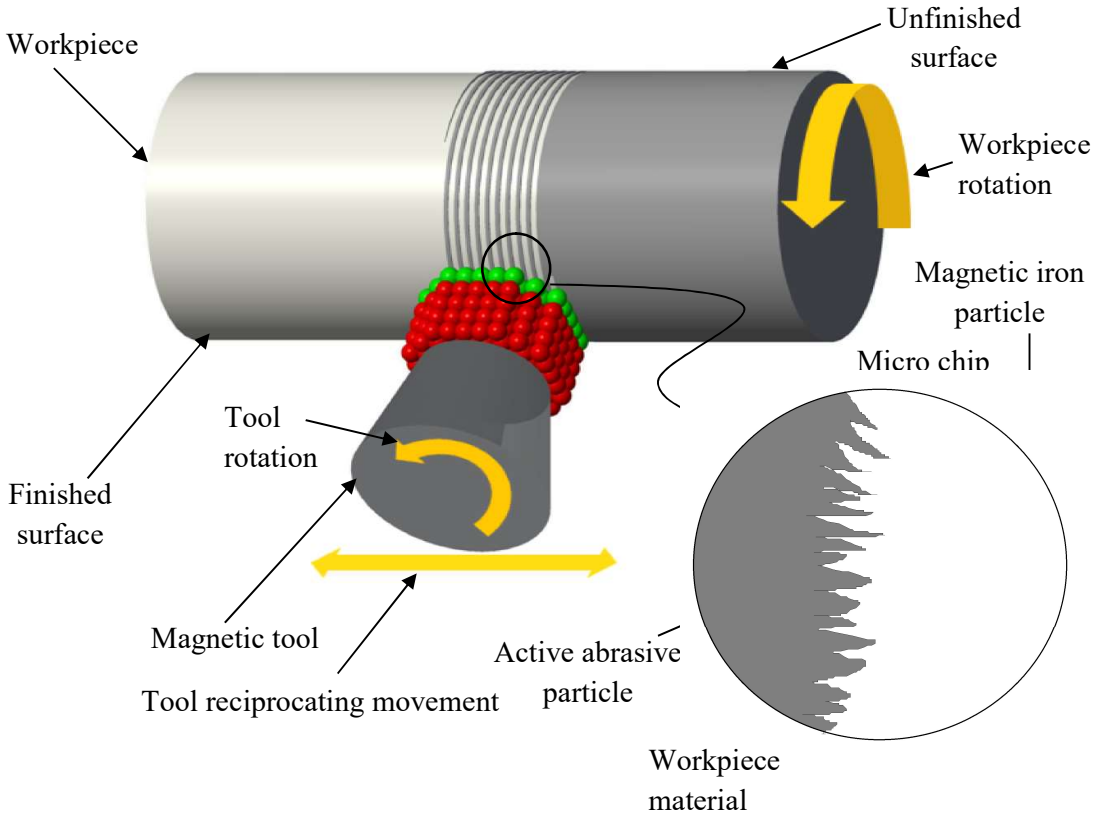

Figure 3.1 Mechanism of material removal and formation of helical path on cylindrical workpiece

The material was removed in the form of micro-chips by the interaction of abrasive particles and cylindrical workpiece surface. The forces acting on abrasive particles were studied to understand the mechanism of material removal. The mechanism of material removal is shown in Figure 3.1. It can be seen that material was removed along the helical path on the cylindrical workpiece. The helical path was created by combination of three motions namely rotation of cylindrical workpiece, rotation of magnetic tool, and translation of magnetic tool along axis of workpiece .

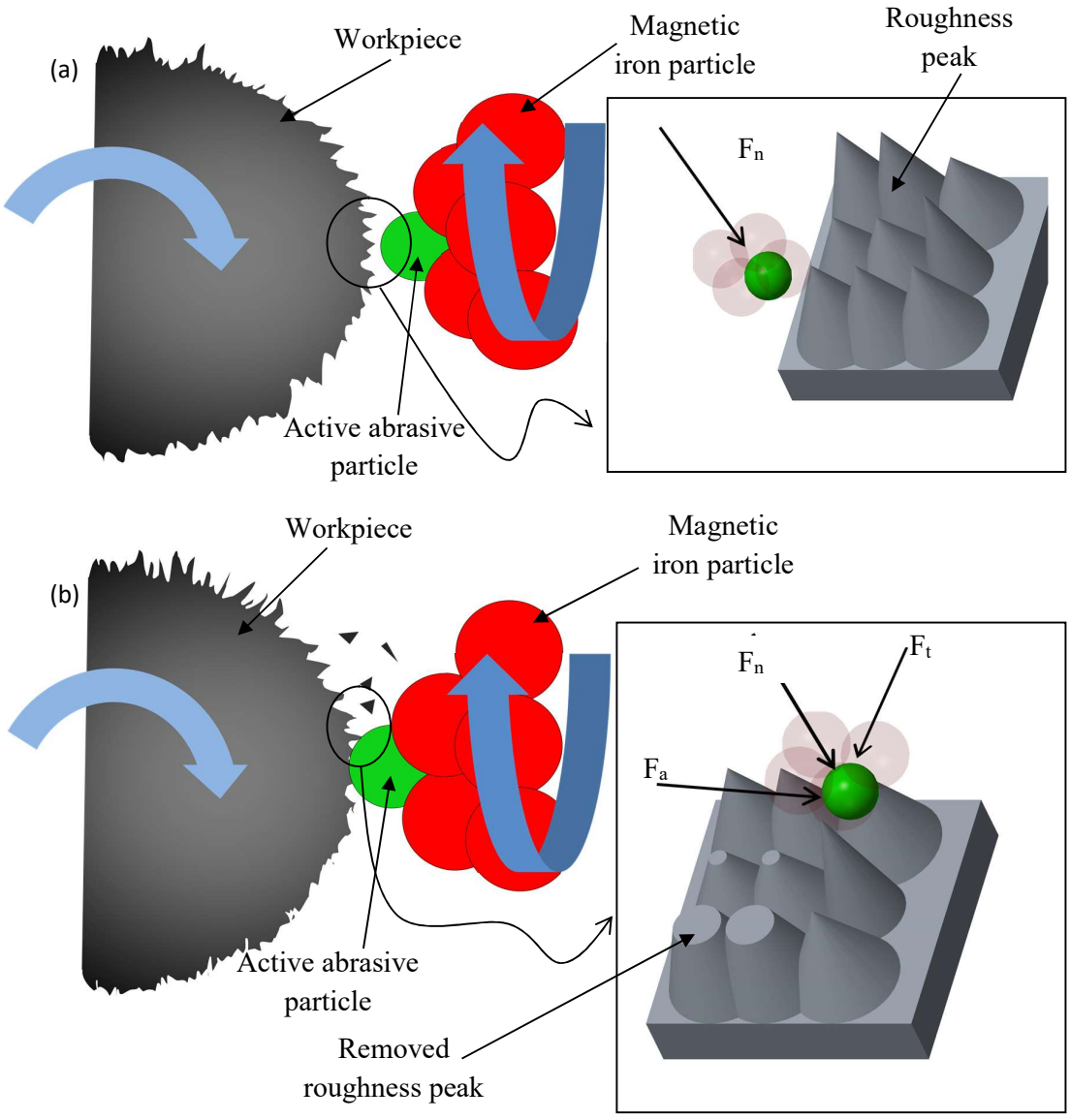

Figure 3.2 Mechanism of material removal (a) force acting on abrasive particles before collision of abrasive particle with roughness peak and (b) forces acting during collision of abrasive particle with roughness peak and shearing of peaks (side view)

The magnetic iron particles arranged themselves in the form of chain under the influence of magnetic field and move toward high magnetic field region whereas abrasive particles move toward region of lower magnetic field. Active abrasive are the particles which are responsible for material removal of workpiece surface [41]. The strength of magnetic flux density in working gap is responsible for gripping strength of iron particles chains which lock the abrasive particles [41].Greater the gripping of abrasives, better will be the finishing performance. Figure 3.2 (a) represent the condition before collision of abrasive particle and roughness peak on cylindrical surface. Only the magnetic force is acting on iron particles which are holding the abrasive. Figure 3.2 (b) shows, there are three forces acting on the abrasive particles namely normal force (F_n), tangential force (F_t) and axial force (F_a) after the collision of abrasive particle and roughness peak. Iron particles are pushing the abrasive particles on cylindrical workpiece surface due to normal force. Tangential force is due to rotation of tool and cylindrical workpiece. Axial force is due to reciprocating motion of tool along axis of cylindrical workpiece. The resistance offered by roughness peaks to active abrasive particles against tangential and axial forces . The normal force acting is responsible for indentation on workpiece surface whereas the resultant of tangential and axial force is responsible for shearing of roughness peaks on workpiece surface as shown in Figure 3.2(b). The resultant must be greater than the resisting shear force of material for removal of peaks to take place.

3.4 MAGNETOSTATIC MODELLING OF MAGNETORHEOLOGICAL (MR) FINISHING TOOL

The feasibility of the present tool [30] was validated by performing the magnetostatic simulation on ansoft maxwell 13 (student version). Magnetic field strength and variation in working gap was checked by performing the simulation. Maxwell ansoft solve the electromagnetic field problem of a given model by assigning materials, boundaries and source conditions. Maxwell equations was applied over finite region or space. To check the magnetic field for the feasibility of the tool, the model was created in the creo 3.0 and was imported to the maxwell ansoft. Tool along with workpiece was imported to maxwell ansoft. The properties was assigned to each component of the model as given in Table 3.2. Environment was created around the model. Model was analyzed for 10 pass runs. Figure 3.4 represents the finite element analysis (FEA) for the CAD model (Figure 3.3). It can be seen that the magnetic flux density magnitude is around 0.93T to 1.05T in the working gap. Figure 3.4(a) show the graphical representation of variation of magnitude of magnetic flux in the working gap. The magnitude of magnetic flux density on tool side is 1.05 T and it decreases to the magnitude of 0.93 T towards workpiece surface as shown in Figure 3.5.

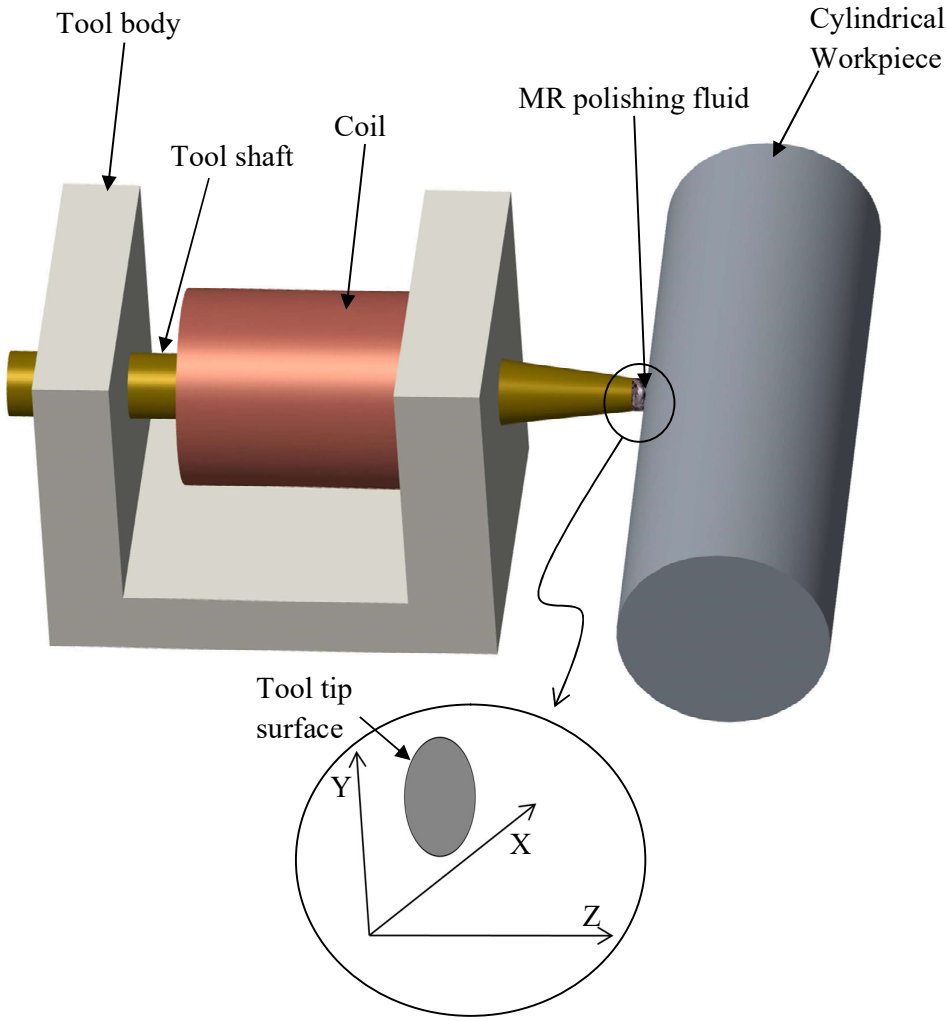

Figure 3.3 CAD model of electromagnetic tool along with MR polishing fluid and ferromagnetic cylindrical workpiece prepared for magnetostatic simulation on creo 3.0

Table 3.2 Input parameters for analyzing of magnetostatic magnetic field

Component	Material	Relative permeability
Tool body	Aluminium	1
Coiling	Copper	0.99
Rotating shaft	Mild steel	200
Finishing medium	MR polishing fluid	5
Ferromagnetic cylindrical workpiece	H13 die steel	180

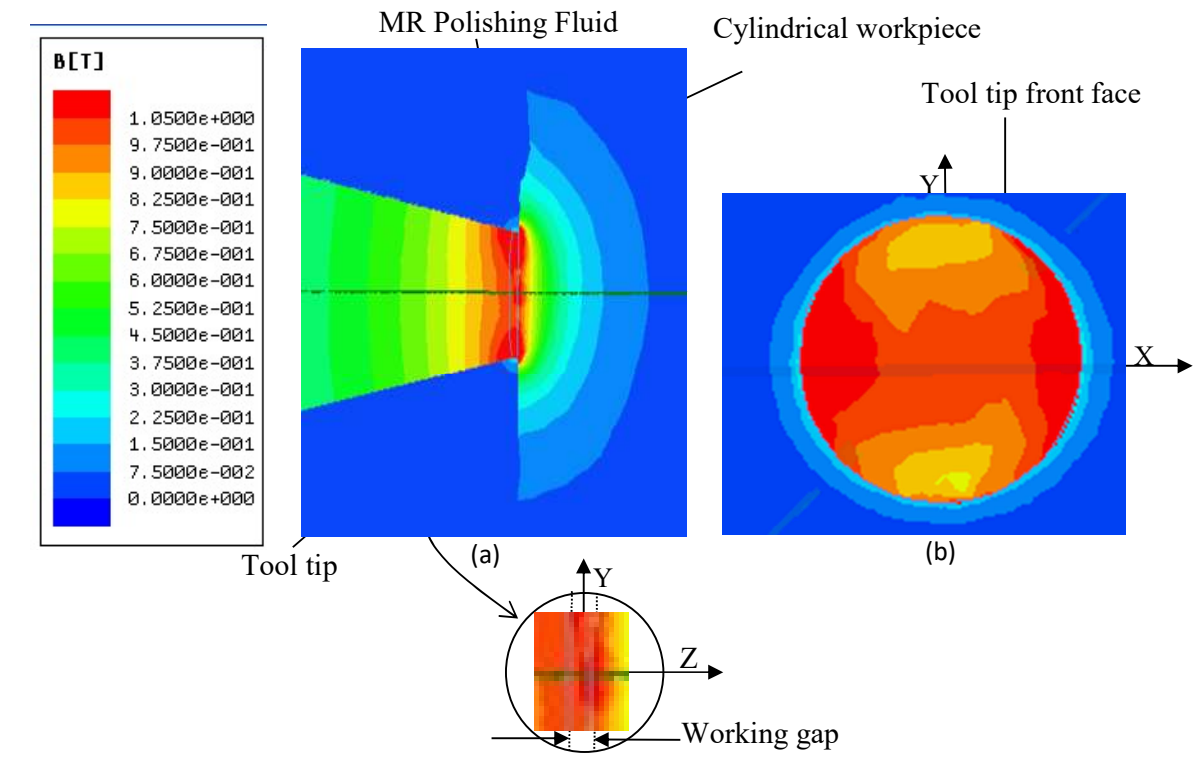

Figure 3.4 (a) Magnetostatic finite element analysis (FEA) for the working gap between tool tip surface and ferromagnetic cylindrical workpiece and (b) magnetic flux density variation on tool tip surface

Figure 3.5 Magnetic flux density variation in the working gap along Z axis (Figure 3.4 (a))

Due to such variation of magnetic flux density in working gap, magnetic iron particles move towards region of high magnetic strength and non magnetic iron particle move towards region of low magnetic strength [8]. Figure 3.6 represents the variation of magnetic flux on tool surface. It can be seen that the active region for abrasive is 10mm along the tool surface.

Active abrasive region is in circular area of radius 10 mm. In this region the magnetic field is varying from 0.80 T to 1.2 T. This region is responsible for holding the abrasive particles for finishing the workpiece surface and was used in later section for calculation of active abrasive particles.

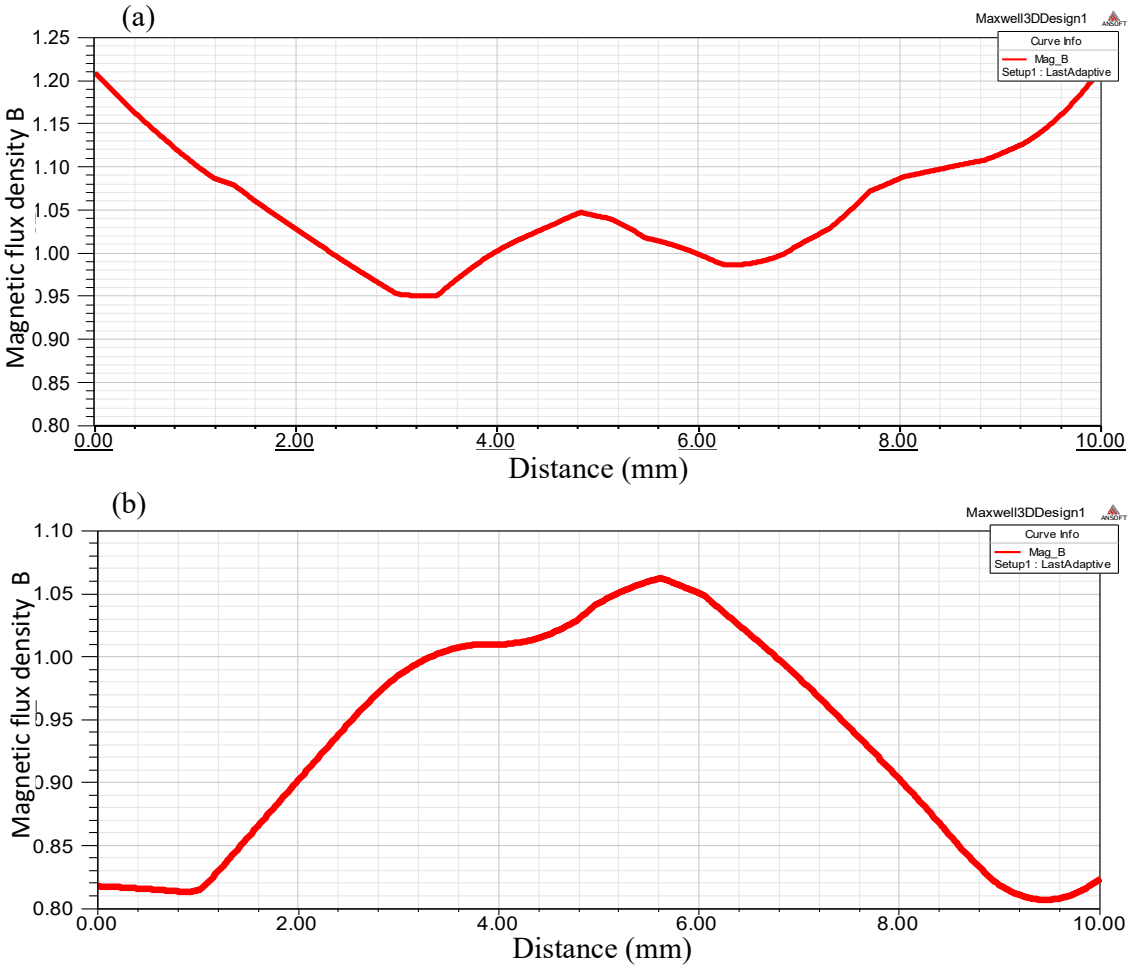

Figure 3.6 Magnetic flux density variation on tool face (a) along x-axis (Figure 3.4 (b)) and (b) along y-axis (Figure 3.4 (b))

3.5 SURFACE ROUGHNESS MODEL FOR MAGNETORHEOLOGICAL FINISHING OF THE CYLINDERICAL WORKPIECE

The mechanism of material removal in term of reduction in surface roughness can be analysed by understanding various forces acting on the abrasive particles. Various forces act while finishing which reduce the roughness peaks. Indentation of abrasives on workpiece surface is due to normal force, tangential and axial forces are responsible for overcoming the shear strength of roughness peaks.

The following assumptions are taken in to account as discussed below.

- Abrasive particles and iron particles are of spherical and uniform shape.

- Distribution of abrasive and iron particles are uniform throughout the working gap.
- Magnetic leakage or losses calculation are not considered in calculation of normal magnetic forces.
- For surface roughness model, calculations are done assuming uniform surface roughness throughout the cylindrical surface.
- The normal magnetic force is responsible for indentation of abrasives on workpiece whereas resultant of tangential and axial force is responsible for shearing of roughness peaks.
- Due to low material removal rate, MR polishing fluid properties are not altered by mixing of removed material.
- Abrasive particles are embedded in the iron particles chain structure and chains are continous in the working gap.
- For calculation of helix effect on active abrasive region, active region was assumed to be circular.

Figure 3.7 shows the resistant forces when abrasive particle come in contact with the workpiece surface. When the normal force (F_n) and shear force (F_s) acts on abrasive particle, resisting normal force (R_n) and resisting shear force (R_s) occurs. The indentation as well as shearing of peaks take place when $F_n > R_n$ and $F_s > R_s$ respectively [39].

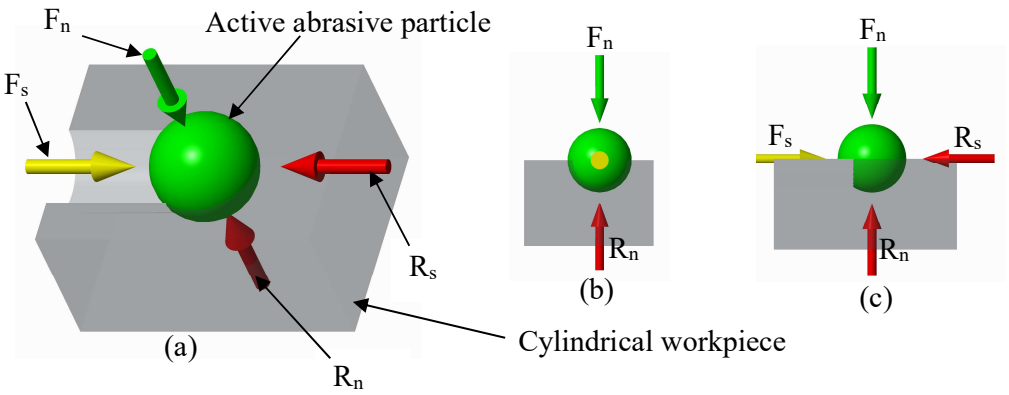

Figure 3.7 (a) Different forces acting on workpiece surface on interaction of abrasive particle, (b) side view representing normal forces, (c) front view representing shear as well as normal forces acting on abrasive particle

3.5.1 Unit Cell and Iron Particles in Chain Structure

To understand the forces acting an abrasive particles, it is important to analyze the effect of magnetic field on magnetic iron particles and non-magnetic abrasive particles. Iron particles attain magnetic dipole moment under effect of magnetic field [8]. It was found that when the dipole interaction forces exceeds thermal interaction, magnetic iron particles arrange

themselves in the form of dipole chains [8]. A magnetic field gradient is created in the working gap under the effect of magnetic field. The non-magnetic abrasive particles moves toward low magnetic field gradient region and iron particles move towards high magnetic field gradient region[8]. It was found the abrasive particles arrange themselves in the iron particles chain structure, chains are still continuous [41]. Iron particles were assumed to be spherical in shape. The chains are formed by alignment of spherical particles in magnetic field[41]. Abrasive particles are also spherical in shape and movement of abrasive particles are very less. For calculating the number of iron particles, it was assumed that the unit cells are repeated in the MR polishing fluid column. So the main focus was on to study the number of abrasives and iron particles in a unit cell.

3.5.1.1 Unit cell

In this research, MR polishing fluid was comprises of 30 % by vol magnetic iron particles of 400 mesh size and 15 % by vol abrasive particles of 800 mesh size. The diameter of abrasive and iron particle was calculated by using Eq 3.1 [42].

$$d_{\mu} = \frac{15000}{m} \tag{3.1}$$

Where d_{μ} is diameter of particle in micron and m represent mesh size of particle.

By using the Eq.3.1, it was found that diameter of iron particle was 38µm for 400 mesh size and diameter of abrasive was 19µm for 800 mesh size.

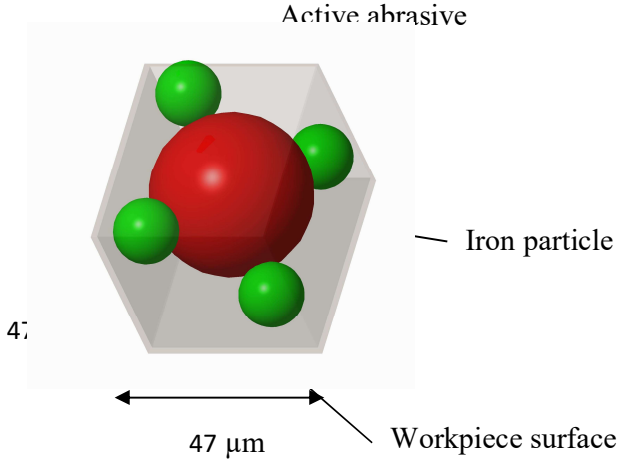

Figure 3.8 Possible arrangement of four abrasive particles with the single iron particle in a unit cell

Number of iron particles (N_{IP}) in a given volume V of MR polishing fluid is given by Eq. 3.2 [41].

$$N_{IP} = \frac{\emptyset_{IP} \times V}{V_{IP}} \tag{3.2}$$

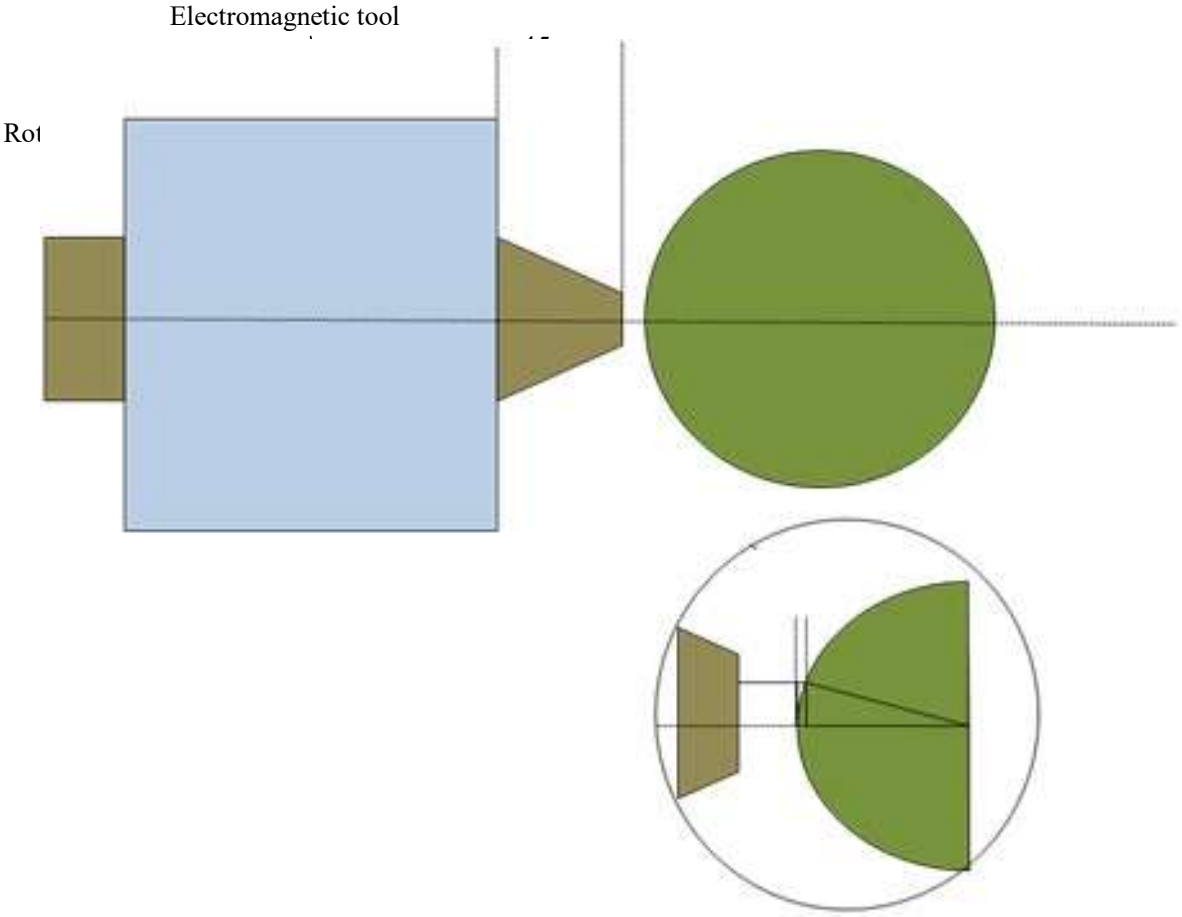

Figure 3.9 Schematic for working gap between tool and cylindrical workpiece

Where V is volume of MR polishing fluid, $\emptyset_{IP}$ is volume fraction of iron particles in MR polishing fluid and V_{IP} volume of single iron particle.

While using the values $\emptyset_{IP}$= 30% , V = 1 mm^3 and V_{IP} = 2.873×10^{-5} mm^3 then it was found that 10,441 iron particles present in MR polishing fluid by using Eq.3.2. Volume occupied by single iron particle was 9.57×10^{-5} mm^3 in 1mm^3 MR polishing fluid. Similarly abrasive particles was 41,767 in 1mm^3 MR polishing fluid and volume occupied by single abrasive was 2.35×10^{-5} mm^3. The edge length of cubic unit cell was found to be 47µm. Number of abrasive particles for a single iron article was two. The possible arrangement of active abrasives for single iron particle is shown in Figure 3.8.

3.5.1.2 Magnetic iron particle in single chain in working gap

The working gap between the tool and cylindrical workpiece is shown in Figure 3.9. the working gap (UQ) was calculated at radius of 3 mm from tool face.

PR was calculated from 6PQR shown in Figure 3.9 using Eq. 3.3.

$$PR = \sqrt{PQ^2 - QR^2} \tag{3.3}$$

For PQ = 30 mm, QR = 3mm, the value of PR = 29.84 mm.

Working gap (UQ) was calculated from Figure 3.9 using Eq. 3.4

$$UQ = US + SQ \tag{3.4}$$

US = 0.6 mm, SQ = PT - TR = 0.16 mm, the value of UQ =0.76 mm.

Number of iron particles (N_{IPC}) in the chain in working gap can be calculated by using the

$$N_{IPC} = \frac{Working\ gap}{Unit\ cell\ edge\ length} \tag{3.5}$$

Where N_{IPC} is the number of iron particle in the chain

By using Eq.3.5, for working gap of 0.76 mm and unit cell edge length of 47 µm number of iron particles in chain was 16.

3.5.2 Modelling of Magnetic Flux in Working Gap

The magnetic field present in the working gap is responsible for magnetisation of ferromagnetic particles. Magnetic flux density at any point in a working gap was calculated by using Eq.3.6 [39].

$$B = \mu_0(H + M) \tag{3.6}$$

Where B is magnetic flux density, μ_0 is permeability of free space, H is magnetic strength at a point and M is magnetization of a particle.

The value of H has to be calculated at each point to measure magnetic field in the gap along axis of tool by using Eq.3.7 [43].

$$H = \sqrt{(H_{xij}^2 + H_{yij}^2 + H_{zij}^2)} \tag{3.7}$$

Where H_{xij} represent component of magnetic strength along x-axis, H_{yij} represent component of magnetic strength along y-axis, H_{zij} represent component of magnetic strength along z-axis as shown in Fig.3.10.

All the three components of magnetic strength can be calculated by using Eqs. 3.8, 3.9 and 3.10 [43].

$$H_{xij} = \frac{I{a_j}^2}{4(R^2 + {a_j}^2)^{\frac{3}{2}}} \left(\frac{3xz_i}{\left(R^2 + a_j^2\right)} + \frac{105a_j^2x^3z_i}{8\left(R^2 + a_j^2\right)^3} + \frac{105a_j^2xy^2z_i}{8\left(R^2 + a_j^2\right)^3}\right) \tag{3.8}$$

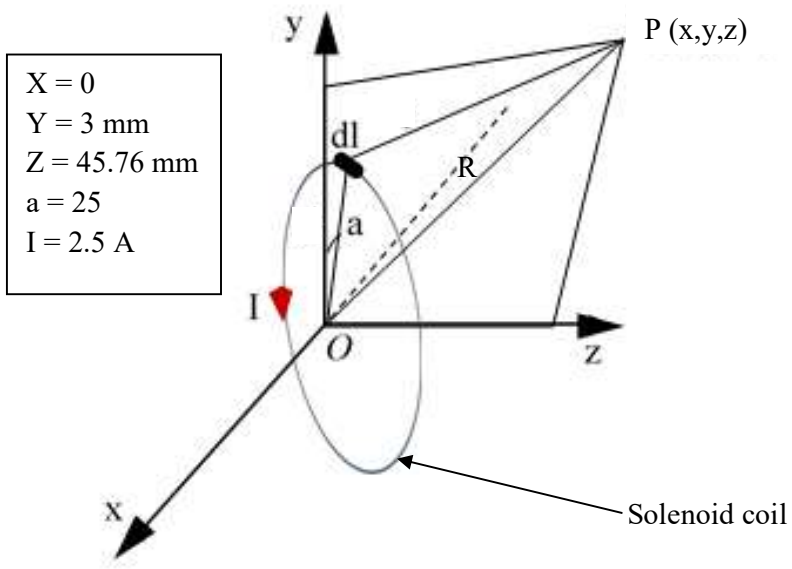

Figure 3.10 Co-ordinate of magnetic field strength at a point [44]

$$H_{yij} = \frac{I{a_j}^2}{4(R^2 + {a_j}^2)^{\frac{3}{2}}} \left(\frac{3yz_i}{\left(R^2 + a_j^2\right)} + \frac{105a_j^2y^3z_i}{8\left(R^2 + a_j^2\right)^3} + \frac{105a_j^2yx^2z_i}{8\left(R^2 + a_j^2\right)^3}\right) \quad (3.9)$$

$$H_{zij} = \frac{I{a_j}^2}{4(R^2 + {a_j}^2)^{\frac{3}{2}}} \left(2 - \frac{3(x^2 + y^2)}{\left(R^2 + a_j^2\right)} + \frac{15a_j^2(x^2 + y^2)^2}{2\left(R^2 + a_j^2\right)^2} - \frac{105a_j^2(x^2 + y^2)^2}{8\left(R^2 + a_j^2\right)^3}\right) \quad (3.10)$$

Where I is current through the coil of electromagnet (2.5A for present case), a_j is radius of coil varying in y direction, z_i is the distance from the measuring point along z-axis, x and y represent the co-ordinates of measuring points and $R = \sqrt{x^2 + y^2 + z_i^2}$.

From the Eqs. 3.8 , 3.9 and 3.10 , it can be seen that a_j and z_i are varying in y and z direction respectively. These two parameters can be calculated by using Equations 3.11 and 3.12.

$$a_j = a + jd_g \; ; \; 0 < j <= n \quad (3.11)$$

$$z_i = z + id_g \; ; \; 0 < i <= m \quad (3.12)$$

Where j represent number of turns radially in y direction and i represent number of turns axially in z direction, n represent the number of turns radially, m represents the number of turns axially and d_g is gauge diameter of electromagnet coiling wire.

In the present tool n = 26, m = 130 and d_g = 1 mm.

Table 3.3 Magnetic strength in the working gap

Distance from tool surface (mm)	Magnetic strength H (A/m)
0.047	1464.37
0.094	1462.37
0.141	1460.37
0.188	1458.37
0.235	1456.37
0.282	1454.37
0.329	1452.67
0.376	1450.67
0.423	1448.57
0.470	1446.67
0.517	1444.67
0.564	1442.67
0.611	1440.67
0.658	1438.67
0.705	1436.67
0.752	1426.67

Magnetic strength of solenoid (H) in the working gap was calculated by using Eq.3.7 at each iron particle in a single chain and reported in Table 3.3. The magnetic strength was calculated at the tool face radius of 3 mm along the working gap. A working gap of 0.76 mm was calculated for the tool radius of 3mm between the flat tool and cylindrical workpiece surface. After obtaining the magnetic strength at each point , the magnetic flux density can be calculated by using Eq.3.6 in working gap. Magnetic flux density can be calculated by substituting the value of magnetization in Eq. 3.6 of magnetic iron particles around the working gap. In this research, the ferromagnetic materials are tool shaft, workpiece and MR polishing fluid having relative permeability of 200, 180 and 5 [40] respectively .

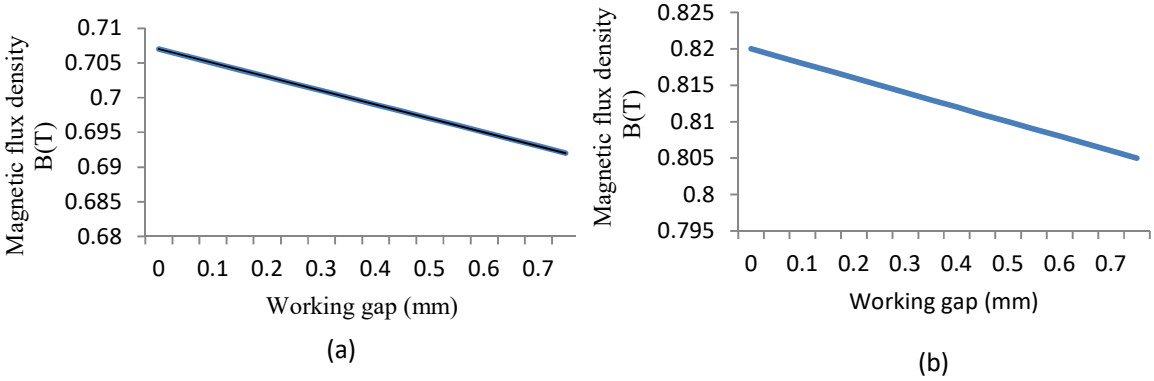

Figure 3.11 Variation of magnetic flux in working gap (a)calculated theoretically and (b) obtained from magnetostatic finite element analysis

The magnetic flux density is obtained at each point inside the working gap and reported in Table 3.4 . As it can be observed from the Table 3.4, magnetic flux density gradient is developed along the working gap. Magnitude of magnetic flux density is more towards the tool surface as compared to that of workpiece surface. The variation of magnetic flux density obtained theoretically (Table 3.4) is shown in shown in Figure 3.11 (a). The variation of magnetic flux density obtained after magnetostatic simulation in working gap is shown in Figure 3.11 (b).The magnitude is more in magnetostatic simulation as compared to theoretical because of idle conditions during simulation. Linear equation for variation of magnetic flux density in working gap is obtained from Figure 3.11 (a) and given as Eq.3.13.

$$B(x) = -0.001x + 0.708 \quad (3.13)$$

Table 3.4 Magnetic flux density in the working gap

Distance from tool surface (mm)	Magnetic flux density B (T)
0.047	0.7065
0.094	0.7055
0.141	0.7046
0.188	0.7036
0.235	0.7026
0.282	0.7017
0.329	0.7007
0.376	0.6998
0.423	0.6988
0.470	0.6978
0.517	0.6969
0.564	0.6959
0.611	0.6949
0.658	0.6939
0.705	0.6929
0.752	0.6919

3.5.3 Calculation of Magnetic Force on Iron Particle and Indenting Force on an Abrasive Particle

The indentation on workpiece surface is caused by the active abrasive particles. The magnetic iron particles under the effect of magnetic field exerts normal force on the abrasive particles. Finishing performance depends on the force acting normally on the abrasive particles which are responsible for indentation. The magnetic force acting on an iron particle calculated by using Eq. 3.12 [39].

$$F_m = \frac{m_{IP}\chi_m B\nabla B}{\mu_0} \quad (3.14)$$

Eq.3.14 was further modified to Eq.3.15.

$$F_m = \frac{m_{IP}\chi_m B(\mathrm{z})\frac{\mathrm{dB(z)}}{\mathrm{dz}}}{\mu_0} \tag{3.15}$$

Where $F_m$is the magnetic force exerted by the iron particle, m_{IP} is the mass of iron particle, χ_m is the mass of magnetic susceptibility, μ_0 is the magnetic permeability of free space and B(z) is variation of magnetic flux along the working gap.

m_{IP} is the mass of iron particle = 2.3989×10^{-11} kg

μ_0 is the magnetic permeability of free space = $4\pi \times 10^{-7}$ (N/A^2)

Mass of magnetic susceptibility for iron particle can be calculated by using Eq. 3.16.

$$\chi_m = \frac{\mu_0 M}{B} \tag{3.16}$$

M was calculated approximately from the Figure 3.12. Figure 3.12 represent the M-B curve for CS grade iron particle . M-B curve was derived experimentally by vibrating sample magnetometer (VSM) test [16].

The indentation force (F_{ind}) acting on abrasive particle was calculated by calculating the magnetic force (Eq. 3.13) acting on the iron particle in the working gap. The magnetic force acting on iron particles is reported in Table 3.5.

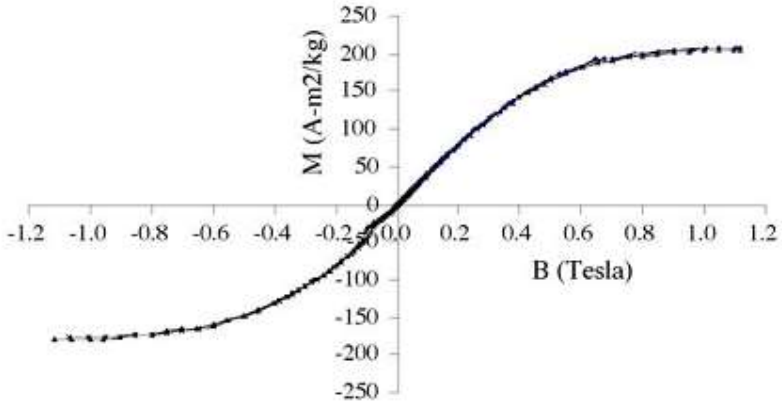

Figure 3.12 M-B curve for CS grade iron particles [16]

F_{ind} can be calculated by using Eq. 3.17 [45] . Eq.3.15 represent the total force exerted by individual iron particle in working gap. The indentation force was equals to 3.15×10^{-10}N.

$$F_{ind} = \sum_{i=1}^{n} \frac{m_{ip}B_i(\frac{dB(z)}{dz})_i\chi_i}{\mu_0} \tag{3.17}$$

Where n= 16 (number of iron particles in working gap in single chain)

3.6 MODELLING OF SURFACE ROUGHNESS

3.6.1 Calculation of Material Removal by Single Abrasive

The indentation force (F_{ind}) acting on abrasive particles was calculated in the previous section. This force is responsible for indenting the abrasives in the workpiece. Indentation causes depression in workpiece surface as shown in Figure 3.13(a). Brinell model is used to calculate the indentation in the workpiece surface. Brinell hardness number (H_{BHN}) given by Eq. 3.18 [39] was used .

$$H_{BHN} = \frac{2F_{ind}}{\pi D_{abr}(D_{abr} - \sqrt{{D_{abr}}^2 - D_i^2})} \quad (3.18)$$

Where F_{ind} is the indentation force on the abrasive particle, D_{abr} is the diameter of abrasive particle, D_i is the indentation diameter, H_{BHN} is brinell hardness number measured in kgf/mm^2.

For $F_{ind} = 3.15 \times 10^{-10}$N, H_{BHN} =400Kgf/mm^2 (H13 steel), D_{abr}= 19µm.

The value of D_i from Eq. 3.18 is calculated as $D_i = 3.0786 \times 10^{-10}$ m.

Table 3.5 Magnetic force acting on iron particles in working gap

Distance from tool surface (mm)	Magnetic flux density (B) (T)	Mass of magnetic susceptibility (χ_m)×10^{-4} (m^3/kg)	Magnetic force (F_n)×10^{-11}(N)
0.047	0.7065	3.502	-2.034
0.094	0.7055	3.472	-2.014
0.141	0.7046	3.459	-2.003
0.188	0.7036	3.446	-1.993
0.235	0.7026	3.433	-1.982
0.282	0.7017	3.420	-1.972
0.329	0.7007	3.406	-1.962
0.376	0.6998	3.393	-1.950
0.423	0.6988	3.380	-1.941
0.470	0.6978	3.367	-1.931
0.517	0.6969	3.354	-1.921
0.564	0.6959	3.340	-1.910
0.611	0.6949	3.327	-1.900
0.658	0.6939	3.314	-1.890
0.705	0.6929	3.300	-1.880
0.752	0.6919	3.287	-1.870

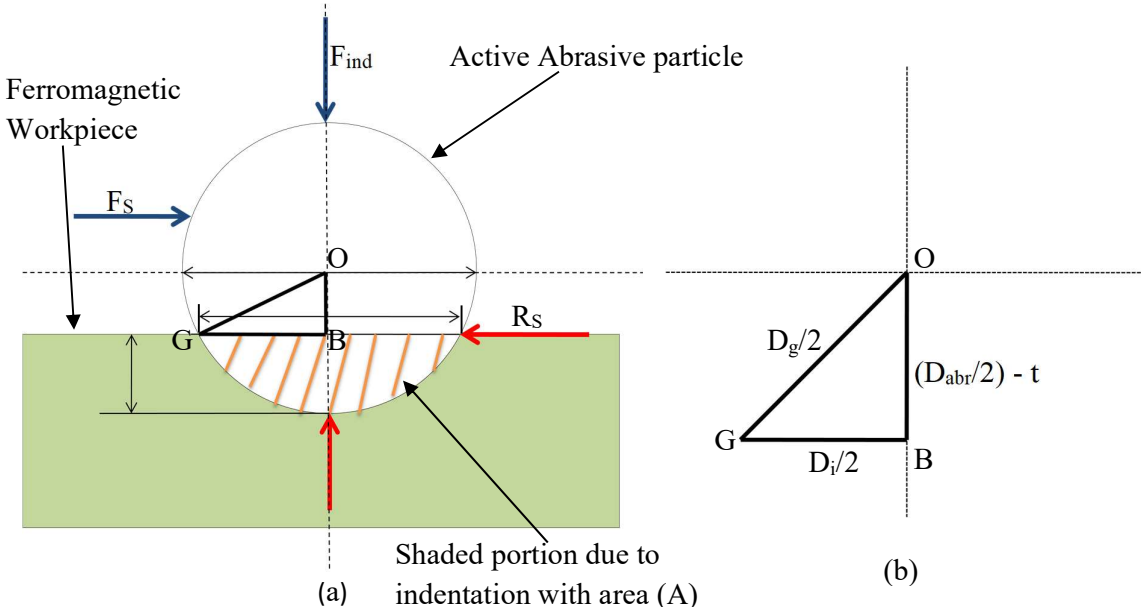

Figure 3.13 (a) Forces acting during interaction of abrasive particle with workpiece and (b) geometrical diagram for calculation of depth of indentation

From 6OGB Figure 3.13(b), depth of indentation can be calculated by using Eq. 3.19 [39]

$$t = \frac{D_{abr}}{2} - \frac{1}{2}\sqrt{D_{abr}^2 - D_i^2} \tag{3.19}$$

For D_{abr} = 19µm and D_i = 3.0786×10^{-10} m, the value of depth of indentation is calculated using Eq. 3.19 as $t = 4.988 \times 10^{-15}$ m.

From the Figure 3.13 (a), the area of groove generated by abrasive particle on workpiece surface calculated by using Eq. 3.20 [39] .

$$A = \frac{D_{abr}^2}{4}\sin^{-1}\frac{2\sqrt{t(D_{abr}-t)}}{D_{abr}} - \sqrt{t(D_{abr}-t)}\left(\frac{D_{abr}}{2} - t\right) \tag{3.20}$$

For D_{abr} = 19µm and $t = 4.988 \times 10^{-15}$ m, area of groove $A = 2.92 \times 10^{-15}$ m^2.

Volume removed by single abrasive (V_a) calculated by the Eq 3.21 [40].

$$V_a = A \times L_a \tag{3.21}$$

Where A is area of cross-section ofindented groove, L_a is actual contact length by abrasive particle on workpiece surface.

3.6.2 Number of Active Abrasive

The abrasive particles which are responsible for finishing operation are known as active abrasives . The active abrasive particles were decided on the basis of magnetic flux density at the workpiece surface from the tool tip surface. Magnetostatic finite element analysis was performed, as discussed above (Figure 3.6). It was found that a region of a circular area of 10 mm was having a minimum magnetic flux of 0.95 T shown in Figure 3.6 (a) . In the active abrasives region, magnetic flux density varies from 0.95 T to 1.2 T. Active abrasives can be calculated by calculating the area of active abrasives ABCD as shown in Figure 3.14 (b). Projected area of the circular tool tip form an ellipse on the surface of workpiece. Area of ellipse shown in Figure 3.14 (b) has to be calculated.

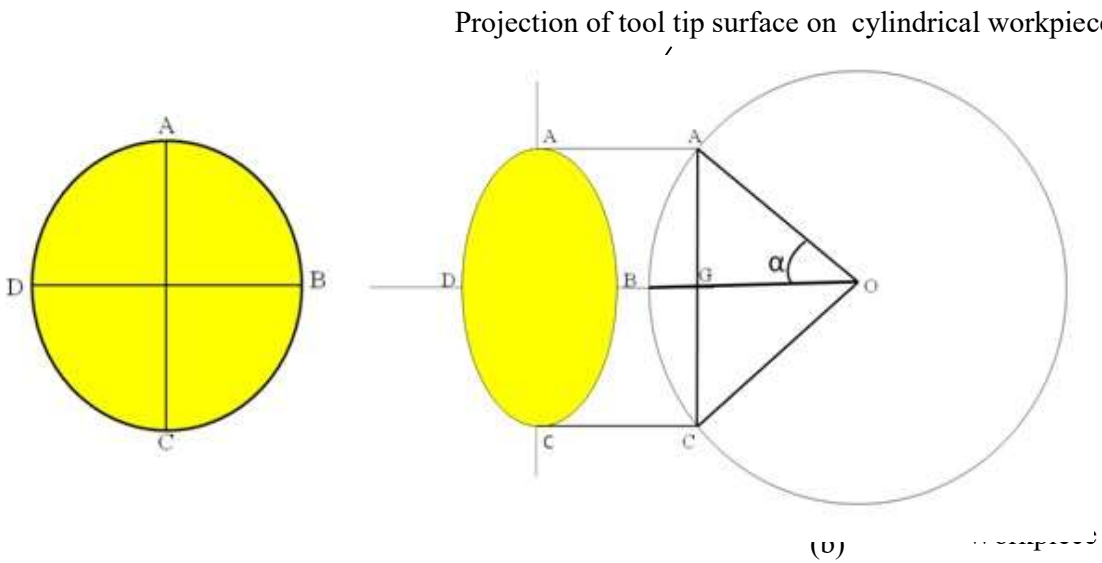

Figure 3.14 (a) The area of active abrasives over tool tip face ,and (b) geometrical representation of region of active abrasives on cylindrical workpiece surface (side view)

From Figure 3.14 (b),

OP is radius of cylindrical workpiece = 30 mm

PC is projection of active abrasives region on workpiece surface = 10 mm

To measure the angle α , Eq. 3.20 was used .

$$\sin\alpha = \frac{PG}{PO} \tag{3.22}$$

For PG = 5 mm and PO = 30 mm , the value of α was found as 0.16 rad.

Length of arc AC was calculated by using Eq. 3.23.

$$PC = 2\alpha \times PO \tag{3.23}$$

For α = 0.16 and PO = 30 mm, the length of PC = 10.04 mm.

Area (E') of region of active abrasive (PBCD) $= \frac{\pi \times \text{PC} \times \text{PD}}{4}$

For PC = 10.04 mm and PD = 10 mm , value of E' = 78.84 mm^2 .

For circular tool tip surface area A' was calculated using Eq. 3.24.

$$A' = \frac{\pi(BD)^2}{4} \tag{3.24}$$

For BD = 10 mm, the value of A' calculated using Eq. 3.24 as A' = 78.53 mm^2.

The difference between A' and E' is not much, so for further calculations A' is used.

From Section 3.2.1, it was found that there are two active abrasives interacting with workpiece surface and are placed at corners of the unit cell of length 47 μm.

Number of active abrasives (N_s) calculated using Eq. 3.25.

$$N_s = 2 \times \frac{A'}{Area\ of\ unit\ cell\ face} \tag{3.25}$$

For A' = 78.84 mm^2 and area of unit cell = 2.209 × 10^{-3} mm^2 , the number of active abrasives was calculated using Eq. 3.24 as N_s = 71100.

3.6.3 Calculation of Surface Roughness Reduction

Volume removed by active abrasives in ith stroke (V') was calculated by using Eq. 3.26.

$$V' = V_a \times N_s \tag{3.26}$$

Material removed in ith stroke (V^i)= actual contact length × width of workpiece × total height of material removed [40]

$$= L_a \times 2\pi R_w \times h \tag{3.27}$$

Where R_w is radius of cylindrical workpiece, h is the height of material removed.

Substituting Eq.3.26 in Eq.3.27 . Eq.3.28 was obtained

$$V_a \times N_s = L_a \times 2\pi R_w \times h \tag{3.28}$$

Subsituting the value of V_a from Eq.3.21 and $h = 7(R_a^{i-1} - R_a^i)$ [40].

$$R_a^{i-1} - R_a^i = \frac{N_s \times A}{7 \times 2\pi R_w} \tag{3.29}$$

Where R_a^{i-1} is the surface roughnesss in (i-1)th stroke, R_a^i is the surface roughness in ith stroke, N_s is the number of active abrasives, R_w is the radius of cylindrical workpiece and A is indenting area by single abrasive Eq.3.29 represent the material removed in single cycle.

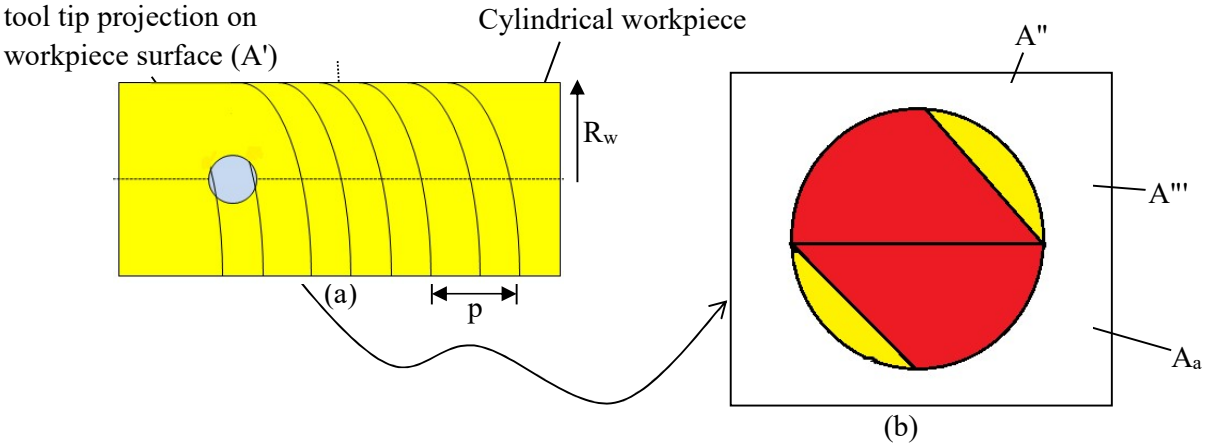

Figure 3.15 (a) Effect of helix angle on workpiece surface due to rotation of workpiece and translation motion of tool and (b) schematic of active abrasives region under effect of helix

3.6.4 Effect of Helix angle on Region of Active Abrasives

As two movements are responsible for finishing of workpiece surface namely translation motion of tool and workpiece rotation. Figure 3.15 (a) shows material is removed in the form of helical path from workpiece surface due to combination of these two motions. The helix angle varies with these motions . The helix angle (β) can be calculated by using the Eq. 3.30.

$$\tan\beta = \frac{p}{\pi D} \tag{3.30}$$

Where p is the pitch of helix , D is diameter of workpiece.

Pitch of the helix (p) can be calculated using Eq. 3.31.

$$p = F \times T' \tag{3.31}$$

Where F is the feed of tool and T is the time taken to complete path in one rotation along helix.

Time T' can be calculated using Eq. 3.32

$$T' = \frac{2\pi R_w}{\pi D R} \tag{3.32}$$

where R_w is radius of workpiece, D is diameter of workpiece and R is rotational speed of workpiece.

Pitch for three different combinations of tool feed and workpiece rotation is calculated using Eq.3.31 and reported in Table 3.6.

Area of region PMNIP (A") can be calculated by using sprandtl Eq. 3.33

$$A'' = \frac{MN \times MP}{(n+1)} \tag{3.33}$$

Where MP = 5 mm, MN= MP tan(β) =5 tan(β), n=2 for circle.

Figure 3.15, shows variation in the helix angle, results in the variation of the region of active abrasives . The varying area of active region (A''') can be calculated by using Eq . 3.34.

$$A''' = (0.5 \times MP^2 \times \tan\beta) - A'' \quad (3.34)$$

The area of active abrasive (A^a) varying with helix angle can be calculated using Eq.3.35 and reported in Table 3.6.

$$A^a = A' - 2A''' \quad (3.35)$$

Table 3.6 Variation of active abrasive region with helix angle

Feed (F) (cm/min)	Workpiece rotation (R) (rpm)	Pitch (mm)	A^a (mm^2)
10	100	1	78.81
30	90	3.33	78.76
20	140	1.428	78.80

After calculation of active abrasives region varying with helix angle, number of active abrasives due to helix effect (N_h) calculated by using Eq. 3.36 and reported in table 3.7.

$$N_h = 2 \times \frac{A^a}{Area\ of\ unit\ cell} \quad (3.36)$$

Eq. 3.37 represent material removed in single stroke by varying translation motion of tool and rotation of cylindrical workpiece as given in Table 3.8.

$$R_a^{i-1} - R_a^i = \frac{N_h \times A}{7 \times 2\pi R_w} \quad (3.37)$$

Table 3.7 Number of active abrasives

A^a (mm^2)	Number of active abrasives
78.81	71353
78.76	71308
78.80	71344

As can be seen from the Table 3.7, the number of active abrasives is not varying much for different combination of workpiece rotation as well as tool feed. From Table 3.6, it can be seen that range of pitch is from 1 mm to 3.33 mm for the selected range of tool feed and workpiece rotation. The active abrasive region will vary up to large extent as shown in Figure

3.15 (b) , if helix angle increases the difference between number of active abrasive will also increases.

Table 3.8 Change in surface roughness for single stroke

Feed (cm/min)	Workpiece rotation (rpm)	6R_a in single stroke (nm)
10	100	0.1575
30	90	0.1578
20	140	0.1578

3.7 RESULTS AND DISCUSSION

The analysis of developed tool was done to check for the feasibility of tool to finish the H13 die steel material. Finite element analysis (FEA) was done on tool using maxwell ansoft (student version). It was found that magnetic flux of 0.8 T to 1.2 T was generated in the working gap. Magnetic flux density gradient is maximum towards the tool surface and decreasing towards workpiece surface. A theoretical model was developed to calculate the magnetic flux density in working gap. Magnetic flux density was calculated using Eq. 3.6. Magnetic flux varies from 0.68 T to 0.7 T. The variation of magnetic flux gradient in working gap is similar to that obtained by FEA. After calculating the magnetic flux density, indenting force was calculated. Roughness model was developed for H13material. The theoretical model developed for surface roughness was validated experimentally during the MR finishing of cylindrical workpiece. In this section the results obtained during validation are discussed.

3.7.1 Experimental Validation for Surface Roughness Model

Theoretical model developed was validated experimentally. Experiments were performed on H13 workpiece. For the experimentation, MR polishing fluid was prepared. MR polishing fluid with composition of 30% iron particles, 15% abrasive particles and 55% carrier medium (80% heavy paraffin and 20 % grease) was used.

Table 3.9 Parameters for experimental validation

Experiment	Feed (cm/min)	Workpiece Rotation (rpm)
1	10	100
2	20	140
3	30	90

Experiment for 20 min was performed on each combination of parameters. The parameters for experiment are given in Table 3.9. The surface finish after experimentation was measured using mitutoyo SJ-400 surf test . Experiments were performed to check for the validation of

the theoretical roughness model given in Table 3.10 . The number of cycles was calculate by using Eq. 3.38 .

$$Number\ of\ cycles\ = \frac{Total\ Duration}{Cycle\ Time} \tag{3.38}$$

Total duration of the experiment was 20 minutes. The movement of the tool was set for 5mm. Cycle time was calculated using Eq. 3.39 .

$$Cycle\ time = \frac{Tool\ movement}{Feed\ of\ tool} \tag{3.39}$$

Eq.3.40 was used to check the percentage error between theoretical and experimental data.

$$\%Error = \frac{Experimental\ data - theoretical\ data}{Experimental\ data} \tag{3.40}$$

Table 3.10 Percentage error between theoretical and experimental value of surface roughness

S. No	Number of cycles	Experimental R_a(µm)	Theoretical R_a(µm)	% Error
0	0	0.380	-	-
1	400	0.320	0.316	1.25
2	800	0.267	0.254	4.86
3	1200	0.206	0.192	6.79

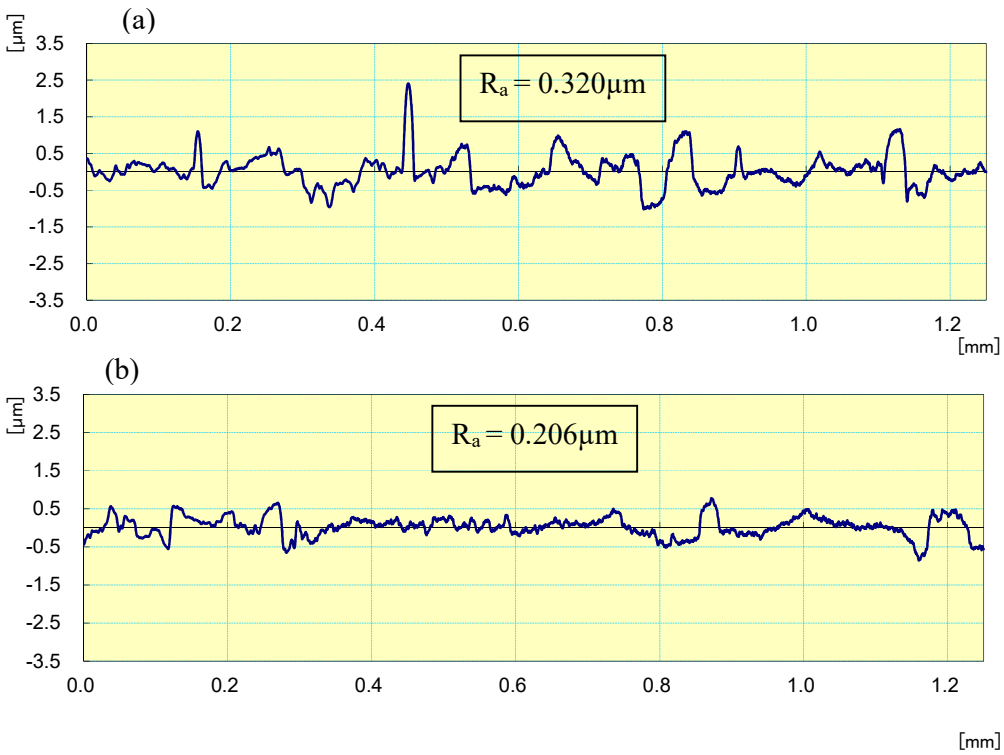

Figure 3.16 Surface roughness profile (a) 400 cycles and (b) 1200 cycles

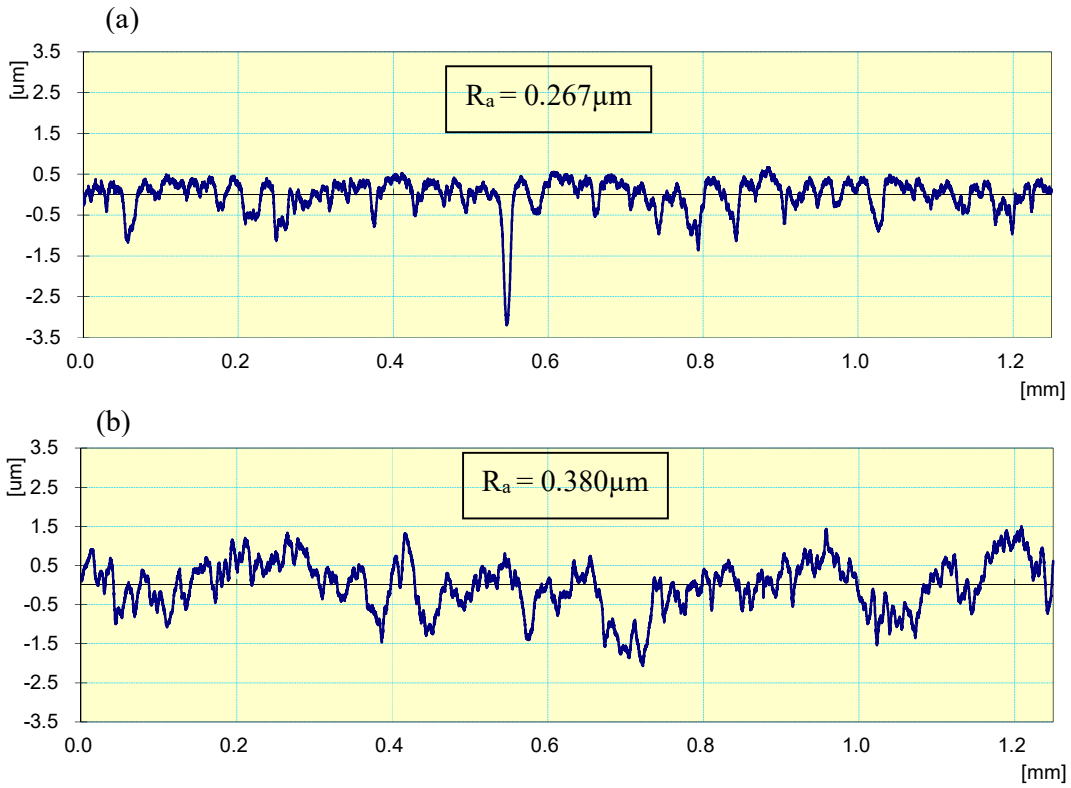

Figure 3.17 Surface roughness profile (a) 800 cycles and (b) 0 cycle

The surface roughness after experimentation was measured using mitutoyo SJ-400 surftest. Initial surface roughness was measured around 0.380µm (Fig 3.17(b)). After experimentation it was reduced to 0.320µm (Fig 3.16(a)) , 0.267µm (Fig 3.17(a)) and 0.206µm (Fig 3.16(b)) in 400 ,800 and 1200 cycles respectively as reported in Table 3.5. The maximum error obtained was 6.79%.

Mechanism of material removal was studied to predict the surface roughness reduction for finishing of cylindrical object made of H13 material using MR fluid based finishing process. In industries, process parameters are selected on basis of hit and trial. Selecting parameters by hit and trial is time consuming. This mechanism study will help to predict the results obtained after finishing as well as effect of selected parameters on the finishing performance for H13 material. The predicted value will be having error in range of 1.25% to 6.79 %. By using this mechanism lot of time will be saved in deciding the parameters for finishing operation.

3.8 CONCLUSIONS

Study of mechanism of material removal during finishing of cylindrical workpiece made of H13 die steel material using magnetorheological fluid based finishing process has been done.

Magnetic flux density, indentation force and surface roughness reduction have been calculated. The main conclusion from the above work are as follows.

- Magnetic flux density at the tool face was obtained as 0.707 T and decreased towards cylindrical workpiece surface linearly to value of 0.69T.
- Indentation force acting on abrasive particles is affected by the magnetic flux density in the working gap and size of magnetic iron particles in the working gap.
- In the decided range of tool feed and workpiece rotation, the effect of helix angle is negligible. The Active abrasive area is not affected much as reported in Table 3.7.
- After the experiment for validation of theoretical model, surface roughness for the cylindrical workpiece was reduced from 0.38 μm to 0.320 μm ,0.267 μm and 0.206 μm respectively in 400 , 800 and 1200 number of finishing cycles.
- Percentage error between the results from the theoretically calculated surface roughness value and experimental value was found in the range of 1.25 % to 6.79 %.
- The percentage error (6.79%) is due to the assumptions made during the theoretical calculation of surface roughness value.

CHAPTER 4

PARAMETRIC STUDY FOR FINISHING OF FERROMAGNETIC CYLINDRICAL WORKPIECE

In this research, the finishing of ferromagnetic cylindrical workpiece was done by using the magnetic field assisted finishing process. Magnetic field control the forces in the magnetic field assisted processes. The finishing operation was performed by MR polishing fluid in the working gap between tool and cylindrical workpiece. In this process various process parameters such as workpiece rotation, tool feed, tool rotation, current intensity through electromagnet and MR polishing fluid composition affects the performance of finishing process. In this chapter, parametric study was done on the process using response surface methodology. To effectively perform the finishing operation, optimum process parameters was calculated using response surface methodology (RSM).The percentage contribution of each parameter on the finishing performance of process was also calculated. The optimum parameters obtained from the parametric study was used to perform the finishing of industrial extrusion punch. After finishing operation, the extrusion punch was sent to industry . In industry, effect of surface roughness of punch in extrusion process was analyzed for its functional life.

4.1 SELECTION OF MATERIAL

The material is generally selected on the basis of operation conditions. In this research, the study is focused on improving the performance of hot-extrusion process. The material that is being used in hot forming process must be able to maintain its strength at elevated temperature and must have minimum deformation during operation to maintain dimensional accuracy of end product. H-series steel are generally used for manufacturing of dies and punches in industries because they are having a good combination of high ultimate strength, high hardness, good fracture toughness at elevated temperature as well as room temperature [46]. H13 has the second highest chromium percentage as compared to the other H-series and average amount of vanadium and molybdenum. The presence of these elements in the composition has made it suitable for hot forming processes [46]. The presence of chromium and molybdenum results in increase in thermal resistance and hardenability respectively. In industries tool steels are generally tempered at maximum hardness so that they have sufficient toughness to withstand loading [46]. Therefore H13 tool steel with hardness of 48 HRC is used in industry for hot tube extrusion process.

4.2 WORKPIECE PREPARATION

For finishing of H13 die steel material, the workpiece was prepared from H13 material with the same condition of hardness of 48 HRC and surface roughness of 0.48µm as that of extrusion punch given in Table 4.1. Workpiece was in the form of a shaft having an axial slot to hold the pieces during the experimentation. The specimen pieces which were placed in the slot are of tight fitment in the slot. Additional screw was there in axial direction to lock them in their position during finishing operation. The specimen pieces that was going to be specimen for experiment was H13 material having the same surface roughness as well as hardness that of the extrusion punch given in Table 4.1. The dimensions of specimen pieces were decided on the basis of dimension of specimen that can be placed in chamber for SEM (selective electron microscopy) measurement. Table4.1 shows the sequence of processes which were used for manufacturing of shaft and specimen pieces.

4.3 EXPERIMENTAL SETUP

Figure 4.1 shows the experimental setup. The workpiece was held between the bearing supports, workpiece rotated by the servo motor through belt drive . All this setup was fixed on vice which was placed in front of the tool. The workpiece center height was maintained at the same level as that of tool center height to obtain the uniform finishing at the workpiece surface. The gap between the tool surface and workpiece surface was maintained at 0.6 mm gap [30]. There was three servo motors M1, M2, M3 used for tool rotation, tool reciprocation and workpiece rotation respectively. Programmable logic controller (PLC) system control these three motors. To supply the DC voltage to the coil of electromagnet, DC voltage regulator was used. It converts the AC voltage from main supply to DC voltage for an electromagnet. To cool the electromagnet, a coolant was supplied to the inlet of electromagnet. After extracting heat from the coiling in electromagnet, coolant returns to the coolant sump which is maintained at the temperature of -6^0C.

4.4 MAGNETORHEOLOGICAL POLISHING FLUID PREPARATION

Magnetorheological (MR) polishing fluid is the suspension of magnetic iron particles, abrasives and carrier medium. Under the effect of magnetic field, iron particles get arranged in the form of chains and abrasive particles get trapped in these chain structures [8] (Figure 4.1 b). When the MR polishing fluid is placed in the working gap along with the magnetic field, the iron particles shifts towards region of high magnetic gradient and abrasives are pushed toward region of low magnetic field gradient [8].

Table 4.1 Sequence of operations for preparation of worpiece and specimens

Machining operations	Shaft	Machining operations	Sample pieces
Blank cutting (rod)		Blank cutting (slab)	
Turning	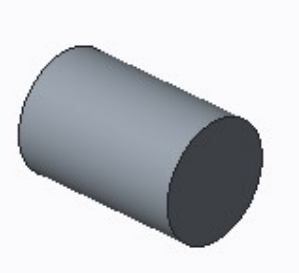	Parting	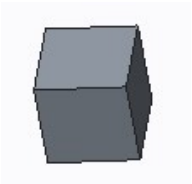
milling	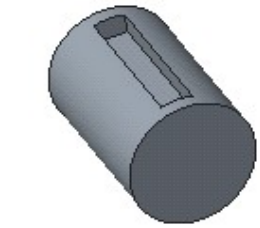	Face grinding	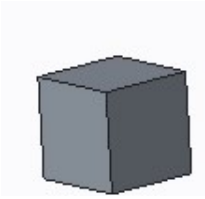
Drilling and tapping	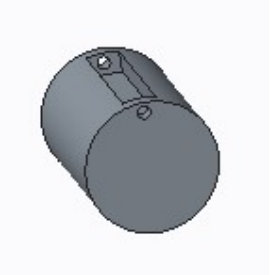	Turning of pieces	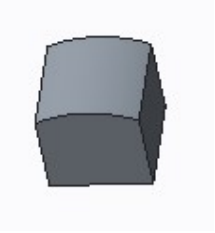
Hardening and tampering	Upto 48 HRC	Hardening and tampering	Upto 48 HRC
Grinding	Upto surface roughness of 0.48µm	Grinding	Upto surface roughness of 0.48µm
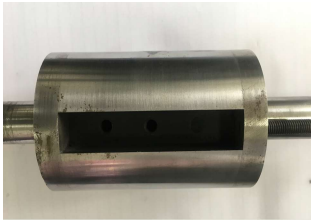			

In this experiment, the components of MR polishing fluid was silicon carbide (SiC) abrasives, iron particles and carrier medium is combination of heavy paraffin and AP3 greese.

(a)

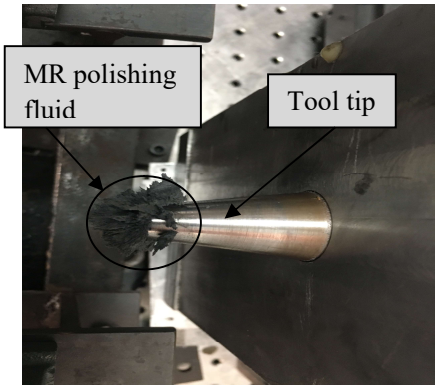

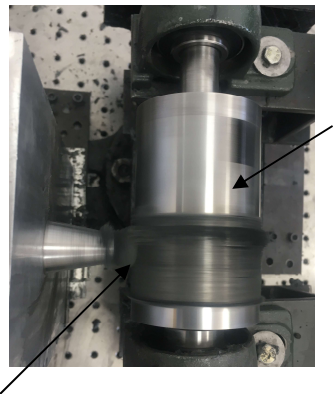

(b) (c)

Figure 4.1 (a) Represent the experimental setup , (b) MR polishing fluid on tool tip under the influence of magnetic field and (c) workpiece for MR finishing

Selection of composition of MR polishing fluid was done on basis of literature review. It was found that 30% carbonyl iron particle (CIP) by volume , 15% abrasives by volume and 55% carrier fluid by volume yields good result for P20 die steel material [30]. The strength of MR polishing fluid increases with increase of percentage volume of iron particles and strength of magnetic field [16]. Based on literature review , the composition of MR polishing fluid was decided by preliminary test on worpiece for 20 minute. The machining parameters along with different composition of MR polishing fluid for the test is given in Table 4.2 and 4.3 . After performing the experiment, the surface roughness was tested on mitutoyo SJ-400 surftest and the results are reported in Table 4.4 and 4.5 respectively. It was found that for MR polishing Fluid, with the composition of electrolytic iron particles (EIP) by 30% volume and silicon carbide (SiC) abrasive particles by 15% volume yields greater percentage change in roughness as compared to 20% by volume EIP and 20% by volume SiC abrasives.

Table 4.2 Machining parameters for experimental Test 1

Test 1	
Parameters	Value
Current (A)	2
Tool rotation(rpm)	1700
Workpiece rotation(rpm)	80
Tool feed(cm/min)	50
SiC concentration(%vol)	15
EIP concentration(%vol)	30

Table 4.3 Machining parameters for experimental Test 2

Test 2	
Parameters	Value
Current (A)	2
Tool rotation(rpm)	1700
Workpiece rotation(rpm)	80
Tool feed(cm/min)	50
Abrasive Concentration(%vol)	20
EIP (%vol)	20

Table 4.4 Experimental results for Test 1

Test 1			
Parameters	Before experimentation (ground surface)	After experimentation (MR finished surface)	Percentage change in surface roughness(%)
R_a(µm)	0.47	0.22	53.16
R_q(µm)	0.56	0.28	50
R_z(µm)	2.5	1.5	40

So MR polishing fluid that was used for experimentation was having 30% by volume EIP, 15% by volume SiC abrasives and 55% by volume carrier fluid (80% heavy paraffin and 20 % AP3 greese by weight). All the components was mixed in a mixture at slow rotation for homogenous mixing.

Table 4.5 Experimental results for Test 2

Test 2			
Parameters	Before experimentation (ground surface)	After experimentation (MR finished surface)	Percentage change in surface roughness(%)
R_a(μm)	0.65	0.39	40
R_q(μm)	0.78	0.47	39.7
R_z(μm)	3.2	2.1	34.3

4.5 EXPERIMENTATION

The MR finishing process was performed for analyzing the effect of various process parameters on H13 die steel material. This research has been done by using the statistical design of experiment . The analysis of various parameters on H13 die steel material was done by using the response surface methodology (RSM). The effect of various parameters individually as well as in combination were examined. The experimental parameters used as based on trial experiments and literature review in experimentation is given in Table 4.6.

Table 4.6 Experimental parameters

Parameters	Condition
Finishing cycle	40 min
Iron articles (30% by V)	400 mesh size
Silicon carbide (15% by V)	800 mesh size
Workpiece material	H13 Ferromagnetic

4.5.1 Selection of Process Parameters

For the experimentation, the parameters and their range were selected based on literature review and machine capability. It was found that magnitude of current plays a very vital role in the MR finishing process. Magnetic field strength is dependent on current intensity through electromagnetic coil [43]. Material with the hardness of 431 VHN has been finished with the MR finishing and machining parameters such as feed and tool rotation was selected for the experimentation [30]. Feed range was selected from 10-50 cm/min and tool rotation was

selected from 700-2300 rpm [30]. The contribution of workpiece rotation can be seen in the research done on cylindrical finishing [30]. On the basis of these findings, the process parameters and their ranges were selected as reported in Table 4.7.

Table 4.7 Process parameters for experimentation

Factors		Levels				
Representation	Description	-2	-1	0	1	2
I	Current(A)	1	2	3	4	5
T	Tool rotation (rpm)	700	1100	1500	1900	2300
F	Feed rate (cm/min)	10	20	30	40	50
W	Workpiece rotation (rpm)	60	80	100	120	140

4.5.2 Experimental Investigation for Determining the Percentage Change in Surface Roughness

To evaluate the effect of certain factors on response, response surface methodology (RSM) technique was used. For optimization of process, RSM uses statistical, mathematical and graphical techniques. In RSM the influence of several parameters are studied on response. In RSM the relationship between the variables and response is given by Eq.4.1 [47].

$$Z = f(I, T, F, W) \quad (4.1)$$

where z is the response and f is the response function and I,T,F,W represent current , tool rotation , tool feed rate and workpiece rotation respectively.

The influence of process parameters were studied by fitting the second order polynomial response surface in the Eq.4.2 [47].

Table 4.8 Experimental result after finishing the specimen pieces

Experiment number	Current (A)	Tool rotation (rpm)	Tool feed (cm/min)	Workpiece rotation (rpm)	Initial R_a (μm)	Final R_a (μm)	%6R_a
1	3	1500	10	100	0.46	0.16	65.21
2	4	1900	40	80	0.32	0.19	40.62
3	3	700	30	100	0.35	0.10	71.42
4	4	1100	20	120	0.35	0.15	57.14
5	3	1500	30	60	0.38	0.11	71.05
6	2	1900	40	120	0.42	0.23	45.23
7	2	1100	40	80	0.3	0.09	70
8	3	1500	30	140	0.34	0.13	61.76
9	4	1100	20	80	0.36	0.17	52.77
10	4	1900	20	80	0.41	0.21	48.78
11	3	1500	30	100	0.35	0.08	74.28
12	4	1900	20	120	0.49	0.23	53.06
13	2	1100	20	80	0.52	0.16	69.23
14	3	1500	30	100	0.3	0.07	76.66
15	3	1500	30	100	0.41	0.10	75.6
16	2	1100	40	120	0.33	0.16	51.51
17	2	1900	40	80	0.38	0.15	60.52
18	2	1100	20	120	0.39	0.16	58.97
19	3	1500	30	100	0.37	0.10	72.97
20	4	1100	40	120	0.4	0.20	50
21	3	2300	30	100	0.35	0.21	40
22	3	1500	50	100	0.28	0.10	64.28
23	4	1100	40	80	0.54	0.22	59.25
24	3	1500	30	100	0.33	0.09	72.72
25	4	1900	40	120	0.47	0.32	31.91
26	2	1900	20	80	0.34	0.14	58.88
27	1	1500	30	100	0.5	0.22	56
28	3	1500	30	100	0.31	0.08	74.19
29	5	1500	30	100	0.4	0.28	30

$$Z = \propto_0 + \sum_{i=1}^{k} \propto_i a_i + \sum_{i=1}^{k} \propto_i a_i^2 + \sum_i \sum_j \propto_i a_i z_i + \varepsilon \quad (4.2)$$

where Z is the response, a_i is the i^{th} process parameter, $\propto$ is regression coeffecient and ε is the residual measure from an experimental error.

The analysis was performed on the Design Expert 6.0.8. The central composite design was created for four factors with five levels. The performance of experiment was calculated in term of the surface roughness reduction percentage. As surface roughness values of workpieces were not same, the response was measured in the form of percentage change.

Table 4.9 ANOVA table obtained along with non-significant terms

Source	Sum of squares	Degree of freedom	Mean square	F-value	Prob>F	
Model	4778.59	14	341.33	18.65	<0.0001	Significant
I	700.61	1	700.61	38.29	<0.0001	
T	620.61	1	620.61	33.92	<0.0001	
F	118.79	1	118.79	6.49	0.0232	
W	175.15	1	175.15	9.57	0.0079	
I^2	2006.43	1	2006.43	109.66	<0.0001	
T^2	849.98	1	848.98	46.40	<0.0001	
F^2	302.60	1	302.60	16.54	0.0012	
W^2	218.63	1	218.63	11.95	0.0039	
IT	21.74	1	21.74	1.19	0.2941	
IF	7.83	1	7.83	0.43	0.5237	
IW	55.65	1	55.65	3.04	0.1031	
TF	86.96	1	86.96	4.75	0.0468	
TW	13.91	1	13.91	0.76	0.3979	
FW	125.22	1	125.22	6.84	0.0203	
Residual	256.17	14	18.30			
Lack of fit	208.67	9	23.19	2.44	0.1693	Not
Pure error	47.50	5	9.50			significant
Total	5034.76	28				

The measurement of the surface roughness of specimen pieces surface were done by using the Mitutoyo SJ-400 surftest with a cutoff length of 0.25mm. After performing the finishing operation, Eq.4.3 was used to calculate percentage change in surface roughness.

$$\%\Delta R_a = \frac{Initial\ Surface\ Roughness - Final\ Surface\ Roughness}{Initial\ Surface\ Roughness} \times 100 \qquad (4.3)$$

Analysis of variance (ANOVA) was performed on the experimental data given in Table 4.8. Regression analysis was performed to obtain a multi-regression model. The verification of the effectiveness of model generated at 95% confidence level was done by comparing F-value obtained in model to that of standard F value.

Table 4.10 ANOVA table obtained with significant terms

Source	Sum of squares	Degree of freedom	Mean square	F-Value	Prob>F	
Model	4664.97	14	341.33	18.65	<0.0001	Significant
I	733.36	1	700.61	38.29	<0.0001	
T	635	1	620.61	33.92	<0.0001	
F	126.30	1	118.79	6.49	0.0232	
W	177.36	1	175.15	9.57	0.0079	
I^2	2008.12	1	2006.43	109.66	<0.0001	
T^2	848.87	1	848.98	46.40	<0.0001	
F^2	301.99	1	302.60	16.54	0.0012	
W^2	218	1	218.63	11.95	0.0039	
TF	94.89	1	94.89	4.62	0.0455	
FW	135.80	1	135.80	6.61	0.0192	
Residual	369.79	18	20.54			
Lack of fit	322.29	13	24.79	2.61	0.1485	Not
Pure error	47.50	5	9.50			significant
Total	5034.76	28				
Std. Dev.	4.53	R-Squared	0.9266			
Mean	58.21	Adj R-Squared	0.8857			
Coeffecient of Variation (C.V)	7.79	Pred R-Squared	0.7640			
Press	1188.41	Adeq Precision	16.370			

On performing the ANOVA, Table 4.9 was obtained. It was found that p-value of model was less than 0.05 which is significant and p-value of lack of fit is greater than 0.05 which is not significant. In the table it was found that there are some terms whose p-value is greater than 0.05 which signifies these terms are non-significant. The IT, IF, IW and TW p-value is greater than 0.05 as can be seen from the Table 4.9.

The model is again developed by removing the non significant parameters given in Table 4.10. It was found that model value is less than 0.05 and lack of fit value is greater than 0.05. All the terms namely I, T, F, W,I^2, T^2, F^2, W^2, TF and FW p-value is less than 0.05. Other parameters such as R-square, R-square predicted and adequete precision. The R-square predicted measure how accurately the model is developed in measuring the value of response. For model to be accurate, the difference between the adj R-square and pedicted R-square must be less than 0.2. In this analysis, the difference between adj R-square and pred R-square value is 0.1714 which shows that our model is accurate. From the regression analysis, the regression Eq.4.4 is obtained.

$$\%\Delta R_a = -197.92 + 45.75521 \times I + 0.11039 \times T + 4.23737 \times F + 1.72969 \times W - 8.5755 \times I^2 - 3.484 \times T^2 - 0.033 \times F^2 - 7.06 \times W^2 - 6.36 \times TF - 0.0152FW \quad (4.4)$$

4.6 RESULTS AND DISCUSSION

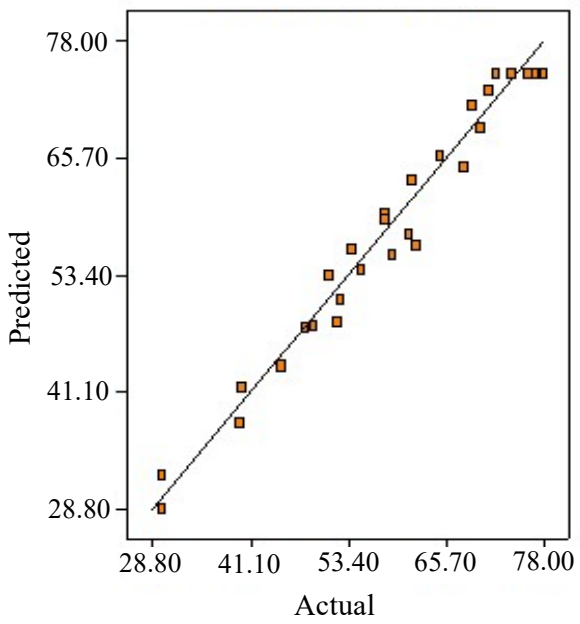

Figure 4.2 Variation between actual vs predicted value obtained from the experimental results

After regression analysis for percentage change in surface roughness, the result has to be summarized in the form of graphs and also have to check for the percentage contribution of each factor. The effect of all the significant parameters individually as well as in the form of interactions is discussed in this section. It can be seen from the Figure 4.2 that predicted values are in close relation with actual values which indicates that the obtained model is accurate enough to predict the percentage change in roughness for the given parameters.

4.6.1 Optimum Parameters

After the regression analysis, optimization of parameters was done to check for the best combination of parameters which gives the maximum percentage change in surface roughness value . After performing the optimization, Table 4.11 was attained which shows the condition under which the optimization has been performed.

Table 4.11 Condition under which optimization performed

Name	Goal	Lower limit	Upper limit	Lower weight	Upper weight	Importance
Current	in range	1	5	1	1	3
Tool rotation	in range	700	2300	1	1	3
Tool feed	in range	10	50	1	1	3
Workpiece rotation	in range	60	140	1	1	3
Response	Maximize	30	78	1	1	3

After obtaining the optimum parameters as given in Table 4.12 , graphs were plotted for individual and interaction effect by keeping three variable constant for individual graphs and two parameters for interaction graphs. The parameters that was kept constant was at optimum value.

Table 4.12 Result obtained after optimization

Solution					
Current (A)	Tool rotation (rpm)	Tool feed (cm/min)	Workpiece Rotation (rpm)	Response (%)	Desirability
2.67	1302.7	30.81	89.23	77.41	0.99

4.6.2 Percentage Contribution (%C) of Each Factor on Percentage Change in Surface Roughness

Percentage contribution tells about the percentage weightage of each factor in regression model of percentage change in surface roughness value. Percentage contribution was

calculated from the ANOVA Table (4.10), it is simply the ratio of sum of square (S.S.) of each factors to that of total sum of square (T.S.S.) is given in Eq.4.5.

$$\%C = \frac{S.S}{T.S.S} \times 100 \tag{4.5}$$

Percentage contribution for each factor is calculated as reported in Table 4.13. Pie-chart is used to display the percentage share of the each factors and their interaction on the response of experimentation as shown in Figure 4.3.

Table 4.13 Percentage contribution of each factors

Parameters	Sum of squares	Total sum of squares	Percentage contribution (%)
I	733.36	5034.76	14.56
T	635		12.61
F	126.3		2.50
W	177.36		3.522
I^2	2008.12		39.88
T^2	848.87		16.86
F^2	301.99		5.99
W^2	218		4.32
TF	94.89		1.88
FW	135.8		2.69

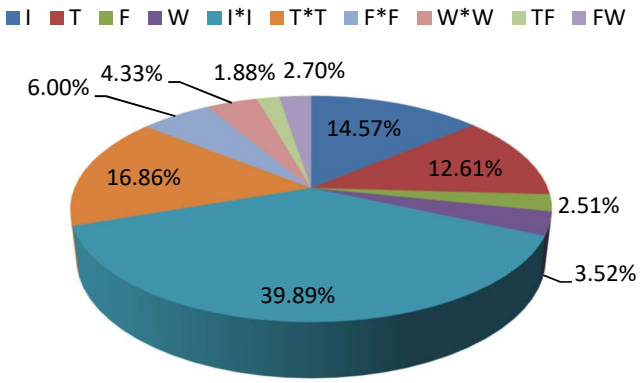

Figure 4.3 Pie-chart representing contribution of each factor on percentage change in surface roughness

4.6.3 Effect of Current (I) on the Percentage Change in Surface Roughness

The effect of magnetization current at tool rotation of 1300rpm, feed of 30cm/min and workpiece rotation of 89rpm is shown in Figure 4.4. Figure 4.4 shows that with increase in magnetization current the percentage change in surface roughness value increases up to an optimum value and then start decreasing. The main reason behind the variation of percentage

change in surface roughness with increasing current is due to the change of magnetic flux density in working gap. As the magnetizing current increases magnetic flux density also increases which results in increase in indentation force by abrasive particles on the workpiece surface. The resultant force obtained from this high indentation force and shear force acting on the abrasive particles is so high that it not only remove the roughness peaks but also remove the base of the material which results in pit formation [20]. Due to pit formation, there is decrease in percentage change in surface roughness. At low current below 2.6A, magnetic flux density is low. The resultant of forces at low current is not sufficient to form the pits on workpiece surface. This the main reason for obtaining an increase in percentage change in surface roughness at lower current as compared to current greater than 2.6A.

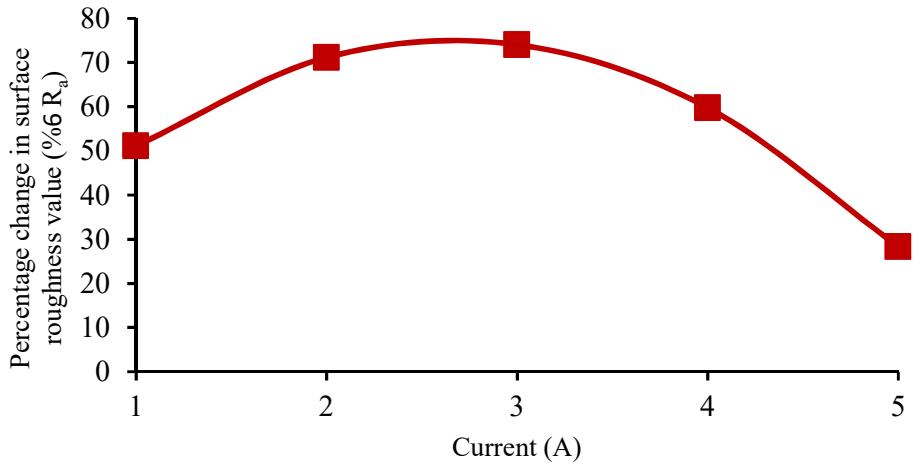

Figure 4.4 Effect of current on percentage change in surface roughness value

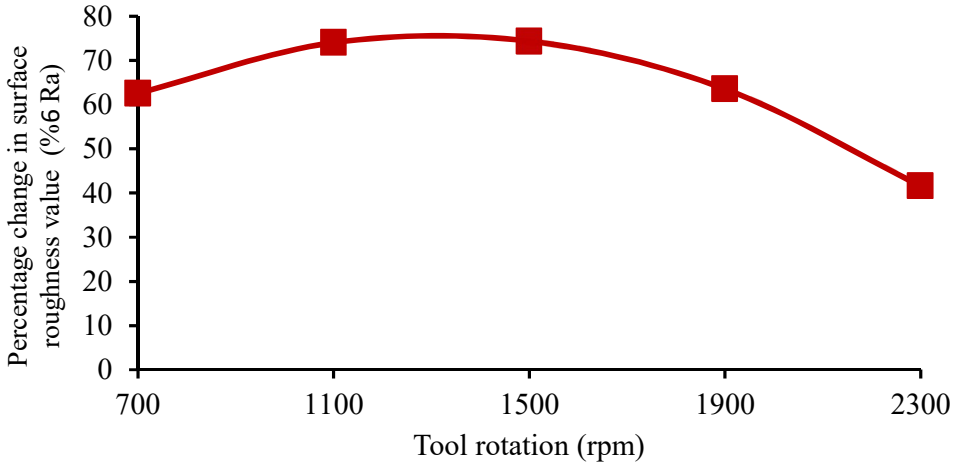

Figure 4.5 Effect of tool rotation on percentage change in surface roughness value

4.6.4 Effect of Tool Rotation (T) on Percentage Change in Surface Roughness

Figure 4.5 shows the effect of tool rotation at magnetization current of 2.6A, feed of 30cm/min and workpiece rotation of 89rpm. It was found that the percentage change in surface roughness value increases up to an optimum value and start decreasing. This type of variation in percentage change in surface roughness value is due to increase of centrifugal force acting on iron particles with increase in rotation of the tool [20]. The centrifugal force magnitude is not sufficient upto 1300 rpm, therefore percentage change in surface roughness increases. The centrifugal force acting on the iron particle chain increases beyond 1300 rpm, which reduces the effect of magnetizing force acting on iron particles in the working gap. Due to reduction of magnetizing force on iron particle in the working gap, the indentation force acting on the abrasive particles is reduced, which results in decrease in percentage change in surface roughness at high tool rotation.

4.6.5 Effect of Feed Rate of Tool (F) on Percentage Change in Surface Roughness

Figure 4.6 shows the effect of feed rate of tool at tool rotation of 1300rpm, magnetization current 2.6A and workpiece rotation of 89rpm. As the feed rate increases, the percentage change in surface roughness increases up to some extent and start decreasing as the feed rate increases. At feed rate of tool below 30cm/min, number of finishing cycles are increasing which results in increase of percentage change in surface roughness. Due to increase in number of finishing cycle, the collision between abrasives as well as roughness peaks increases. The stresses are being developed in MR fluid column. Beyond tool feed of 30cm/min, interaction between abrasive particles and roughness peaks increases up to such an extent that stresses induced in the MR polishing fluid column crosses the yield stress point for fluid column. Deformation of MR fluid column take place [16]. Due to deformation of iron particle chain, active abrasives are not able to remove the peaks more effectively as that at low feed rate.

4.6.6 Effect of Workpiece Rotation (W) on Percentage Change in Surface Roughness

Figure 4.7 shows the effect of workpiece rotation at tool rotation of 1300 rpm, magnetization current of 2.6A and tool feed rate of 30cm/min. As the workpiece rotation increases, the number of roughness peaks passing through the region of active abrasive particles increases. This results in increase of stresses induced in MR polishing fluid column due to increase in collision of peaks and abrasives. Beyond the value of 80rpm, the stress induced in the MR polishing fluid column crosses the yield stress point of MR polishing fluid column. Deformation of MR polishing fluid column take place [16]. That's why the active abrasives

attached to the iron particle chain not able to finish effectively as compared to that at low workpiece rotation.

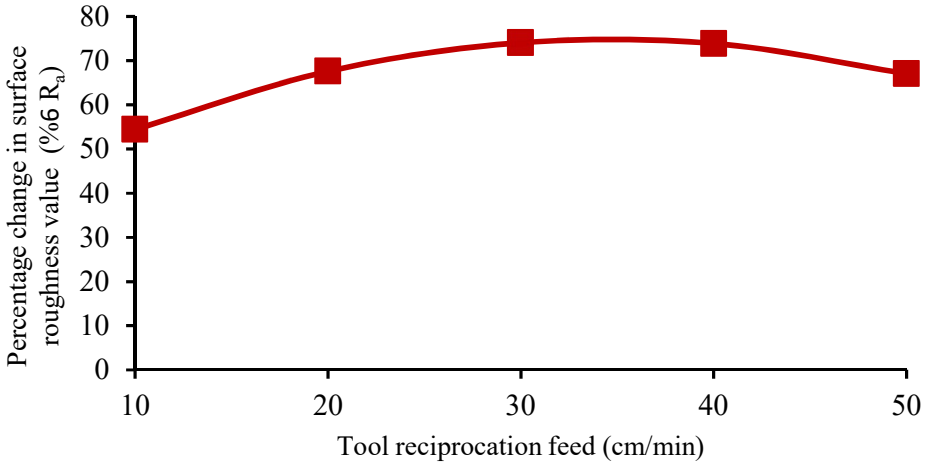

Figure 4.6 Effect of tool reciprocation feed on percentage change in surface roughness value

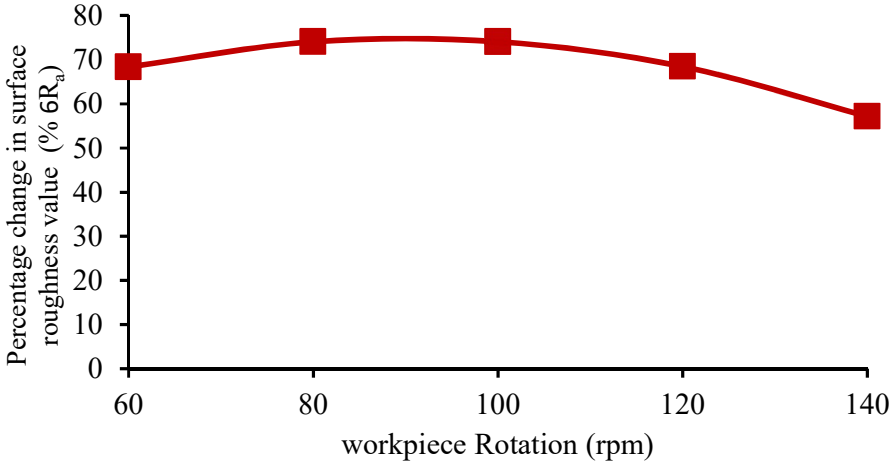

Figure 4.7 Effect of workpiece rotation on percentage change in surface roughness value

4.6.7 Effect of Interaction between Workpiece Rotation and Tool Reciprocation

Figure 4.8 represent the percentage change in surface roughness with respect to tool feed and tool rotation for current of 2.6A and tool rotation of 1300rpm. The percentage change in surface roughness for individual effect of feed rate of tool increases upto 30cm/min and start decreasing afterwards. It can be seen from the Fig.4.8 that optimum value of tool feed rate for percentage change in surface roughness shifts after interaction. For workpiece rotation of 140rpm, the optimum value of percentage change in surface roughness shifts to 20cm/min tool feed. The reason for this change is that at high workpiece rotation, deformation of MR polishing fluid column take place. Domination of this effect results in shifting of optimum feed rate. For workpiece rotation of 60rpm, the optimum feed rate shifts to 40cm/min. The shifting is due to reduction in collision of abrasive particles with roughness peaks due to

which deformation reduces. The optimum value of feed rate doesn't shift much for 100rpm and 80rpm worpiece rotation because optimum value for individual effect of workpiece rotation was 89rpm.

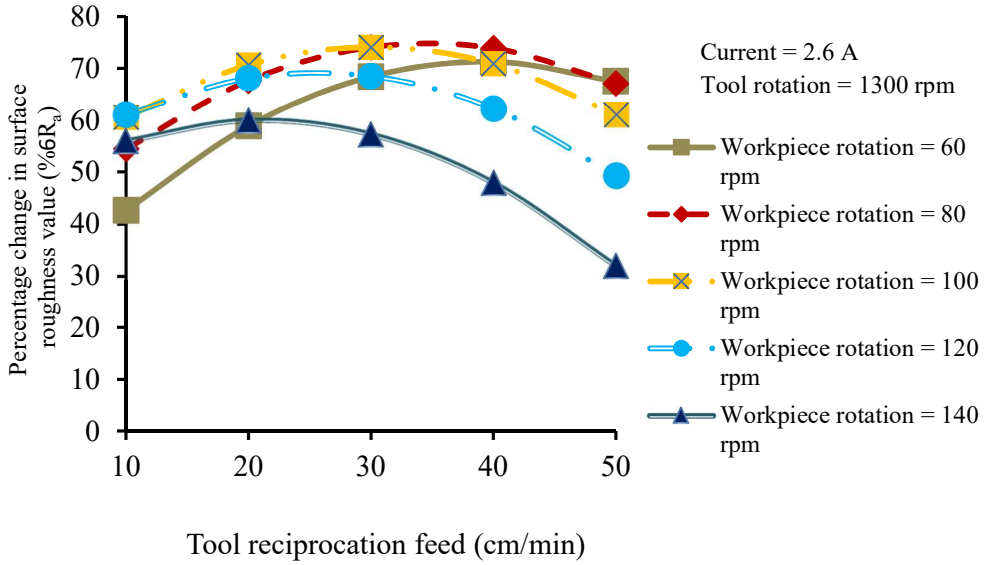

Figure 4.8 Variation of percentage change in surface roughness for tool reciprocating feed and workpiece rotation

4.6.8 Effect of Interaction between Tool Rotation and Tool Reciprocation

Figure 4.9 represent the percentage change in surface roughness with respect to tool feed and tool rotation for current of 2.6A and workpiece rotation of 89 rpm. The percentage change in

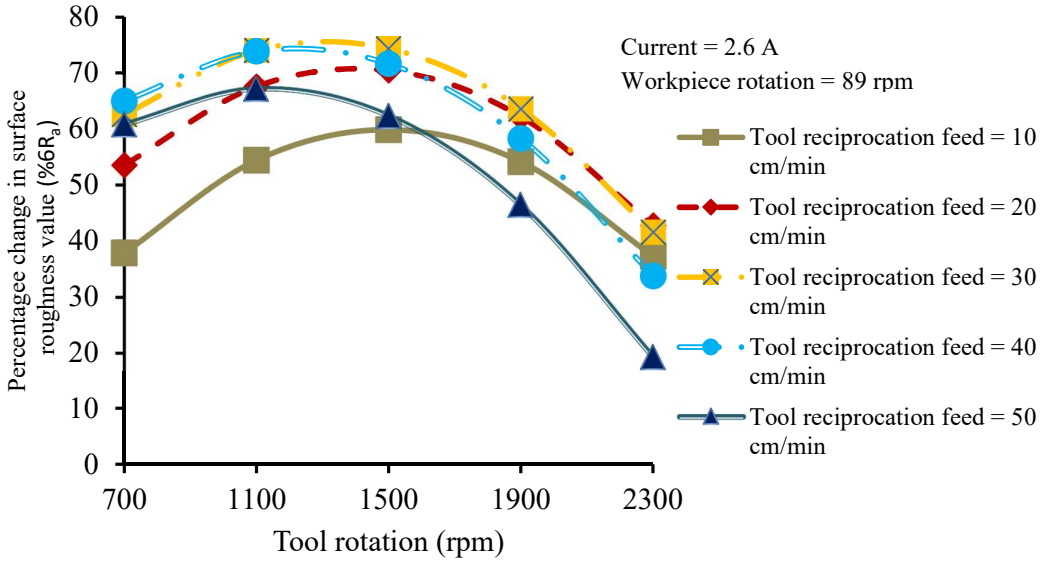

Figure 4.9 Variation of percentage change in surface roughness for tool rotation and tool reciprocating feed

surface roughness for individual effect of tool rotation increases up to 1300rpm and start decreasing afterwards. It can be seen from Fig.4.9 that optimum value of tool rotation for percentage change in surface roughness shifts after interaction. For tool reciprocating feed of 50 cm/min, the optimum value of tool rotation shifts to 1100rpm. The reason for this behavior is that as the tool feed increases, interaction between the abrasive particles and surface roughness increases. Domination of this effect results in shifting of optimum value for tool rotation. For tool reciprocating feed value of 10cm/min, the optimum value of tool rotation shifts to 1500 rpm. The shifting is due to reduction in number of cycles which results in decreasing of collision of abrasive particle with roughness peaks. Domination of this factor results in increasing of optimum too rotation to 1500rpm. For tool reciprocating feed of 20cm/min and 30cm/min, optimum value of feed doesn't shift much because optimum value for individual effect of tool reciprocating feed was 30cm/min.

4.7 CONFIRMATORY TEST FOR REGRESSION MODEL VALIDATION

In this section, the confirmatory test was carried out for checking the model accuracy. Three experiment were performed for optimum parameters. The percentage change in surface roughness was measured after experimentation and calculated theoretically from the regression Eq.4.4 as given in Table 4.14. It can be seen that percentage error between the theoretical and experimental observation is in the range of -2.49% to 3.02%, which shows the good agreement between regression and experimental model. In this investigation the response was percentage change in surface roughness which has to be maximized. After regression analysis, the optimization of response was done on design-expert 6.0.8. It was found that optimized parameters were 2.6A current, 1300rpm tool rotation, 30cm/min tool feed and 89 rpm workpiece rotation.

Table 4.14 Confirmatory test with optimum parameters

Time (min)	Current (A)	Tool rotation (rpm)	Tool reciprocation (cm/min)	Workpiece rotation (rpm)	Experimental %6Ra	Predicted %6Ra	Error %
40	2.6	1300	30	89	79.62	77.21	3.02
40	2.6	1300	30	89	76.74	77.21	-0.61
40	2.6	1300	30	89	75.33	77.21	-2.49

An experiment was performed using optimized parameter and surface roughness was reduced from 0.38 to 0.05 in 50 minutes as shown in Figure 4.10. The surface roughness was checked after 10 minutes interval during its 60 minute finishing.

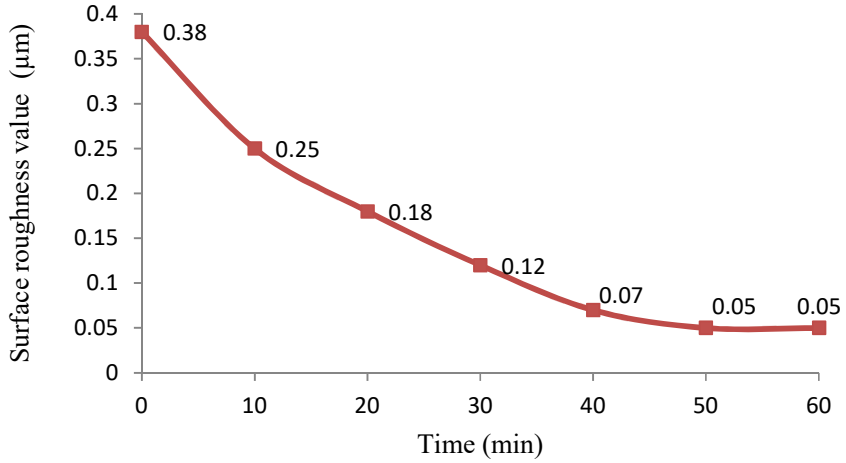

Figure 4.10 Rate of change of surface roughness value with respect to time using optimum parameters

After selecting the optimum process parameters (current = 2.6 A, tool rotation = 1300 rpm, tool reciprocating feed = 30 cm/min and workpiece rotation = 89 rpm), the MR finishing has been performed on the actual extrusion punch. The MR finishing of the extrusion punch was done on a designed fixture using optimum parameters.

4.8 EXPERIMENTATION ON INDUSTRIAL EXTRUSION PUNCH

In the suspension system of an automobile, spindle carries hub and attaches to the steering knuckle. It is the main link which connects the wheel to the steering knuckle. So it has to be dynamically as well as statically stable [48]. For better stability, suitable material is selected which is hardened and tempered for appropriate combination of hardness, strength and toughness. The main process to produce spindle nowadays is extrusion. In extrusion, permanent moulds are used for forming a spindle**.** In extrusion, end product is obtained by heating the metallic billet upto the recrystallization temperature, extrusion punch compresses the hot billet, then the billet plastically deform and flow along the gap between punch and cavity block to get the final shape. The finishing of punch is very much demanded nowadays in industry due to the defects associated with surface roughness in extrusion process. The defects associated with surface roughness are heterogeneity in final product, excessive use of power to overcome the friction loss [36]. Among all these mechanisms, mechanical wear mechanism plays the main role [36]. Factors influencing wear of dies are sliding distance, surface finish, contact area, shape and type of motion [35]. The two factors influencing extrusion flow pattern are die-billet-container friction and billet thermal gradient [36]. It was found that extrusion forces increases up to 0.35 coefficient of friction for 13% and 25% reduction of area. Whereas, there was no significant change after 0.2 coefficient of friction

for 37% to 48% reduction of area [38]. Generally, the process of finishing is done traditionally on die grinders [30], and thus the process has a requirement of very high skill level. Moreover, the materials used for moulds manufacturing are very hard , so finishing of moulds become a very tedious task [30].

4.8.1 Forming of Spindle

In industry, the spindle is produced by hot extrusion in three stages by a vertical press. The billet before extrusion has to be passed through pre-processing as shown in Figure 4.11. The billets are received in the form of long rods. These billets are cut to the required length for extrusion. After cutting these billets are passed through the induction heater. Induction heater heat the billets upto the temperature of 1150^0 C to 1200^0 C. Before passing on to the next station, the billets which are not heated to these temperature are removed from the conveyor. Thermal sensors are placed at the exit of the heater exit to detect the temperature of billet. Heating upto such a high temperature results in scaling on the surface of the billet surface . The scaling on the billet surface is removed by water jets on the next station. These billets are then placed in the three stage on vertical press by the robotic arms shown in Fig.4.12. The extrusion punch before piercing in the billet is lubricated by glass lubricant at all three stages of extrusion. In the first stage, the extrusion punch pierced to some length through billet placed in the mould. The piston at the bottom of the container pushes the billet which is taken to the next station by the robotic arm. In the second stage punch pierce the billet upto the half of length and lastly at stage 3, the punch pierce completely through the billet. The spindle produced is pushed by the piston at bottom of the container. Each time extrusion punch after operation is cooled by water jets and air jets before extrusion of next billet. The spindle is then placed on the conveyor by the robotic arms for further processing. The spindle formed by extrusion is passed for the heat treatment processes.

4.8.2 Extrusion Punch

Extrusion punch is made of H13 material. H13 material is used because of its capability to have the good fracture toughness and hardness at elevated temperature. The thermal resistance and hardenability of H13 material is high due to the presence of chromium and molybdenum. The composition of H13 material is given in Table 4.15. The extrusion punch is a cylindrical billet in raw form. It is machined to its final shape (Figure 4.13) by various machining processes (turning, facing, centering) and heat treatment processes. The extrusion punch is hardened upto 42-46 HRC. The surface roughness obtained after grinding operation has been obtained of 0.48μm.

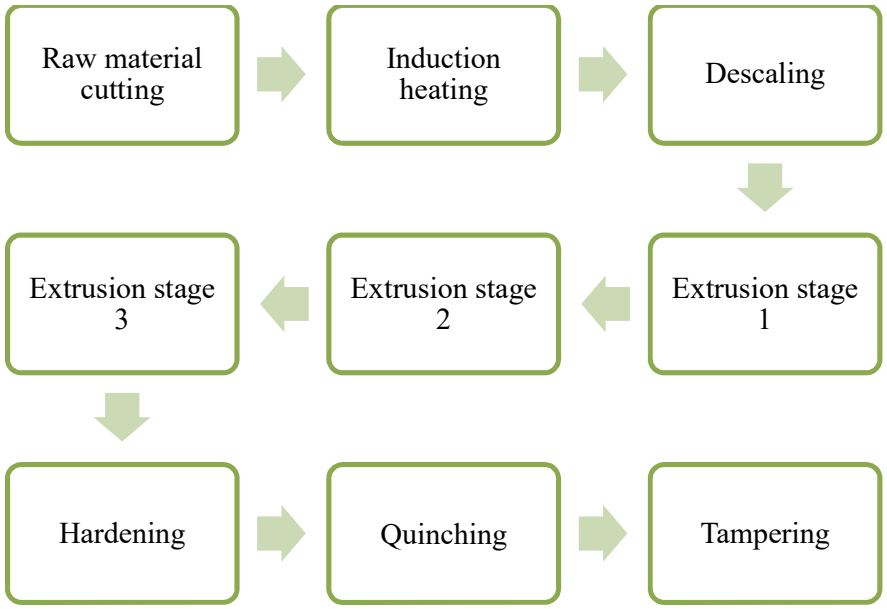

Figure 4.11 Processing chart for spindle

Figure 4.12 Extrusion press

4.8.3 Calculation of Time Based on the Aforesaid Experiment to Perform Experimentation on Actual Extrusion Punch

The time required for the finishing of the industrial extrusion punch was calculated by scaling out the time for the specimen cylindrical shaft specimen. An experiment was performed on the cylindrical shaft (Figure 4.14(a)) at optimum parameters as obtained in

Table.4.15 Composition of AISI H13 steel [46]

Element	Composition(%)
Carbon , (C)	0.32 - 0.40
Chromium, (Cr)	5.13 - 5.25
Iron, (Fe)	>=90.95
Molybdenum, (Mo)	1.33 - 1.4
Silicon, (Si)	1.0
Vanadium, (V)	1.0

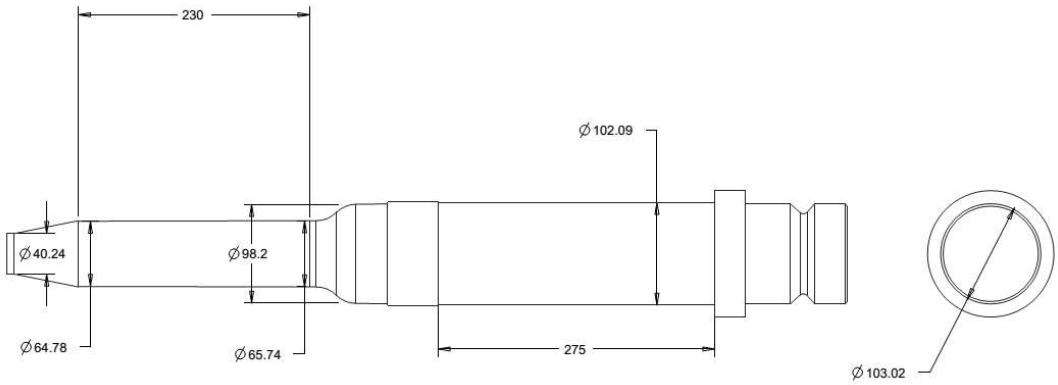

Figure 4.13 Schematic of extrusion punch (all dimensions in mm)

aforesaid experimentation (Table 4.12). The experiment was performed for 50 minutes. After the experimentation, surface roughness was checked on the mitutoyo SJ-400 surftest. Figure 4.14 (b), the surface roughness was reduced to 30 nm from 480 nm. The scaling of the extrusion punch was done for 30 nm surface roughness in 50 minutes. Figure 4.15 shows the working area during experimentation of cylinderical specimen. The finished surface area of the specimen calculated from the Figure 4.15 using Eq.4.6.

$$A_1 = \pi AL \quad (4.6)$$

For A = 25 mm and L = 20 mm,

Then value of A_1 is calculated as given in Eq.4.7.

$$A_1 = 1570\text{mm}^2 \quad (4.7)$$

Figure 4.16 shows the working area of the extrusion punch. The surface area of the extrusion punch A_2 calculated from Figure 4.16 using Eq.4.8.

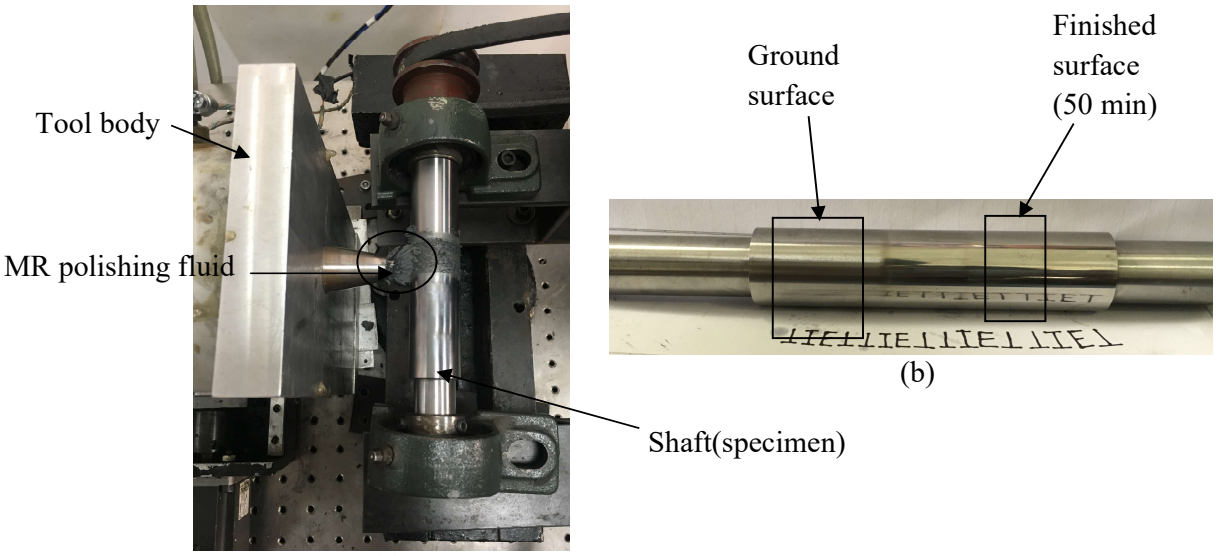

Figure 4.14 (a) Experimentation on AISI H13 steel cylindrical workpiece surface to be used for time scaling, to perform the experiment on actual extrusion punch AISI H13 steel (b) mirror testing of finished surface

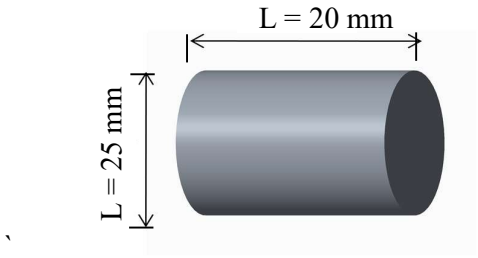

Figure 4.15 Finishing surface dimensions of cylindrical workpiece

$$A_2 = \frac{1}{2}(\pi B + \pi C)L \qquad (4.8)$$

For B = 64.78 mm , C = 65.74 mm and L = 230 mm.

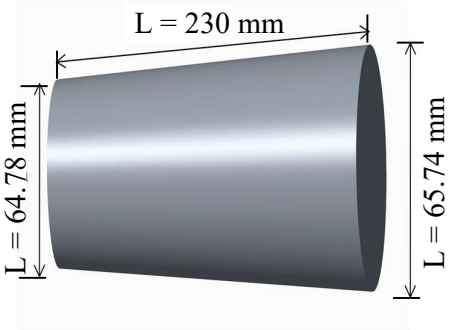

Figure 4.16 Dimensions of the cylindrical extrusion punch surface area to be used for MR finishing

Then value of A_2 is calculated as given in Eq.4.9.

$$A_2 = 47154 \text{ mm}^2 \quad (4.9)$$

Calculation of surface roughness shows that time taken to finish the cylindrical specimen surface area (A_1) is taken 50 minutes. Therefore, to finish the surface area (A_2) of the extrusion punch as shown in Figure 4.16 for achieving surface roughness value of 30 nm, finishing time was calculated as 25 hrs.

4.8.4 Experimentation

Optimum parameters for experimentation of H13 steel was obtained from parametric study. Time required for finishing of industrial extrusion punch was calculated as 25 hrs. The experimentation of the industrial punch was done on the fixture setup shown in Figure 4.17(a).

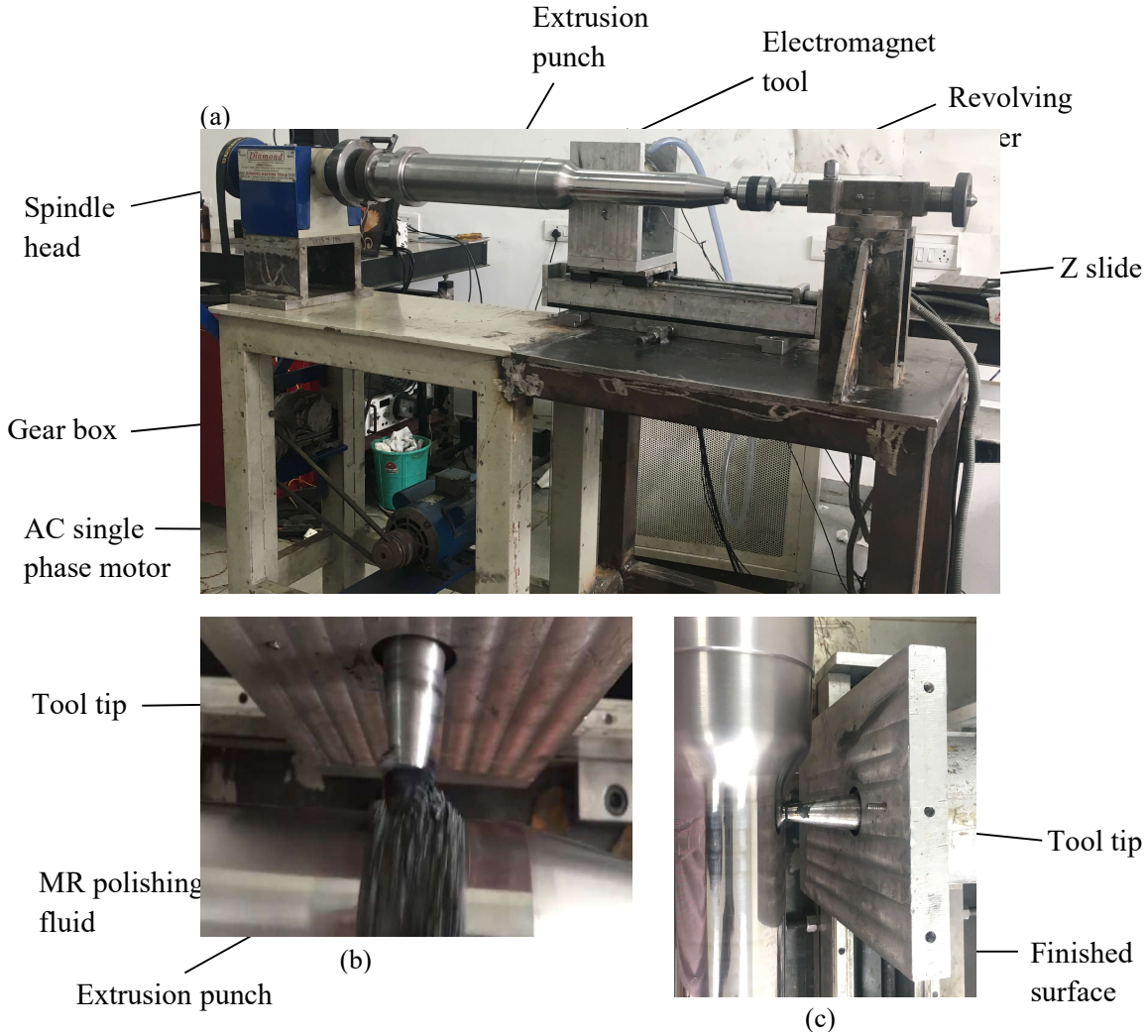

Figure 4.17 MR finishing process for extrusion punch (a) experimental set up, (b) MR polishing fluid between tool and workpiece and (c) Finished punch surface area

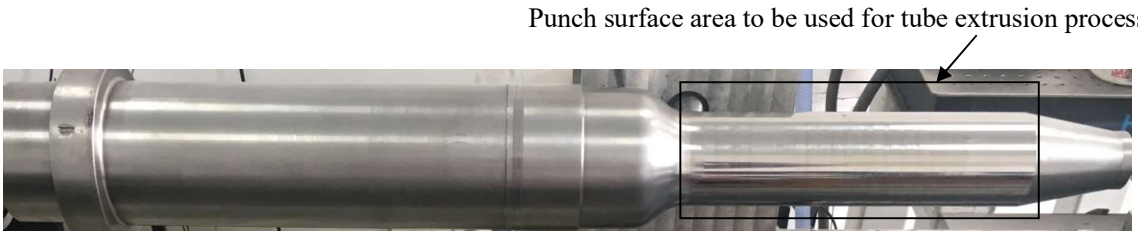

Figure 4.18 Working surface area for finishing of extrusion punch using MR fluid based finishing process

The fixture setup was designed and fabricated for the finishing of the extrusion punch surface area. Figure 4.17(a) shows that the workpiece was held between the revolving centers at both the end of the setup. The workpiece was rotated by the 1Hp single phase AC motor. AC motor was having the fix rpm of 1440. Motor rpm was reduced to 90 rpm by the use of gear box and belt drive which is equal to the optimum rpm as obtained from the experimental analysis. The workpiece was rotating with the run-out less than 5µm. The run-out was measured using the dial gauge. The tool was reciprocating on the horizontal Z slide shown in Figure 4.17(a). Figure 4.17(b) shows the finishing of punch surface by MR polishing fluid. Figure 4.17(c) shows the finished punch surface obtained after the present MR finishing process. The movement of tool was set for 7mm. The workpiece was finished by distributing the 230 mm working length in to small length of 7mm. Figure 4.18 shows the working area finshed to nano level range by using MR fluid based finishing process. The working length of the workpiece is in taper which was eliminated by setting the Z slide axis parallel to axis of the workpiece. The experiment was performed on the 6 mm region for 40 minute with 20 minute interval for changing the MR polishing fluid. 0.6 mm gap was maintained between tool and workpiece.

4.9 RESULTS AND DISCUSSION

After the experimentation, the improvement in surface characteristics of the extrusion punch was diagnosed. The reduction in surface roughness as well as improvement in surface quality (SEM image) were obtained. The extrusion punch was taken to industry to check the effect of surface finish improvement in the extrusion process.

4.9.1 Surface Characteristics of Extrusion Punch

After the experimentation, improvement in surface roughness was measured using mitutoyo SJ-400. The roughness profiles are shown in Figure 4.19. R_a value of the extrusion punch surface was reduced from 480 nm to 70 nm in 25 hrs. The mirror image of extrusion punch surface before and after MR finishing shown in Figure 4.20.

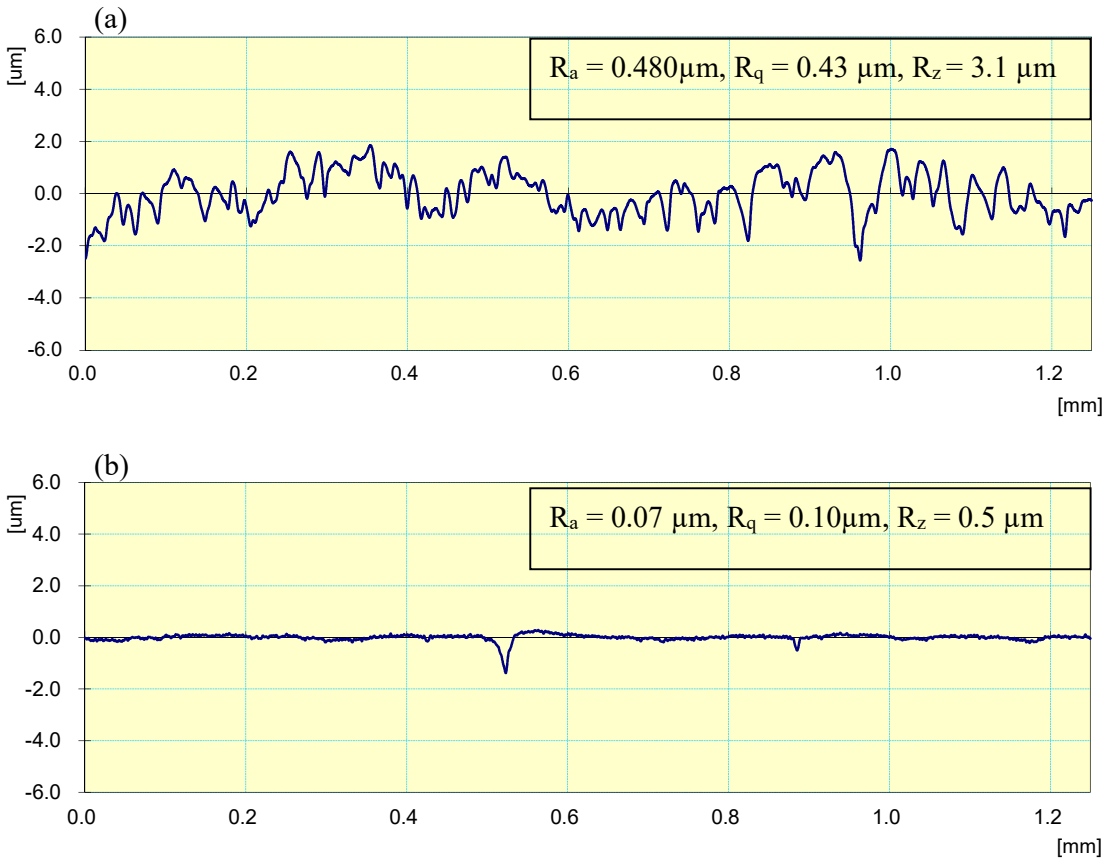

Figure 4.19 Surface roughness profile (a) grinded initial surface and (b) MR finished surface after 25 hrs of finishing

Scan electron microscopy (SEM) images shown in Figure 4.21 (a) and (b). From Figure 4.21 (b) it can be seen that grinding lays has been removed and a smooth surface is obtained. Due to improvement in texture of surface, material can flow easily along the surface.

4.9.2 Improvement in Extrusion Process

The punch after finishing was taken to industry to check for the performance in the extrusion process. Before loading the punch on the vertical press as shown in Figure 4.12, the punch was machined to make the die angle. The punch was loaded on the press. To check the effect of surface roughness improvement of punch, stage 1 was analyzed. The power consumption was measured with the help of clamp multimeter. Motor is attached to the pump responsible for discharging the hydraulic oil to the press. The discharged hydraulic oil by pump make the extrusion punch holder to move while operation. The power consumption of the motor was checked using multimeter. Current reduction was reduced to 39A from 52A for the single cycle. It take 2 minutes to complete the single cycle of stage1. The reduction in current consumption shows the reduction of friction forces. Generally 3300 to 3500 spindles are formed in stage 1 using grinded extrusion punch. After MR finishing, extrusion punch was

tested in industry for life. Extrusion punch was cracked and worn out after extruding 3515 spindles. There is an improvement in the life of the extrusion punch.

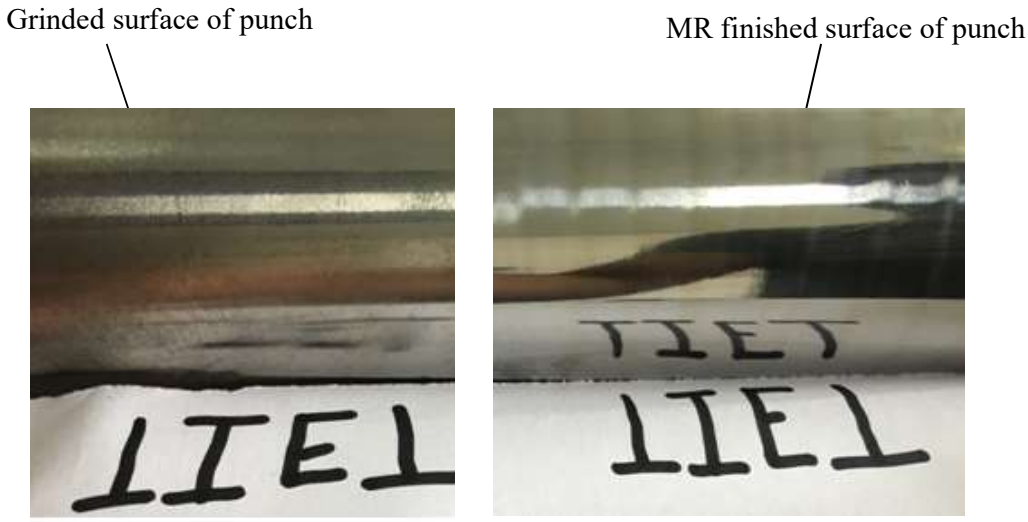

(a) (b)

Figure 4.20 Mirror image of punch surface (a) before finishing and (b) after MR finishing

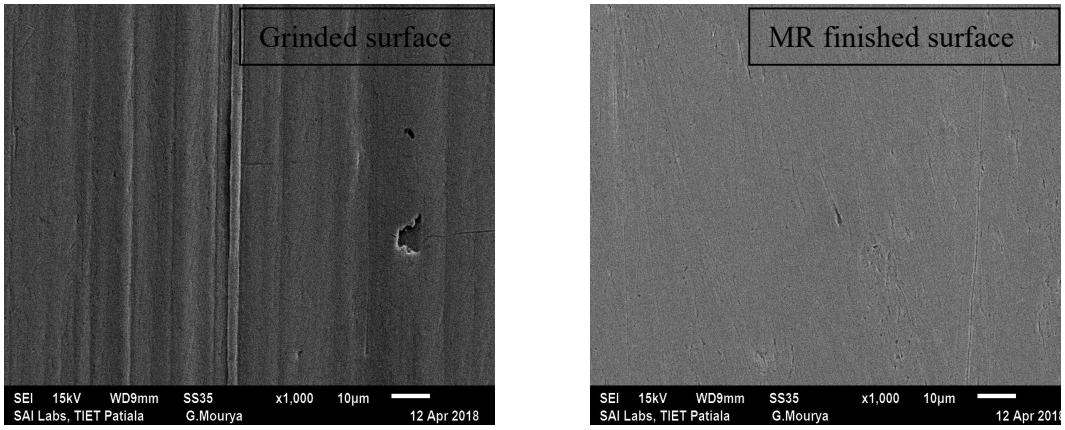

(a) (b)

Figure 4.21 Scan electron microscopy (SEM) images (a) before MR finishing and (b) after MR finishing

4.10 CONCLUSIONS

The parametric study for the H13 die steel material was carried out. Response surface methodology with central composite design has been used to statistically design the experiment and analyze the effect of various parameters on percentage change in surface roughness. Optimized parameters were obtained through RSM. Optimum parameters were used to finish the actual extrusion punch on the fabricated fixture (Fig.4.16). After MR finishing, the extrusion punch surface characteristics were compared to the grinded surface. Extrusion punch was taken to industry to analyze the change in extrusion process after improvement in surface finish.

- The regression analysis revealed that current played the major role in finishing the H13 die steel material. The contribution of current was found as 14.57% contribution of current as compared to 12.61%, 2.50% and 3.522% for tool rotation, tool reciprocation feed and workpiece rotation respectively on surface roughness value.
- The optimum parameters are predicted as current 2.6 A, tool rotation 1300 rpm, workpiece rotation 89 rpm and tool reciprocating feed 30 cm/min.
- The surface roughness value of the specimen was reduced to 50 nm from 380 nm in 50 minutes while finishing performed with optimum parameters.
- After performing the confirmatory test for regression model, the percentage error between the theoretical model observations and experimental observations was found in the range of -2.49 to 3.02 %. The range of percentage error showed good agreement between theoretical as well as experimental data.
- The surface roughness of the finished industrial punch surface reduced to 70 nm from 480nm in 25 hr. SEM images showed the great improvement in surface quality of punch. The surface become smooth after the removal of grinding lays.
- The reduction in surface roughness value from 480 nm to 70 nm after the present MR finishing process on the extrusion punch surface resulted in decrease of current consumption of the press from 52 A to 39 A as compared to grinded punch surface.
- Also the present MR finished surface of the punch were capable to extrude 15 spindles more as compared to the highest obtained earlier using grinded punch surface.

CHAPTER 5

CONCLUSION AND FUTURE SCOPE

In this chapter, the results obtained after mathematical modelling, parametric study of process parameters and testing of extrusion punch are discussed.

5.1 CONCLUSIONS

- Magnetic flux density was obtained as 0.707 T at tool tip surface and decreases linearly to 0.69 T towards the surface of cylindrical punch workpiece surface.
- Indentation force acting on abrasive particles is affected by the magnetic flux in the working gap and size of magnetic iron particles in the working gap.
- The designed fixture in the experimental setup ensured the accurate movement of magnetic tool in finishing of industrial extrusion cylindrical punch surface.
- Percentage error between the results from the theoretically calculated surface roughness value and experimental data ranges from 1.25% to 6.79%. The percentage error (6.79%) is due to assumption made during theoretical calculation of surface roughness value.
- The regression analysis revealed that current play the major role in finishing the H13 die steel material. The contribution of current was founded 14.75% as compared to 12.61%, 2.50% and 3.522% for tool rotation, tool reciprocation feed and workpiece rotation respectively in reduction of surface roughness value.
- The optimum parameters are predicted as current 2.6 A, tool rotation 1300 rpm, workpiece rotation 89 rpm,and tool reciprocating feed 30 cm/min.
- The Surface roughness value of the specimen was reduced to 50 nm from 380 nm in 50 minutes while finishing performed with optimum parameters.
- After performing the confirmatory test for regression model, the percentage error between the theoretical model observations and experimental observations was found in the range of 2.49% to 3.02 %. The range of percentage error showed good agreement between theoretical as well as experimental data.
- The surface roughness of the finished industrial punch surface reduced to 70 nm from 480nm in 25 hrs. SEM images showed the great improvement in surface quality of punch. The surface became smooth after the removal of grinding lays.
- The reduction in surface roughness value from 480 nm to 70 nm after the present MR finishing process on the extrusion punch surface resulted in decrease of current consumption of the press from 52 A to 39 A as compared to grinded punch surface.

- Also the present MR finished surface of the punch were capable to extrude 15 spindles more as compared to the highest obtained earlier using grinded punch surface.

5.2 FUTURE SCOPE

- While developing the model for surface roughness, rotation of tool has no effect on the surface roughness reduction. The main reason for this behaviour is neglecting of centrifugal force on abrasives as well as iron particles. Percentage error can be reduced by eliminating the assumptions of the model.
- While performing the parametric experiment on H13 material, the colour of the surface changes to brown on reducing the gap. This change in characteristics needs to be further analyzed. The surface roughness was not reduced even after 40 minutes of operation.
- Tool design was altered to reduce the finishing time by attaching the permanent magnet along with electromagnet. Disc shape magnet was used. There was no effect on the surface roughness. The main reason was working gap was varying between the flat disc magnet and cylindrical workpiece. The permanent magnet with curvature should be used to maintain the working gap.
- Time taken to finish the extrusion punch was 25 hrs. Time for finishing can be reduced by using two electromagnetic tool .
- The reduction in surface roughness results in low power consumption. The mould through which the billet flow plastically should be finished as well to increase the efficiency of the process.

REFERENCES

[1] Jain V.K (2008). An abrasive based nano finishing techniques : an overview, *Machining Science and Technology*, 12:3, 257–294.

[2] Samaria-al R.A, Haftirman, Ahmed K.R and Al-douri Y (2012). The influence of roughness on the wear and friction coefficient under dry and lubricated sliding, *International Journal of Scientific and Engineering Research*, 3, 1–6.

[3] Farago F.T. *Abrasive Methods Engineering*. New York: Industrial Press Inc., 1980.

[4] Zhang X, Wang X, Wang D, Yao Z, Xi L and Wang X (2017). Methodology to improve the cylindricity of engine cylinder bore by honing, *Journal of Manufacturing Science and Technology*,139, 1–10.

[5] Jain V.K. *Nano Finishing Science and Technology: Basic and Advanced Finishing and Polishing Processes*. CRC Press, 2016.

[6] Gostimorvic M, Rodic D, Kovac , Jesic D and Kulundzik N (2015). Investigation of the cutting forces in creep freed surface grinding process, *Journal of Production Engineering,* 8(2).

[7] Jiao F and Zhao B (2017). Research on ultrasonic-assisted fixed-abrasive lapping technology for engineering ceramics cylindrical part, *Journal of Micro- and nano-finishing*, 5, 1–7.

[8] Jain V.K. (2009). Magnetic field assisted abrasive based micro- / nano-finishing, *Journal of Materials Processing Technology,* 209, 6022–6038.

[9] Rhoades L.J. (1988) Abrasive flow machining, *Manufacturing Engineering*, 28, 107–116.

[10] Jha S and Jain V.K. (2004). Design and development of the magnetorheological abrasive flow finishing process, *Machine Tool and Manufacture*, 44, 1019–1029.

[11] Kordonski W.I. (1996). Magnetorheological finishing, *International Journal of Modern Physics B*, 10(23–24), 2837–2849.

[12] Hayashi Y, Nakajima T and Kunio T (2001). Ultra-uniform chemical mechanical polishing (CMP) using a hydro chuck featured by wafer mounting on a quartz

glass plate with fully flat water supported surface, *Japanese Journal of Applied Physics*, 35, 1054–1059.

[13] Nanz G and Camilletti L.E. (1995). Modelling of chemical-mechanical polishing: A review, *IEEE Trans. on Semiconductor Manufacturing*, 8, 382–389.

[14] Komanduri *R,* Lucca D.A and Tani Y (1997). Technological advances in fine abrasive processes, *Annals of CIRP*, 46(2), 545–596.

[15] Tsuwa H, Ikawa N and Sugiyama M.Y (1979). Numerically controlled elastic emission machining, *Annals of CIRP*, 28(1), 193–197.

[16] Sidpara A, Das M and Jain V.K (2009). Rheological characterization of magnetorheological finishing fluid, *Materials and Manufacturing Process*, 24, 1467–1478.

[17] Pintaude, G. Characteristics of abrasive particles and their implications on wear . Available at (https://www.researchgate.net/publication/221912389) (Accesed 12th January 2018)

[18] Singh A.K, Jha S and Pandey P.M (2013). Mechanism of material removal in ball end magnetorheological finishing process, *Wear*, 302, 1180–1191.

[19] Singh M, Singh A and Singh A.K (2017). A rotating core based magnetorheological nano- finishing process for external cylindrical surfaces, *Material and Manufacturing processes,* 33, 1160–1168.

[20] Maan S and Singh A.K (2017). Nano surface finishing of hardened AISI 52100 using magnetorheological solid core rotating tool, *International Journal of Advanced Manufacturing Technology*, 95, 513–526.

[21] Judal K.B, Yadava V and Pathak D (2014). Experimental investigation of vibration assisted cylindrical – magnetic abrasive finishing of aluminum workpiece, *Materials and Manufacturing Processes,* 28, 1196–1202.

[22] Jung B, Jung K.I, Min B.K, Lee S.J and Seok J (2009). Magnetorheological finishing process for hard materials using sintered iron-CNT compound abrasives, *International Journal of Machine Tools and Manufacture,* 49, 407–418.

[23] Song W.L, Choi S.B, Cai Q.C Choi J.Y and Lee C.H (2011). Finishing performance of magneto-rheological fluid under magnetic field finishing, *Mechanics of Advanced Materials and structures,* 20:7, 529–535.

[24] Wang J, Chen W, and Han F (2015). Study on the magnetorheological finishing method for the WEDMed pierced die cavity, *International Journal of Advanced Manufacturing Technologies,* 76:1, 1969–1975.

[25] Wang Y, Zhang Y and Feng Z (2016). Applied surface science analyzing and improving surface texture by dual-rotation magnetorheological finishing, *Applied Surface Science,* 360, 224–233.

[26] Singh D.K, Jain V.K and Raghuram V (2005). On the performance analysis of flexible magnetic abrasive brush, *Machining Science and Technology*, 9, 601–619.

[27] Jayswal S.C, Jain V.K and Dixit P.M (2005). Modeling and simulation of magnetic abrasive finishing, *International Journal of Advanced Manufacturing Technologies,* 26, 477–490.

[28] Singh A.K, Jha S, and Pandey P.M (2013). Mechanism of material removal in ball end magnetorheological finishing process, *Wear*, 302, 1180–1191.

[29] Sidpara A and Jain V.K (2013). Analysis of forces on the freeform surface in magnetorheological fluid based finishing process, *International Journal of Machine Tools and Manufacturing,* 69,1–10.

[30] Maan S, Singh G, and Singh A.K (2017). Nano-surface-finishing of permanent mold punch using magnetorheological fluid-based finishing processes, *Material and Manufacturing Processes,* 32,1004–1010.

[31] Bedi T.S and Singh A.K (2017). Magnetorheological finishing of ferromagnetic blind-hole type surfaces, *Material and Manufacturing Processes*, 33, 1169–1176.

[32] Bedi T.S and Singh A.K (2017). Development of magnetorheological fluid-based process for finishing of ferromagnetic cylindrical workpiece, *Machining Science and Technology,* 22, 120–146.

[33] Ohmori H, Li W, Makinouchi A and Bandyopadhya B.P (2000). Effecient and precision grinding of small hard and brittle cylindrical parts by the centerless grinding process combined with electro-discharge truing and electrolytic in-process dressing, *Journal of Materials Processing Technology,* 98, 322–327.

[34] Hocheng H and Pa P.S (2003). Electropolishing of cylindrical workpiece of tool materials using disc-form electrodes, *Journal of Materials Processing Technology,* 142, 203–212.

[35] Hassan A.M, Al-jalil H.F, and Ebied A.A (1998). Burnishing force and number of ball passes for the optimum surface finish of brass components, *Journal of Materials processing Technology,* 83, 176–179.

[36] Arif A.F.M, Sheikh A.K, Qamar S.Z, Raza M.K and Al-Fuhaid K.M (2015). Product defects in extrusion. Available https://www.researchgate.net/publication/281905425 (Accessed at 12th December).

[37] Ebrahimi R, Reihanian M, Kanaeni M and Moshksar M.M (2007). An upper-bound analysis of the tube extrusion process, *Journal of Material Processings,* 9, 214–220.

[38] Gattmah J, Ozturk F and Orhan S (2017). Effects of process parameters on hot extrusion of hollow tube, *Arab Journal of Science and Engineering,* 42, 2021–2030

[39] Alam Z and Jha S (2017). Reprint of Modeling of surface roughness in ball end magnetorheological finishing (BEMRF) process, *Wear*, 374, 54–62.

[40] Jain R.K, Jain V.K and Dixit P.M (1999). Modeling of material removal and surface roughness in abrasive flow machining process, *Machine Tools and Manufacture,* 39,1903–1923.

[41] S. Jha and V. K. Jain (2006). Modelling and simulation of surface roughness in magnetorheological abrasive flow finishing (MRAFF) process, *Wear*, 261, 856–866.

[42] Kirk D. A quick and easy formula for mesh-micron particle size conversions. Available at https://www.powderbulk.com/wp-content/uploads/2014/05/pbe 20081201 0018.pdf (Accessed on 10th Febraury 2018).

[43] Xudong G, Cheng W and Ronnguo Y (2011). An electromagnetic localization method for medical micro-devices based on adaptive particle swarm optimization with neighbourhood search, *Measurement*, 44, 852–858.

[44] Sawhney A.K. *Electrical Machine Design*. Dhanpat Raj and Co, 2016.

[45] Das M, Jain V.K and Ghoshdastidar P.S (2018). Analysis of magnetorheological abrasive flow finishing (MRAFF) process, *Machine Tools and Manufacture,* 48, 415–426.

[46] Marashi J, Yakushina E, Xirouchakis P, Zante R and Foster J (2017), An evaluation of H13 tool steel deformation in hot forging conditions, *Journal of Materials processing*, 246, 276–284.

[47] Yang A, Yang H, Yuhang P, Hongwei P and Jinze P (2017). Optimum surface roughness prediction for titanium alloy by adopting response surface methodology, *Results in Physics*, 7, 1046–1050.

[48] Rajput R.K. *Automobile Engineering.* Laxmi Publications, 2008.